Title
Genome-scale CRISPR screening reveals that C3aR signaling is critical for rapid capture of fungi by macrophages

Author
Cohen, Allison Leah

Publication Date
2022

Peer reviewed|Thesis/dissertation

Genome-scale CRISPR screening reveals that C3aR signaling is critical for rapid capture of fungi by macrophages

by
Allison Cohen

DISSERTATION
Submitted in partial satisfaction of the requirements for degree of
DOCTOR OF PHILOSOPHY

in

Cell Biology

in the

GRADUATE DIVISION
of the
UNIVERSITY OF CALIFORNIA, SAN FRANCISCO

Approved:

DocuSigned by:
Hiten Madhani
242AFD8ACF95471...

Hiten Madhani
Chair

DocuSigned by:
Anita Sil
DocuSigned by:
A2...

Anita Sil

Alexander Marson
7F25CDCE383C4A8...

Alexander Marson

Committee Members

This dissertation is dedicated to Steven Cohen, Karen Cohen, Ted Cohen, and Lilly Cohen. Without your constant love and support I would not be where I am today.

Acknowledgements

Many individuals and institutions have contributed to the work presented in this dissertation, and I am indebted to everyone involved. First and foremost, I would like to acknowledge Anita Sil, my advisor and mentor, for providing me with the guidance, resources, and support necessary to complete this challenging project, and for helping me to stick with it through all of the unexpected twists and turns. I feel that I've grown tremendously as a scientist due to her steadfast mentorship. The other members of my thesis committee, Alex Marson and Hiten Madhani, have also provided valuable guidance, insight, and encouragement along the way.

I would like to thank Mike Bassik and many folks in his lab who have been generous with their time, resources, and expertise in large-scale CRISPR screening and phagocytosis. In particular, Edwin Jeng contributed an immense amount of work and creativity to this project. He provided critical reagents, cell-lines, and protocols, in addition to guidance and technical support during the screen design phase, and his sequencing and analysis skills. Mark Voorhies enthusiastically provided indispensable guidance and resources for analyzing and visualizing our datasets, and has been a joy to work with and learn from. A brilliant infectious disease fellow and postdoc, Jane Symington, performed the challenging *Coccidioides posadasii* infections. Nebat Ali, a talented graduate student in the lab, generated the Gnb2 CRISPR knockout data in BMDMs, and I am very excited to see what else she will discover. Rosa Rodriguez has been instrumental in conducting the animal experiments, and in general is a fantastic scientist and supportive colleague and friend. I also want to thank Keith Walcott for

babysitting me in the BSL3 while I counted plates. Mark Roxas, our superb lab manager, helped keep us well stocked and running smoothly, in addition to skillfully pouring liters of specialized plates. I am also indebted to current and former lab members who work on *Hc*-macrophage interactions who provided hands-on training and support early in my career, and also helped foster a collaborative and friendly environment, including Bevin English, Lauren Rodriguez, Dinara Azimova, and Nancy Van Prooyen. Other lab members have also provided valuable feedback and support throughout this process.

I have also gotten loads of help and feedback from the broader UCSF community, including the Engel, Noble, Madhani, Cyster, and Barber labs, who have been generous with equipment, reagents, and expertise. In particular, Eric Dang, a brilliant immunologist, has provided indispensable insight and expertise that has helped me push this project forward. I'd also like to thank Nathaniel Meyer in Diane Barber's lab for gifting the LifeAct plasmid, and Carrie Graham in Sandy Johnson's lab for helping me with the *Candida albicans* phagocytosis studies.

None of this work would have been possible without the support of the UCSF Laboratory Animal Resource Center (LARC) and the Parnassus Flow Cytometry Core facility. Both institutions have exceptional staff whose expertise and rigor have immensely benefited this work. I would especially like to thank Alyssa Tafoya, who helped with blood collection, and Ashley Carlos for support and training on the flow cytometers and cell sorters.

I want to thank the lab mentors who have made a big impact on my decision to pursue a career in molecular biology research. Mya Breitbart and many talented marine microbiologists in Florida first introduced me to the wonderful world of microbes. Songtao Jia taught me how to use genetic tools, and Elias Coutavas taught me biochemistry. My high school biology teacher, Mr. McGonnegal, also got me excited about biology early on.

I've also leaned heavily on my grad school cohort, the famous (perhaps infamous) and inimitable Tetrad class of 2014 for scientific insight, emotional support, and adventure. I'd like to give a special shout-out to the 1260 roommates Valentina Garcia, Efren Reyes, and Austin Walter for helping me survive the pandemic lockdown and in general being amazing to live with, and to my fellow Parnasties Sumitra Tatapudy and Nick Sanchez. Nairi Harooni, Kelsey Haas, and Karen Cheng have also been great friends and confidants. The UCSF school of fighting (AKA Rick Garcia's boxing group) has been godsend when I needed to blow off some steam and hang out with amazing people. I feel much better prepared to move to Philly and start bar fights with Eagle's fans now thanks to you. I also want to thank my college and high school friends for supporting me and visiting me in SF (or even moving here for a few years!).

I, of course, would never have been able to do this without the unconditional love and support of my parents, Karen and Steven Cohen, my brilliant and hilarious siblings Ted and Lilly, and Grandma Beverly, the trailblazing physicist. Grandpa Murray, Granny Kitty and Granpda Leon have been a source of inspiration. May they rest in peace.

Contributions

The data presented in this dissertation has been prepared in the following manuscript, which is being revised for re-submission to *PLoS Pathogens*:

Cohen, A., Jeng, E.E., Voorhies, M., Symington, J., Ali, N., Rodriguez, R., Bassik, M.C., Sil, A. Genome-scale CRISPR screening reveals that C3aR signaling is critical for rapid capture of fungi by macrophages.

I (Allison Cohen) conceived, designed, and implemented experiments, collected and analyzed data, and wrote this dissertation. Dr. Anita Sil directed and supervised the research, provided financial support, and edited the document

Genome-scale CRISPR screening reveals that C3aR signaling is critical for rapid capture of fungi by macrophages

Allison Cohen

Abstract

The fungal pathogen *Histoplasma capsulatum* (*Hc*) invades, replicates within, and destroys macrophages. In chapter 2, to interrogate the molecular mechanisms underlying this interaction, we conducted a host-directed CRISPR-Cas9 screen and identified 361 genes that modify macrophage susceptibility to *Hc* infection, greatly expanding our understanding of host gene networks targeted by *Hc*. We identified pathways that have not been previously implicated in *Hc* interaction with macrophages, including the ragulator complex (involved in nutrient stress sensing), glycosylation enzymes, protein degradation machinery, mitochondrial respiration genes, solute transporters, and the ER membrane complex (EMC). The highest scoring protective hits included the complement C3a receptor (C3aR), a G-protein coupled receptor (GPCR) that recognizes the complement C3 cleavage product, anaphylatoxin C3a. Although it is known that the serum complement system reacts with the fungal surface, leading to opsonization and release of small peptide fragments such as C3a, a role for C3aR in macrophage susceptibility to fungi has not been elucidated. In chapter 3, we demonstrated that, whereas C3aR is dispensable for macrophage phagocytosis of bacteria and latex beads, it is critical for optimal macrophage capture of pathogenic fungi, including *Hc*, the ubiquitous fungal pathogen *Candida albicans*, and the causative agent of Valley Fever *Coccidioides posadasii*. We explored the role of serum

complement in macrophage phagocytosis of *Hc,* and found that the ability of serum to stimulate macrophage phagocytosis of *Hc* is dependent on complement, and involves C3a and C5a signaling, which can act redundantly to stimulate phagocytosis. We showed that C3aR localizes to the early phagosome during *Hc* infection, and coordinates the formation of actin-rich membrane protrusions that promote *Hc* capture. We also found that the EMC promotes surface expression of C3aR, likely explaining its identification in our screen. In chapter 4, we investigated the role of C3aR in the macrophage cytokine response to *Hc* and mouse susceptibility to *Hc* infection. Taken together, our results provide insight into host processes that affect *Hc*-macrophage interactions, and uncover a novel role for C3aR in macrophage recognition of fungi.

Table of Contents

List of Figures

List of Tables

List of Abbreviations

BMDMs	Bone-marrow-derived macrophages
Cas	CRISPR-associated sequence
CasTLE	Cas9 high-Throughput maximum Likelihood Estimator
Cbp1	Calcium binding protein 1
CLR	C-type lectin receptor
CRISPR	Clustered, regularly interspersed palindromic repeats
CRISPRKO	CRISPR knockout
CR3	Complement receptor 3
C3aR	Complement C3a receptor
C5aR	Complement C5a receptor
EDTA	Ethylenediaminetetraacetic acid
EGTA	Ethylene glycol-bis(β-aminoethyl ether)-N,N,N'N'-tetraacetic acid
FBS	Fetal bovine serum
FDR	False-discovery rate
GFP	Green-fluorescent protein
GPCR	G-protein coupled receptor
Hc	*Histoplasma capsulatum*
Inf	Infected
MOI	Multiplicity of infection
NHS	Normal human serum
NMS	Normal mouse serum

PBS	Phosphate-buffered saline
PRR	Pattern-recognition receptor
RT	Room temperature
sgRNA	single guide-RNA
Thio-Pmacs	Thioglycollate-ellicited peritoneal macrophages
TLR	Toll-like receptor
WT	Wild-type
Zy	Zymosan

Chapter 1: Introduction

The global disease burden of invasive fungal pathogens

Human fungal pathogens that cause invasive disease lead to significant morbidity and mortality worldwide. An estimated 1.5 million people are killed by fungal infections per year, with the majority of disease caused by a handful of clades such as *Candida*, *Aspergillus, Cryptotoccus*, *Pneumocystis*, and the endemic thermally dimorphic fungi (1, 2). While invasive fungal infections are rare and typically occur when the host is immune compromised, they are difficult to treat and associated with high fatality rates (3). The closely related clade of thermally dimorphic fungi share the ability to change their morphology depending on the temperature and to cause pulmonary or disseminated disease in immune competent individuals (4). These include the causative agent of Histoplasmosis, *Histoplasma capsulatum*, which is endemic to the Ohio and Missisippi valleys in the United States, and is the main focus of this work (5), and *Coccidioides*, the causative agent of Valley Fever, which is endemic to the central valley of California and the South-western United States (6). Despite their clinical importance, the biology of these organisms and how they interact with their hosts is under-studied.

The role of phagocytes in the pathogenesis of fungal infections

Professional phagocytes, including neutrophils, macrophages, and dendritic cells, are critical for defense against invading fungal pathogens (7, 8). These cells are highly efficient at ingestion of large (≥ 0.5 μm in diameter) particles, including microbes and damaged or cancerous cells, by a process called phagocytosis (9). Neutrophils, fast-moving cells armed with highly microbicidal granules and reactive oxygen and

nitrogen species, can initiate early clearance of fungi, such as *Candida albicans* and *Aspergillus spp.* (10, 11). Their importance is illustrated by the dramatically increased susceptibility of neutropenic individuals to infections with these fungi (12). However, for certain fungal infections, including pulmonary Cryptococcosis, neutrophil infiltration is associated with exacerbated host damage and impaired fungal clearance (13). Dendritic cells ingest pathogens and present antigens to prime the adaptive immune response (14). Macrophages, which exhibit remarkable diversity and phenotypic plasticity (15-17), participate in tissue surveillance, direct fungal killing, and antigen presentation during the innate phase of infection (7). They are also important for the clearance of apoptotic neutrophils, wound healing, and the resolution of inflammation that prevents inflammatory pathology (18, 19). Following initiation of the adaptive immune response, macrophages can be activated by cytokines secreted by CD4+ T-cells, such as interferon gamma (IFN-γ) (14). Activation increases the microbicidal activity of macrophages (20). IFN-γ activated macrophages are critical for the control of granulomatous pathogenic fungi such as *Hc* (21), and activated macrophages can inhibit intracellular fungal replication (22).

Fungi have also evolved strategies to subvert phagocyte functions. They can block phagocytosis, interfere with phagosome maturation, survive and replicate intracellularly, dampen the immune response, escape the phagosome, and exit or kill the cell (23). Disseminating fungi that survive inside macrophages may coopt them as transport to access the bloodstream, other tissues, and even to cross the blood-brain-barrier (24). Given the importance of phagocytes and phagocytosis to the outcome of

fungal infections, understanding the molecular details underlying phagocytosis of pathogenic fungi by innate immune cells is of vital importance to developing successful immunotherapeutic agents that can help to treat fungal infections.

Phagocytosis and phagosome formation

Phagocytosis receptors expressed on innate immune cells can directly recognize molecular patterns of their targets and engage opsonins, which are soluble components such as complement or antibodies that bind to the target surface. Engagement of phagocytosis receptors by either type of ligand triggers a complex cascade of intracellular signaling events, involving small GTPase activation, membrane phospholipid remodeling, and actin cytoskeleton polymerization that drives plasma membrane deformation and encircling of the targeted particle (9, 25). The mechanism of FcγR-mediated phagocytosis of antibody-opsonized targets, and to a lesser extent CR3-mediated phagocytosis of complement-opsonized targets, are well studied and are reviewed in the following references (25-28). Briefly, ligand binding and clustering of these receptors upon target contact leads to activation of Src family kinases, which phosphorylate the cytoplasmic tails of phagocytosis receptors, driving the recruitment of the kinase Syk. Syk then orchestrates the activation of phosphoinositide (PI) kinases, GTPases, and phospholipases that coordinate membrane remodeling and force generation via actin cytoskeleton polymerization. Branched, ARP2/3-complex-mediated actin nucleation, regulated by SCAR/WAVE and Rho-family GTPases, plays an important role in force generation that drives phagocytosis (29). The specific signaling events and cytoskeleton remodeling machinery involved in phagocytosis differ

depending on the composition of the particle, the cell-type and activation state, and the receptors engaged (26).

Microbes harbor a complex array of ligands, and are usually recognized by more than one receptor, which often participate in complex cooperative or antagonistic interactions that regulate internalization dynamics, phagosome maturation, and signaling (26). Receptors that can confer phagocytic activity to normally non-phagocytic cells are referred to as canonical phagocytosis receptors, which include Fcγ-R, Dectin-1, and CR3. However, many other receptors participate in phagocytosis or influence signaling, but are not sufficient to trigger uptake by non-phagocytic cells (30). In recent years, phagocytosis has been dissected systematically using genome-wide CRISPR screens, identifying new regulators, and clarifying the contribution of genes in phagocytosis of diverse substrates (31).

Following internalization, the phagosome undergoes a series of physiological changes termed phagosome maturation, which together create a degradative compartment that is hostile to microbial growth and important for antigen processing and presentation (32). These changes are orchestrated by phosphoinisitide remodeling at the phagosome membrane by PI kinases and phosphatases (33), and effector recruitment driven by Rab GTPases (34). The recruitment of the Vacuolar-type ATPase (v-ATPase) acidifies the phagosome (32). Depending on the phagocytic target and the influence of other activating signals, NADPH oxidase delivery to the phagosome leads to the generation of microbicidal and immune-modulatory reactive oxygen species

(ROS) (35). Finally, fusion with lysosomes delivers hydrolytic enzymes into the lumen of the mature phagolysosome that digest the contents (36).

Phagocytosis receptors for non-opsonic recognition of fungi

Common fungal cell-wall components are directly recognized by pattern-recognition-receptors (PRRs) expressed on innate immune cells, which drive phagocytosis and regulate pro-inflammatory signaling and activation. These include the integrin, C-type lectin, and Toll-like receptor families. The role of such receptors in recognition of fungi is extensively reviewed here (7, 30, 37). C-type lectin receptors (CLRs) are a family of receptors that bind carbohydrates, many of which play a role in direct recognition of the carbohydrate-rich fungal cell-wall (30, 38). The ubiquitous cell-wall polysaccharide β-glucan is recognized by receptor Dectin-1, which is sufficient to stimulate phagocytosis of un-opsonized fungi by non-phagocytic cells, and is also necessary for efficient recognition of many opportunistic fungi, including *Candida albicans* (39, 40). Other C-type lectin receptors, including dectin-2, mincle and DC-SIGN, recognize mannose structures (30). The mannose receptor recognizes α-mannans (30). Of these, mincle, DC-SIGN, and mannose receptor can directly trigger phagocysosis of fungi (30). While not sufficient to drive phagocytosis, dectin-2 plays an important role in the macrophage response to fungi, and can alter phagosome maturation and cytokine production (38). A recently described CLR, Mel-Lec, directly recognizes DHN-melanin on *Aspergillus* conidia (41). However, in mice, it is not expressed on leukocytes (though it is in humans), and its role in innate immune recognition and phagocytosis of fungi not well understood (37).

β2 integrin receptors (42, 43) are formed through dimerization of CD18 (*Itgb2*) with various α subunits. These include complement receptor 3 (CR3 or Cd18Cd11b), leukocyte function-associated antigen 1 (LFA-1 or Cd18Cd11a), or complement receptor 4 (CR4 or Cd18Cd11c) (44). Unstimulated integrin receptors adopt a bent, low-affinity conformation. When activated by external signals, they switch to an extended conformation, which better exposes ligand binding sites and increases the affinity of the interaction (44). Active integrin receptors recognize diverse ligands (28), including C3b, glucan, and other proteins to facilitate fungal recognition. They are also known to cooperate with other fungal phagocytosis receptors, such as dectin-1, to promote phagocytosis and the cytokine response to fungi (45, 46).

Toll-like receptors (TLRs), important and highly conserved PRRs, are critical for host defense against fungal pathogens. Mice deficient in the key TLR signaling adaptor MyD88 are more susceptible to fungal infections, including histoplasmosis (47, 48). In addition, *TLR4-/-* mice show enhanced susceptibility to opportunistic fungal infections (47), and *TLR7/9-/-* mice are more susceptible to infection with *Hc* (49). Some TLRs, such as TLR2, appear to interfere with protective immunity to certain systemic fungal infections (47). TLRs recognize diverse components of the fungal cell-wall. TLR2 has been proposed to recognize phosphomannan, chitin, and α-glucan; TLR4 binds mannans and mannosylated proteins; and TLR9 recognizes fungal DNA found in endosomes and chitin (37). While these receptors are not thought to directly participate in phagocytosis of fungi, TLR ligands promote macrophage cytokine production, and may enhance the activity of phagocytosis receptors such as CR3 (28).

Chemotaxis

Chemotaxis, which is directed movement of cells along a concentration gradient of a chemical signal (50), such as a chemokine or microbial byproduct, is important for antimicrobial defense. Chemotaxis mediates the recruitment of inflammatory cells to infected tissue (51), and for efficient hunting and capture of phagocytic targets (52). Chemotaxis is predominantly driven by G-protein coupled receptors (GPCRs). These multi-pass transmembrane receptors signal through heterotrimeric G-proteins to initiate spatially coordinated cytoplasmic and plasma membrane second messenger signaling (53, 54). Similar to phagocytosis, the protrusive force driving chemotaxis is generated by dynamic remodeling of the actin cytoskeleton (55). The SCAR/WAVE, ARP2/3, and WASP complexes coordinate actin polymerization at the leading edge of the cell. Following activation, GPCRs are rapidly internalized via clathrin-mediated endocytosis, and can be trafficked back to the plasma membrane via retrograde trafficking. GPCR trafficking regulates their activity and allows them to retain their sensitivity to small changes in chemoattractant levels, in addition to facilitating endosomal signaling (53).

Potent chemokines generated at sites of infection orchestrate the long-range recruitment of phagocytes from the bloodstream. GPRCs expressed on inflammatory monocytes respond to signals such as CCL2, and migrate from the bloodstream to the site of infection, where they respond to local signals to differentiate into inflammatory macrophages or dendritic cells (51). Neutrophils are also recruited to sites of fungal infection by CXC chemokines (11). Elimination of the recruitment of monocytes or neutrophils can dramatically impair the anti-fungal response (56).

Phagocytes also respond chemotactically to local signals generated by microbes or target cells that promote homing and improve the efficiency of microbial capture (52, 57). A uniform concentration of chemokines or cytokines also increases the rate of membrane ruffling and sampling of the extracellular milieu, which improve the likelihood of microbial capture (58). GPCR signaling can activate the high-affinity conformation of integrins through the activity of the GTPase Rap1(28). Microbial-derived chemotactic signals include byproducts of microbial metabolism, such as formylated peptides recognized by formyl-peptide receptors expressed on phagocytes, which are important for bacterial capture (59). There is some evidence that certain fungi can generate non-serum-dependent chemoattractants, though their identity and role in fungal capture is not well understood (60). As described below, complement components react with microbial surfaces, undergo proteolysis, and release the anaphylatoxins C5a and C3a. C5a and C3a can both stimulate chemotaxis of innate immune cells (61). C5a has been shown to drive local chemotaxis of neutrophils towards fungi to facilitate fungal capture (62). C3a has been assumed to have an analogous function, although this has not been thoroughly investigated to our knowledge.

The complement pathway and its role in fungal recognition

Innate and antibody-dependent cellular recognition of pathogens is supported by the complement system (63). While complement factors are predominantly synthesized in the liver and delivered to the bloodstream, innate immune cells such as macrophages can locally secrete complement components (64-66). Around 50 complement factors and regulators participate in this process, and are found biological fluids such as serum

and bronchoalveolar fluid (67, 68), where they react with foreign particles and facilitate their destruction and recognition by innate immune cells, in addition to performing other homeostatic and immune modulatory functions (69, 70).

The complement cascade is be triggered by three main pathways: the antibody-dependent classical pathway, the lectin pathway, through recognition of microbial sugars by the soluble mannan binding lectin, and the non-specific alternative pathway. These activation pathways all culminate in the self-cleavage and activation of the central complement component C3 (63). Following C3 activation, C3b is covalently attached to the microbial surface, and is recognized by complement receptors (CRs) expressed on immune cells, which mediate phagocytosis (28). C3b can be further processed by proteolytic cleavage into inactivated C3b (iC3b), which is also recognized by CRs. C3 cleavage also releases the small peptide fragment, anaphylatoxin C3a, which is recognized by the complement 3a receptor (C3aR), a G-protein coupled receptor (GPCR) highly expressed on innate immune cells (71). C3a acts as a chemoattractant for innate immune cells such as neutrophils, eosinophils, and macrophages (72). C3a can also have direct antimicrobial activity (73), modulates the production of cytokines in response to inflammatory stimuli (74), and has been implicated in the pathogenesis of inflammatory diseases such as sepsis and allergic inflammation (61).

Initial activation of C3 initiates a proteolytic cascade that results in the cleavage and activation of downstream components, such as C5. C5 cleavage releases the potent anaphylatoxin C5a, which, like C3a, activates a GPCR, C5aR, that promotes

chemotaxis and innate immune modulation (63). The anaphylatoxins C5a and C3a have other inflammatory effects on both immune and non-immune cells, such as inducing basophil degranulation, smooth muscle contraction, and vasodilation (61). An important role for intracellular C3a-C3aR signaling in regulating T-cell functions has also emerged in recent years (75, 76). C5 also initiates the formation of the membrane attack complex (MAC), a pore-forming complex that can directly drive lysis of bacteria. Since inappropriate complement-mediated attack of host tissue can cause extensive damage, complement activation is tightly controlled and regulated by a number of inhibitors, decay-acceleration factors, and proteases, including carboxypeptidases that remove the C-terminal arginine from C3a and C5a, abrogating their activity (63). Failure to appropriately control complement activation is linked to immune pathology (77).

Ubiquitous opportunistic fungal pathogens, including *Candida albicans*, as well as endemic fungal pathogens such as *Coccidioides immitis* (78) and *Hc* (79), are strong activators of multiple complement pathways (80). Serum is known to enhance the phagocytosis of opportunistic fungal pathogens, and the role of C3b/iC3b opsonization in promoting uptake of fungi due to recognition by complement receptors is well-studied (80-83). In addition, complement plays an important role in host defense against opportunistic fungi, including *Candida albicans* (84) and *Cryptococcus neoformans* (85), as *C3-/-* mice are more susceptible to these infections. Zymosan, a cell-wall preparation of *Saccharomyces cerevisiae*, has been well-established as a model for complement activation for several decades (86). CR3 recognizes other substrates, such as glucans, and promotes complement-independent recognition of fungi such as *Hc* (28, 42, 43).

C3b deposition on fungal surfaces has also been suggested to mask ligands for dectin-1 and dectin-2, and may preclude a strong cytokine response (87). C5a-C5aR signaling can also promote neutrophil migration towards and phagocytosis of *Cryptococcus neoformans* (62) and promote monocyte cytokine production in response to *Candida albicans* infection (88).

Certain pathogenic fungi, the best studied of which is *Candida albicans*, have evolved strategies to interfere with complement (69, 82, 89). The masking of cell-wall glucans can slow the alternative pathway of complement activation. In addition, fungi can either recruit endogenous complement inhibitors or secrete effectors that inhibit complement or degrade complement components to prevent activation. In general, the rigid structure of the fungal cell is thought to preclude MAC formation, though how fungi resist MAC-mediated lysis is incompletely understood.

Notably, the role of complement in innate immune recognition of endemic fungi such as *Hc*, and of C3a-C3aR signaling in macrophage interaction with fungi has not been investigated.

Chapter 2: A large-scale pooled CRISPR screen in J774A.1 macrophage-like cells identified genes required for macrophage susceptibility to infection with *Hc*

Introduction

Histoplasma capsulatum (*Hc*) is a fungal intracellular pathogen of macrophages. Infection with *Hc* occurs when soil containing *Hc* spores or hyphal fragments is aerosolized and fungal particles are inhaled by a mammalian host (90). In the lung, *Hc* invades alveolar macrophages (91, 92), replicates to high intracellular levels, and induces macrophage lysis (93, 94). *Hc* resides in a phagosome, and neutralizes the pH of this phagosome using unknown strategies (95, 96). Though many of the molecular mechanisms underpinning *Hc* pathogenesis are unknown, a number of *Hc* genes that promote immune evasion and virulence have been identified, including genes that detoxify reactive oxygen species, acquire nutrients, and drive macrophage lysis (97-102). However, little is known about the host pathways involved in *Hc* pathogenesis.

Macrophage phagocytosis of *Hc*, unlike that of other fungi, is not dependent on β-glucan recognition by Dectin-1 (43), though Dectin-1 contributes to the macrophage cytokine response to *Hc* (46). *Hc* can prevent such recognition by shielding cell-wall β-glucans with a layer of α-glucan (103) or by secreting glucanases to prune β-glucans (104). Instead, *Hc* recognition and phagocytosis is directly mediated by β2 integrin receptors, the best studied of which is CR3 (42, 43). However, in murine macrophages, inhibiting CR3 with blocking antibodies or mutating the β-2 integrin subunit of CR3 (105) does not fully inhibit phagocytosis of *Hc*, suggesting the involvement of other receptors (43). A ligand for CR3 recognition of un-opsonized *Hc* is chaperone Hsp60, which is

deposited on the *Hc* cell-wall (106). CR3 recognition of glucans may also play a role in *Hc* phagocytosis, though blocking with soluble glucans does not inhibit phagocytosis of *Hc*. The lipid composition of the macrophage plasma membrane is also important for optimal phagocytosis of non-opsonized *Hc*, as interfering with the sialic acid (43), ganglioside (105), or cholesterol composition (105) of the plasma membrane interfered with optimal phagocytosis, possibly by preventing the formation of lipid rafts that aid in signaling. Blocking polymerization of the actin cytoskeleton has also been shown to prevent macrophage phagocytosis of *Hc* (107). Literature on innate immune recognition of *Hc* by macrophages is reviewed here (97).

To characterize host genes that underlie macrophage susceptibility to infection with *Hc*, we took advantage of a powerful pooled host-side screening platform (108) that has been successfully employed to identify host targets of intracellular pathogens (109, 110) and microbial toxins (111). We screened a CRISPR-Cas9 knockout library in macrophage-like cells challenged with *Hc*, and identified genes required for macrophage susceptibility to *Hc*-mediated lysis. We identified a number of host pathways that affected macrophage susceptibility to *Hc* infection, and focused our studies on molecules that influence *Hc* phagocytosis. Our findings shed light on molecular mechanisms underlying innate immune recognition of fungi, and uncover new host pathways that may be targeted by *Hc* to promote virulence.

Development of Cas9-expressing J774A.1 cells, and validation of screening approach

To identify genes that affect macrophage sensitivity to parasitization by *Hc*, we conducted pooled CRISPR-Cas9 knockout screens in the J774A.1 mouse macrophage-

like cell-line. This cell line has been widely used to model macrophage interactions with pathogenic microbes, including *Hc* (98, 100). We demonstrated that *Hc* can induce lysis of J774A.1 cells in a manner dependent on the secreted effector Cbp1 (Fig. 2.1), which is consistent with studies in primary macrophages (98, 100, 101). We also found that the stress-responsive genes, *Trib3* and *Chop*/*Ddit3*, are up-regulated in J774A.1 cells in a Cbp1-dependent manner, though the upregulation is less pronounced than that observed in BMDMs (Fig. 2.1) (98).

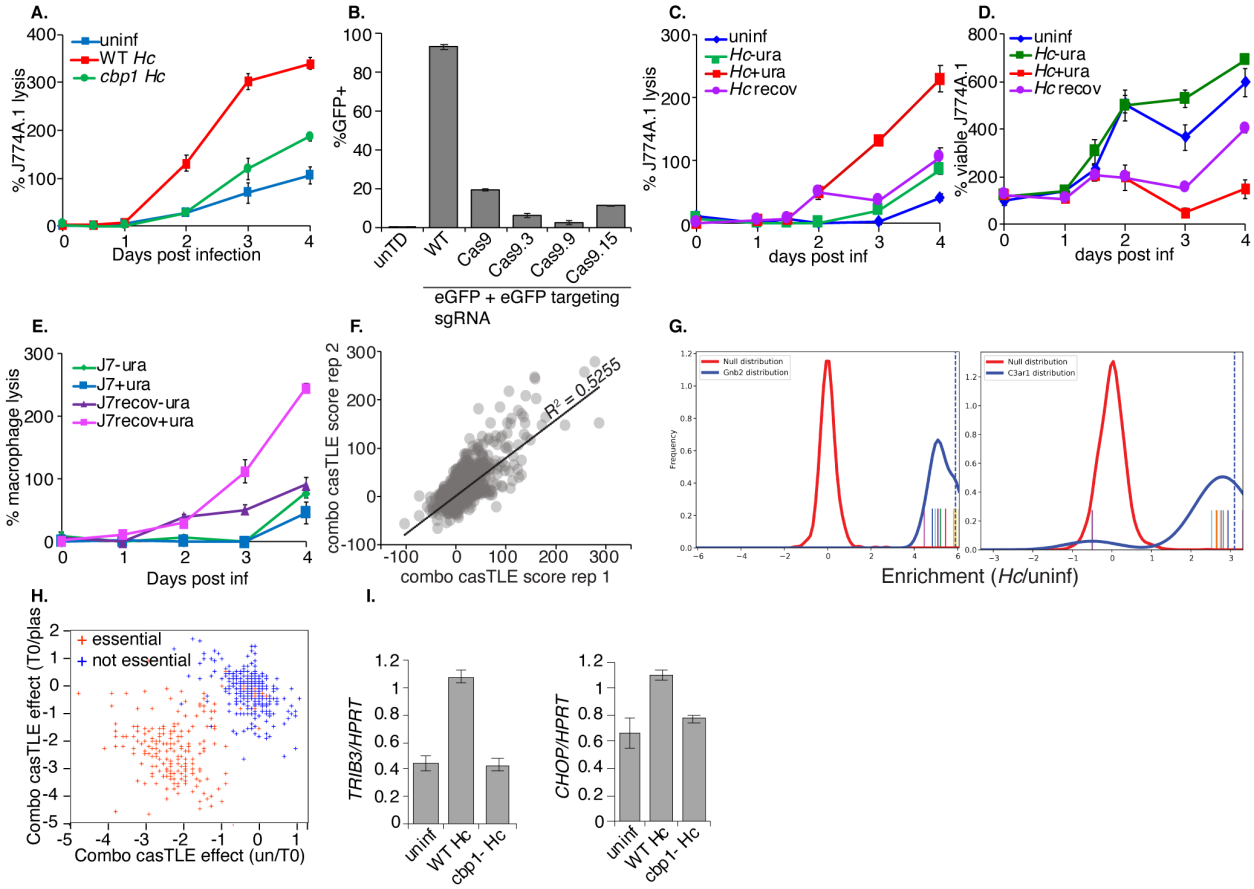

Figure 2.1: Development and validation of Cas9-expressing J7 cell-lines, and validation of screening approach. A. Characterization of *Hc*-mediated lysis in J774A.1 macrophage-like cells. J774A.1 cells were infected with WT *Hc,* or *Hc* with a disruption in a gene, *CBP1*, that is required for *Hc* to lyse macrophages. Lysis over time was measured using the LDH release assay. B. Validation and clonal expansion of Cas9-expressing J774A.1 cells. Cells were transduced with an Ef1a-Cas9-Blast expression vector and grown under blasticidin selection to generate a population of

Cas9-expressing cells. These were subjected to single-cell sorting and clonal expansion to generate Cas9-expressing J774A.1 clones with high Cas9 activity. Cas9 activity was measured by transducing J774A.1 cells with a guide RNA vector that co-expressed GFP with a sgRNA targeting GFP. Cas9 activity leads to silencing of the GFP following puromycin selection. Cas9 clone 9 was chosen for the large-scale CRISPR screens due to its high-efficiency GFP silencing. C-D. Characterizing lysis and recovery from infection with uracil pulses during infection with a Ura5-deficient *Hc*. J774A.1 cells were infected with *ura5ΔHc* in the presence or absence of exogenous uracil (0.4ug/mL). Uracil-containing cultures were washed, and media was replaced with uracil-poor media after 2d of lysis, which allowed the macrophages to recover. Recovery was assessed using LDH release quantification to assess lysis, and the confluency of viable cells in the wells was estimated using the pico-green dsDNA assay kit following lysis of macrophages with water. E. macrophages that had been recovered from lysis by removal of uracil from culture media were passaged for several days, and uracil was added to selected wells. Macrophage lysis over time was monitored by assessing LDH release to determine whether dormant yeast would be able to re-activate upon introduction of uracil. F. Reproducibility of the casTLE confidence score across two replicates of the screens. G. Histograms comparing the distribution of negative control sgRNAs and sgRNAs targeting *Gnb2* or *C3ar* in the *Hc* infected pool compared to the uninfected pool. H. Analysis of essential gene behavior during J7 library growth. Scatter plot showing the gene effect resulting from passaging of J7s, either going from the plasmid pool to the T0 pool, or the T0 pool to the uninfected pool. Genes annotated as "essential" or "non-essential" were plotted to determine whether essential genes appeared more likely to drop out of the uninfected pools. I. Up-regulation of *TRIB3* and *CHOP* stress-responsive transcripts in *J7s* during *Hc* infection is Cbp1-dependent as measured by qPCR 24h post-infection at an MOI of 5.

To create our knockout libraries, we first generated a clonal J774A.1 cell-line with high constitutive Cas9 activity (Fig. 2.1). We then transduced these Cas9-expressing J774A.1 cells with pooled lentiviral sgRNAs. We used a previously designed CRISPR-Cas9 sgRNA library, which targets 23,000 protein-coding mouse genes with 10 sgRNAs/gene. The genome-wide library is split into 20 sub-libraries, each of which covers 500-1500 genes and includes 750 negative control sgRNAs (112). We screened each sub-library separately, covering a total of 16,782 genes. These cells were infected, in duplicate, with *Hc* or were left uninfected and passaged throughout the course of the screen (Fig. 2.2). To improve the sensitivity of our screen, we used a strain of *Hc* with a

mutation in the *URA5* gene (*Hc ura5Δ*) which cannot grow in media without uracil supplementation (113). This strain does not lyse J774A.1 cells in the absence of exogenous uracil, and host cells that survive the initial round of lysis can be recovered by washing the monolayer and incubating in media without uracil supplementation (Fig. 2.2), thereby allowing enrichment of resistant host cells.

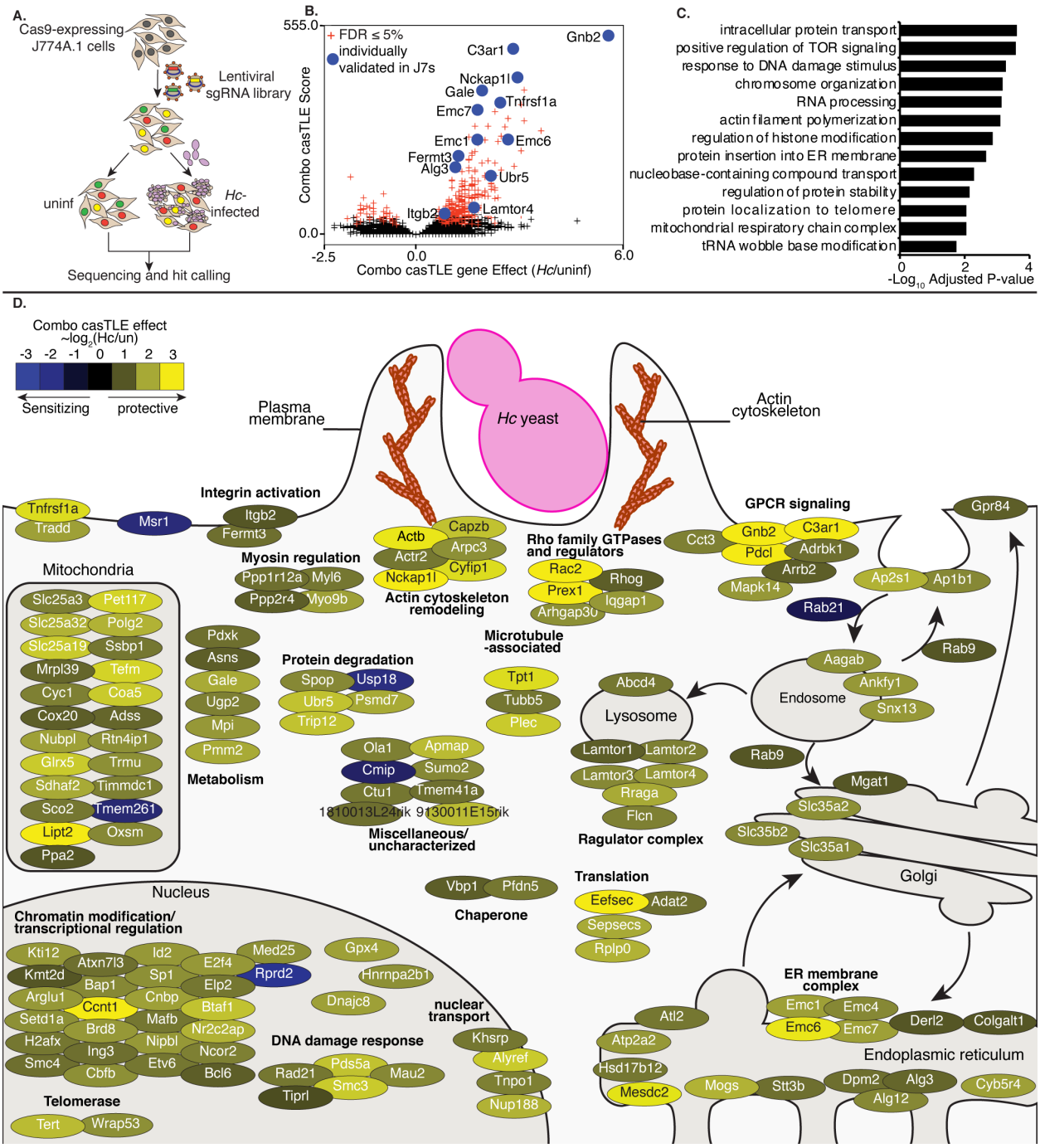

Figure 2.2: A pooled CRISPR screen identifies genes required for macrophage susceptibility to infection with *Hc*. A. Diagram of screen approach. Cas9-expressing J774A.1 macrophage-like cells were transduced with a library of sgRNAs, challenged with *ura5Δ Hc* yeast, and subjected to 2-3 pulses of uracil treatment followed by recovery. sgRNAs amplified from *Hc*-infected and uninfected cells were deep-sequenced, and sequences were analyzed to identify guides that became enriched or depleted in the *Hc*-infected pool relative to the uninfected pool. B. Volcano plot showing the confidence score (casTLE score) versus the effect size (casTLE effect) for all genes. Genes that pass the 5% FDR cutoff are colored red, and genes individually

validated in J774A.1 cells are labelled and colored in blue. C. Adjusted P-values for selected GO biological process annotations enriched in the screen hits. D. The 150 highest-scoring genes identified in the screen grouped based on their annotated function and localization in a cell, functional categories or complexes of genes are noted. Genes are colored according to their gene effect estimate, where yellow indicates enrichment in the *Hc* infected pool and blue indicates depletion.

We infected the J774A.1 pools with *Hc ura5Δ* and performed 2-3 rounds of uracil addition to induce *Hc*-mediated lysis of at least 50% of the J774A.1 cells, followed by uracil removal and recovery (see table 2.1 for sub-library specific details). We pulsed the uninfected cells with uracil during passaging to match the *Hc* infection. The sgRNAs in the final pools were deep-sequenced to determine the enrichment of guides following challenge with *Hc*. We employed the Cas9 high-throughput maximum-likelihood estimator (casTLE) algorithm (114) to estimate the effect of knocking out a gene on macrophage susceptibility to *Hc* (caSTLE effect) based on enrichment of guides targeting each gene compared to the enrichment of negative control sgRNAs. We additionally analyzed uninfected cells at the beginning and the end of passaging using the casTLE algorithm, and we were able to verify that guides targeting genes previously annotated as essential (114) dropped out of the pool during passaging (Fig. 2.1).

Table 2.1: Screen results summary by sub-library

Sub-library	Rounds of *Hc*-mediated lysis	Duration (days)	Δdivisions (uninf-*Hc* inf)	Correlation coefficient (R^2 casTLE score)	genes	desensitizing hits (Hc/un>0)	sensitizing hits (Hc/un<0)	Total hits
ACOCA	2	16	10.17	0.74	1568	31	1	32
ACOCB	3	10	7.93	0.57	1546	59	1	60
TMMA	2	9	9.9	0.69	972	43	4	47
TMMB	3	7	6.73	0.49	951	37	1	38
DTKPA	2	7	5.53	0.24	1008	20	1	21
DTKPB	2	8	4.9	0.48	1003	15	0	15
SPA	2	9	8.5	0.49	1333	31	9	40

Sub-library	Rounds of *Hc*-mediated lysis	Duration (days)	Δdivisions (uninf-*Hc* inf)	Correlation coefficient (R^2 casTLE score)	genes	desensitizing hits (Hc/un>0)	sensitizing hits (Hc/un<0)	Total hits
SPB	2	9	8.45	0.68	1478	21	2	23
MPAB	3	10	6.2	0.73	953	14	4	18
GEA	2	8	5.6	0.54	954	9	6	15
GEB	2	9	6.2	0.46	962	14	4	18
U1A	2	8	5.2	0.19	1019	8	1	9
U1B	2	8	5.3	0.53	932	19	2	21
U2AB	2	8	6.3	0.0028	2103	1	3	4

Identification of host genes that modulate macrophage susceptibility to Hc infection

We identified 361 genes whose deletion modulated macrophage susceptibility to *Hc* infection at a 5% false-discovery rate cutoff (Fig. 2.2). Confidence scores between screen replicates were moderately correlated (Fig. 2.1). Disruption of 322 of these genes conferred protection against *Hc* (combo casTLE effect >0), and disruption of 39 conferred greater susceptibility to infection (combo casTLE effect <0) (Fig. 2.2). We noticed that the protective hits include genes known to be required for macrophage phagocytosis, such as members of the SCAR/WAVE and ARP2/3 complexes (Fig. 2.2). Such regulators have been well-studied for their role in phagocytosis and chemotaxis (25, 31, 115). Similarly, we identified *Itgb2* (CD18), which encodes the β-subunit of CR3 that has been previously shown to facilitate recognition and phagocytosis of *Hc* (42, 43), and *Fermt3*, which promotes activation of integrins (116) (Fig. 2.2).

Of note, we identified a number of pathways and complexes among the resistance-promoting hits that have not been previously implicated in *Hc* interaction with macrophages (Fig. 2.2), such as the ragulator complex, glycosylation enzymes, protein

degradation machinery, mitochondrial respiration genes, solute transporters, and the ER membrane complex (EMC). The ragulator complex promotes nutrient stress sensing (117), and the EMC facilitates the folding of transmembrane proteins with multiple membrane-spanning regions (118, 119). The highest-scoring protective hits include a group of genes (*Gnb2*, *Pdcl*, AP-1 subunits, AP-2 subunits, *Arrb2*) that regulate G-protein coupled receptor (GPCR) signaling and receptor trafficking following GPCR engagement (Fig. 2.2) (120, 121). The gene identified with the second-highest confidence score encodes the GPCR C3a receptor 1 (*C3ar1/C3aR*) (Fig. 2.2). Histograms demonstrating the enrichment of negative control sgRNAs and sgRNAs targeting *Gnb2* and *C3ar* in the *Hc*-infected pool are shown in Fig. 2.1. We went on to investigate whether these factors play a role in macrophage phagocytosis of *Hc*.

Identification of genes required for phagocytosis of yeast in J774A.1 macrophage-like cells and primary macrophages

We selected 16 high-confidence hits to individually validate in J774A.1 macrophage-like cells, including two genes, SCAR/WAVE subunit *Nckap1l*, and CR3 subunit *Itgb2*, which were expected to play a role in macrophage phagocytosis of *Hc*. We prioritized genes that would shed light on novel aspects of macrophage interactions with *Hc* and that did not appear to strongly inhibit macrophage replication. We chose the three top-performing guides, based on enrichment or depletion in the screen, for further validation. CRISPR targeting was validated by TIDE analysis of sequence traces from amplicons of the targeted locus. The sequences of sgRNAs used and their estimated INDEL frequencies are listed in Table 2.2.

Table 2.2: sgRNAs used in this study and CRISPR targeting efficiency measured by TIDE analysis.

sgRNA	Cell-type	Target sequence	Targeting efficiency (INDEL frequency)
Neg control		GCAGGATCGCGCCGTATAAT	N/A
Gnb2sg1	J7	GGCCACAAAGTTCCCTGAGG	30.60%
Gnb2sg3	J7	GAACACGGAGGACCCTCCG	45.70%
Gnb2sg7	J7	GCTTGATGGAGGCGTCAC	31.80%
C3ar1sg1	J7	GAAACAGAGGCCGTGAGTGT	69.20%
C3ar1sg5	J7	GCACAGGAACAAGCCATA	95.80%
C3ar1sg8	J7	GGAAATCGGCCAGGGTGAGA	71.70%
Nckap1Lsg8	J7	GGATGAGCGTGATGTACA	66.20%
Nckap1Lsg9	J7	GAAGCTGACAGAAGAATT	80.60%
Nckap1Lsg10	J7	GGTTCCTCCGAACAAAG	91.30%
Galesg3	J7	GGCCGTCATCCACTTTGC	42%
Galesg7	J7	GAGGCGTGGGCGCCTAT	82.10%
Galesg10	J7	GAACCCCCAGTACCTGCCTC	27.90%
Tnfrsf1asg2	J7	GTGTCTCACTCAGGTAGCGT	31.30%
Tnfrsf1asg6	J7	GTGTGTAACTGCCATGCA	54.80%
Tnfrsf1asg8	J7	GGCAAGGAGAGATCTCCACC	
Emc7sg4	J7	GCCTCAGGACTGGATCTCCG	94.40%
Emc7sg6	J7	GTGGTTCATGATATTCCCTC	84.60%
Emc7sg7	J7	GATTTCATTTGGAGAGGATA	76.90%
Emc6sg4	J7	GGTGAGGCCGAGGATGCCGG	85.50%
Emc6sg5	J7	GCTCCTCATTCTCAAAGC	75.20%
Emc6sg6	J7	GAGGCCTCCCGTAAAGAG	92.10%
Emc1sg2	J7	GCATGAGGCGCCCTCCGT	82.70%
Emc1sg8	J7	GCTGTGCTGCTCGTCCCTG	92.70%
Emc1sg9	J7	GTGGATGCCATGCTGGTCCA	61.40%
Fermt3sg3	J7	GTCTGTTGGGCAGTCGC	54.10%
Fermt3sg6	J7	GCCCCTCTTCCAAACGG	81.80%
Fermt3sg9	J7	GGTCTGACCATGCCATT	69.60%
Alg3sg5	J7	GCCTCTGCATAGCAGAGGT	54.50%
Alg3sg7	J7	GATGTACAAAAACCCAGCT	81.90%
Alg3sg9	J7	GAAGGAATAGCAATCCCG	85.50%
Ubr5sg1	J7	GACGTCCATCCATTTCG	96.10%
Ubr5sg5	J7	GAGCTGGTCCTCGGTGCC	83.10%
Ubr5sg8	J7	GGCGTGTTCTTCTTATCC	73.50%
Rab21sg1	J7	GCTCGGGGAAGGCTGCGT	

sgRNA	Cell-type	Target sequence	Targeting efficiency (INDEL frequency)
Rab21sg2	J7	GAGCCTACTCCTTCAAGG	
Rab21sg8	J7	GATGAGAGAGCAAAAGGCAA	46.30%
Atl2sg3	J7	GCCATATGAGTGCTCATA	55.40%
Atl2sg6	J7	GGGATCTTAACATAGTCG	60.10%
Atl2sg7	J7	GCTGGTCCTGATAACGG	83.20%
Lamtor4sg2	J7	GCTTGCTCATCGTTCTCA	87.40%
Lamtor4sg5	J7	GGGATTCGCTCCAGCCCTT	93.20%
Lamtor4sg6	J7	GAGCGAATCCCAGACCAGCT	88%
Arrb2sg2	J7	GTCGCGCTTGCCCAAGTACA	70%
Arrb2sg4	J7	GACAGGCCCAGTACATCC	88.20%
Arrb2sg9	J7	GTGCGGCTTATCATCAGAA	
ITGB2sg1	J7	GGATTAGCGATGCTCCTG	71.60%
ITGB2sg2	J7	GATCAATGGGGTATCCCT	49.60%
ITGB2sg3	J7	GGGCAAGCAGCAGTGAGTGT	58.60%
Gnb2sg1	BMDM	GGCCACAAAGTTCCCTGAGG	60.80%
Gnb2sg3	BMDM	GAACACGGAGGACCCTCCG	65.70%
Gnb2sg7	BMDM	GCTTGATGGAGGCGTCAC	71.90%
C3ar1sg1	BMDM	GAAACAGAGGCCGTGAGTGT	68%
C3ar1sg5	BMDM	GCACAGGAACAAGCCATA	77.90%
C3ar1sg8	BMDM	GGAAATCGGCCAGGGTGAGA	75.30%
ITGB2sg1	BMDM	GGATTAGCGATGCTCCTG	53.50%
ITGB2sg2	BMDM	GATCAATGGGGTATCCCT	66.40%
ITGB2sg3	BMDM	GGGCAAGCAGCAGTGAGTGT	62.50%
Emc1sg2	BMDM	GCATGAGGCGCCCTCCGT	64.30%
Emc1sg8	BMDM	GCTGTGCTGCTCGTCCCTG	75.80%
Emc1sg9	BMDM	GTGGATGCCATGCTGGTCCA	70.80%

To verify susceptibility/resistance phenotypes in J774A.1 cells, we mixed GFP+, CRISPR-knockout (KO) cells with Cas9-expressing unlabeled cells, infected one pool of this mixture with *Hc*, and in parallel passaged the uninfected pool. Following one round of lysis and recovery, the pools were then harvested, and the proportion of GFP-expressing cells was measured by flow cytometry (Fig. 2.3). The ratio of GFP+ cells in the *Hc*-infected compared to the uninfected pool demonstrated whether targeting a

specific gene conferred a fitness advantage (>1) or disadvantage (<1) to macrophages during co-culture with *Hc*. Of the 16 genes tested, 13 conferred a fitness advantage during *Hc* infection when disrupted, including *Gnb2*, *C3ar*, ER membrane complex subunits *Emc1, Emc6,* and *Emc7*, and ubiquitin ligase *Ubr5* (Fig. 2.3). As positive controls, we included knockouts of SCAR/WAVE subunit *Nckap1l*, and the β-2 integrin subunit of CR3, *Itgb2* (Fig. 2.3). The only susceptibility-promoting hit that we tested, *Rab21*, did not promote increased susceptibility to *Hc* infection when disrupted (Fig. 2.3).

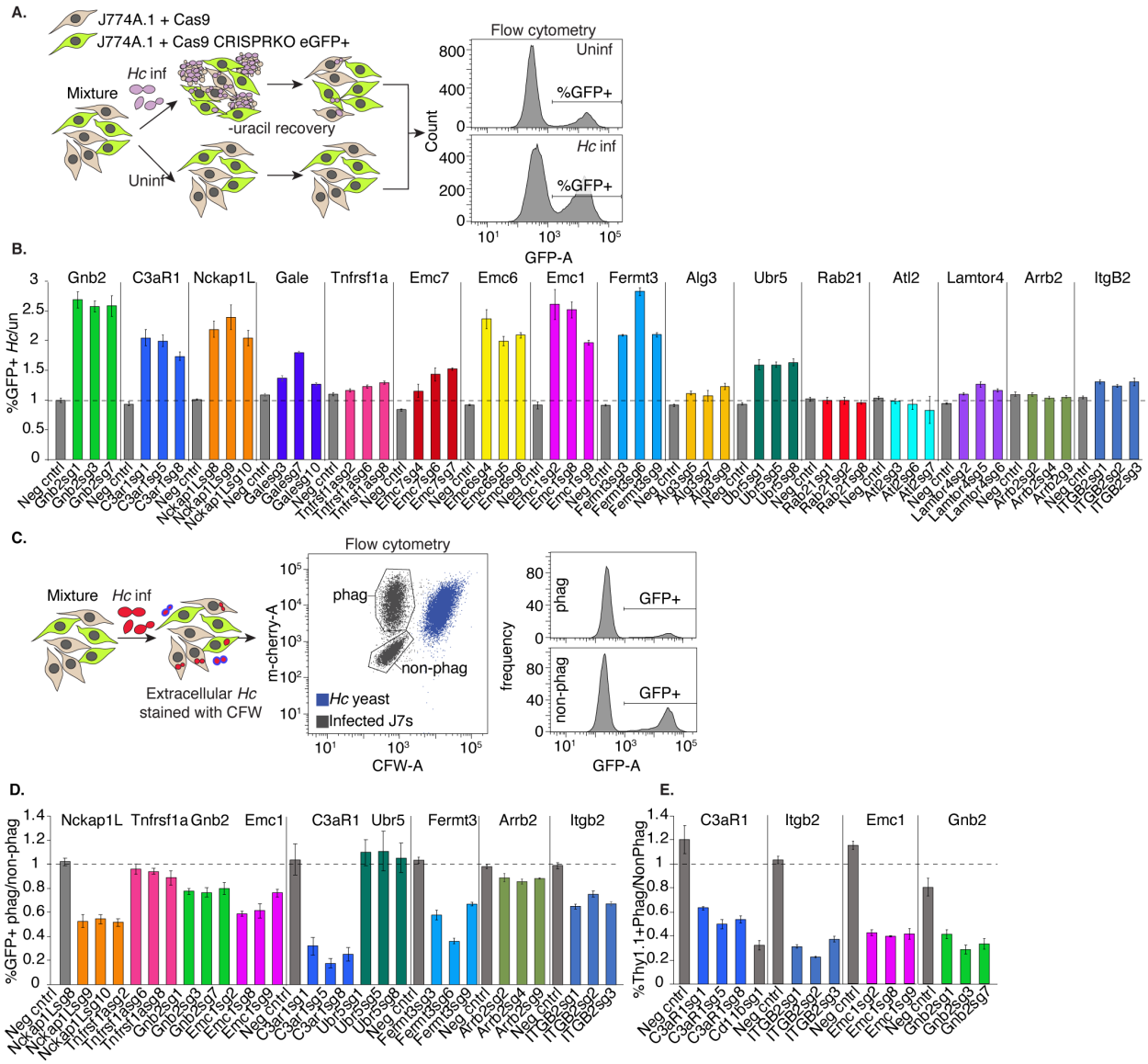

Figure 2.3: Identification of genes required for phagocytosis of *Hc* yeast in J774A.1 cells and primary macrophages. A. Diagram of the approach used to individually validate the role of a gene in macrophage susceptibility to *Hc* infection. A mixture of WT (GFP-) and CRISPRKO (GFP+) J774A.1 cells with gene-targeting or negative control sgRNAs were challenged with *Hc* yeast in the presence of uracil, and allowed to recover. Uninfected cells from the same mixture were passaged in parallel, and the percentage of CRISPRKO cells in the *Hc* infected pools was compared to that of the uninfected pools via flow cytometry (n=3 biological replicates). B. Enrichment of gene-targeting guides in the *Hc* infected pool relative to the control pool, compared to that of non-targeting guides. C. Diagram of approach for determining the role of a gene in phagocytosis of *Hc.* A mixture WT (GFP-) and CRISPRKO (GFP+) J774A.1 cells were infected with mCherry-expressing *Hc* yeast. Non-internalized yeasts were excluded using calcofluor white staining. Flow cytometry was used to determine the representation of CRISPRKO cells in the phagocytic compared to the non-phagocytic

populations (n=3). D. Identification of genes required for phagocytosis of yeast in J774A.1 cells using GFP expression to measure enrichment of sgRNA-expressing cells. E. Validation of gene involvement in BMDM phagocytosis of yeast using CRISPRKO BMDMs (Thy1.1+). A mixture of transduced (Thy1.1+) and untransduced (Thy1.1-) BMDMs were similarly infected with yeast and stained with calcofluor white and a Thy1.1 antibody to determine the representation of mutants in the phagocytic and non-phagocytic populations (n=3 biological replicates).

Next, we tested whether these genes play a role in macrophage phagocytosis of *Hc* yeast. To this end, we mixed GFP+, CRISPR-targeted (CRISPRKO) cells with unlabeled, Cas9-expressing cells, infected the mixture with mCherry-expressing *Hc* yeast, and stained the cells with calcofluor white (CFW) to distinguish between intracellular and extracellular yeast. We used flow cytometry to measure the representation of GFP+ cells in the phagocytic compared to the non-phagocytic population. As expected, targeting of *Nckap1l, Fermt3,* and *Itgb2* led to decreased *Hc* phagocytosis in J774A.1 cells (Fig. 2.3). Additionally, we found that knockout of *Emc1, Gnb2, C3ar1,* and *Arrb2* decreased phagocytosis of *Hc* (Fig. 2.3).

Although J774A.1 cells recapitulate many important features of primary macrophages, including phagocytosis, they also differ in characteristics such as gene expression regulation (122). Therefore, we attempted to reproduce our findings from J774A.1 cells in bone marrow-derived macrophages (BMDMs) using CRISPR-Cas9-mediated gene disruption. We mixed CRISPRKO, Thy1.1+ BMDMs with WT, unlabeled BMDMs, infected the mixture with *Hc* yeast, and assessed phagocytosis as described above. We quantified the proportion of Thy1.1+ cells in the phagocytic compared to the non-phagocytic populations to determine whether the targeted genes promoted BMDM phagocytosis of *Hc* yeast. The four genes that we tested, GPCR *C3ar1*, integrin subunit

Itgb2, ER membrane complex *Emc1*, and Gβ subunit *Gnb2*, were also required for efficient phagocytosis of *Hc* yeast by BMDMs (Fig. 2.3).

Chapter 3: Serum complement and C3aR signaling are critical for efficient macrophage capture of *Hc* yeast

Introduction

Since a role for C3aR in phagocytosis of fungi had not previously been defined, we were intrigued by the result that this receptor is required for efficient phagocytosis of *Hc* by J774.1 cells and BMDMs. C3aR is a GPCR that recognizes the complement C3 cleavage product, anaphylatoxin C3a, and signals through Gαi (61), which is sensitive to pertussis toxin-mediated ADP-ribosylation (123). C3aR has been previously implicated in macrophage chemotaxis in transwell assays (72), and macrophage uptake of certain, though not all, bacterial pathogens (124, 125), and in microglial phagocytosis of several substrates (126-128). C5a, which can be released downstream of C3 activation, has been shown to facilitate neutrophil capture of *Cryptococcus* yeast (62). We further investigated the role of complement, C3aR and GPCR signaling in macrophage phagocytosis of fungi.

C3aR signaling plays a role in macrophage phagocytosis of fungi

We generated BMDMs from *C3ar*-/- mice (129) and age-matched WT mice. We then infected these macrophages with several species of pathogenic fungi, including *Hc* yeast expressing mCherry*, Candida albicans* (*Ca*) yeast detected with a fluorescent antibody, and *Coccidioides posadasii* (*Cp*) arthroconidia labeled with FITC (Fig. 3.1), and determined the extent of phagocytosis over time. We also tested phagocytosis of FITC-labeled zymosan, a cell-wall extract of *Saccharomyces cerevisiae*. We used calcofluor white staining to distinguish between intracellular and extracellular fungi. We observed that C3aR was required for efficient phagocytosis of all three species of

pathogenic fungi, in addition to zymosan, suggesting an important general role for C3aR in macrophage capture and phagocytosis of fungi (Fig. 3.1). The involvement of C3aR did not require fungal viability, as C3aR was equally important for phagocytosis of both live and killed *Hc* yeast, as well as zymosan (Fig. 3.1). The phagocytosis defect was not due to a defect in CD11b or CD18 surface expression in *C3ar-/-* BMDMs (Fig. 3.2). *C3ar-/-* macrophages are still able to eventually phagocytose most of the fungi tested by 30-60min post-infection at an MOI of 2, but uptake is slower. The dynamic range of the phagocytosis assay is higher at an MOI of 5, and the phagocytosis defect of *C3ar-/-* BMDMs appears stronger at an MOI of 5.

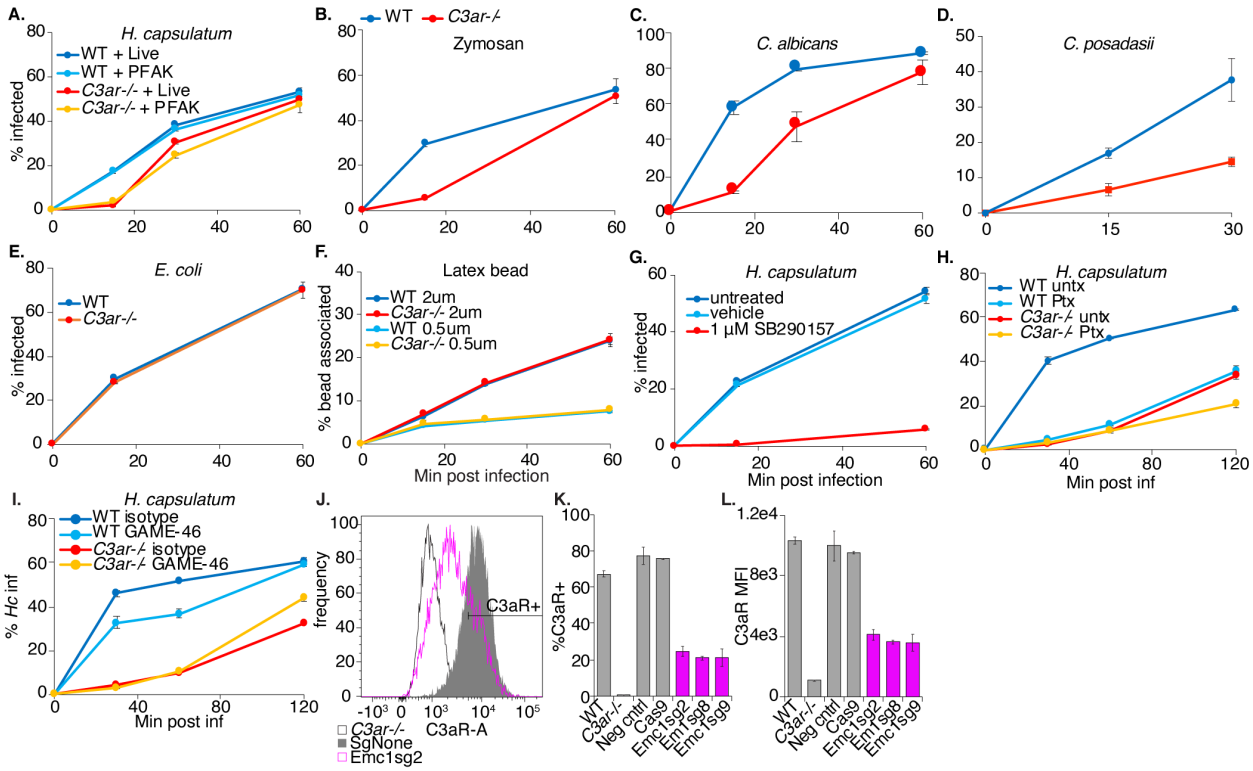

Figure 3.1: C3aR signaling plays a role in macrophage phagocytosis of fungi. A. WT and *C3ar-/-* BMDMs were infected with live or PFA-killed, mCherry-expressing *Hc* yeast (MOI2), and the phagocytosis rate was monitored over-time using flow-cytometry (n=3 biological replicates). B. WT and *C3ar-/-* BMDMs were infected with FITC-labelled zymosan or mCherry-expressing *Hc* (MOI2) and the phagocytosis rate cells was monitored using flow cytometry (n=3 biological replicates). C. BMDMs were infected with *Candida albicans* (*Ca*) (MOI3). Cells were imaged using confocal microscopy to

quantify phagocytosis (n=2 biological replicates, >350 cells/replicate). CFW staining was used to exclude extracellular *Ca.* D. BMDMs were infected with FITC-labelled *Coccidioides posadasii* (*Cp*) arthroconidia (MOI1), and extracellular conidia were labelled with calcofluor white. BMDM infection rates were determined using confocal microscopy (n=3 biological replicates, 200-400 cells/rep). E. BMDMs were infected with FITC-labelled *E. coli* bioparticles (MOI4), and the *E. coli*-association with BMDMs was monitored via flow cytometry (n=2 biological replicates). F. BMDMs were infected with 2 µm or 0.5 µm red fluorescent latex beads (MOI2), and the rate of BMDM association with the beads was measured using flow cytometry (n=3 biological replicates). G. BMDMs were treated with a C3aR antagonist (1 µM SB290157) and infected with *Hc* yeast (MOI2). Phagocytosis was measured using flow cytometry (n=3 biological replicates). H. BMDMs were pre-treated for 2 h with 1 µg/mL pertussis toxin (Ptx), which inhibits Gαi, and infected with *Hc* (MOI5, n=3 biological replicates). I. BMDMs were pre-treated for 90 min with 10 µg/mL CD18 blocking antibody (GAME-46) and infected with *Hc* yeast (MOI5, n=3 biological replicates). Phagocytosis was measured using flow cytometry. Emc1 is required for C3aR expression in BMDMs (J-L). J. *Emc1* CRISPRKO BMDMs and control sgRNA transduced BMDMs were surface-stained for C3aR, and C3aR levels were measured via flow cytometry (n=2 biological replicates). K. Histogram of C3aR levels in control and *Emc1* CRISPRKO BMDMs. L. Frequency of C3aR+ cells in the indicated BMDMs. M. The mean fluorescence intensity (MFI) of the C3aR signal in the indicated BMDMs.

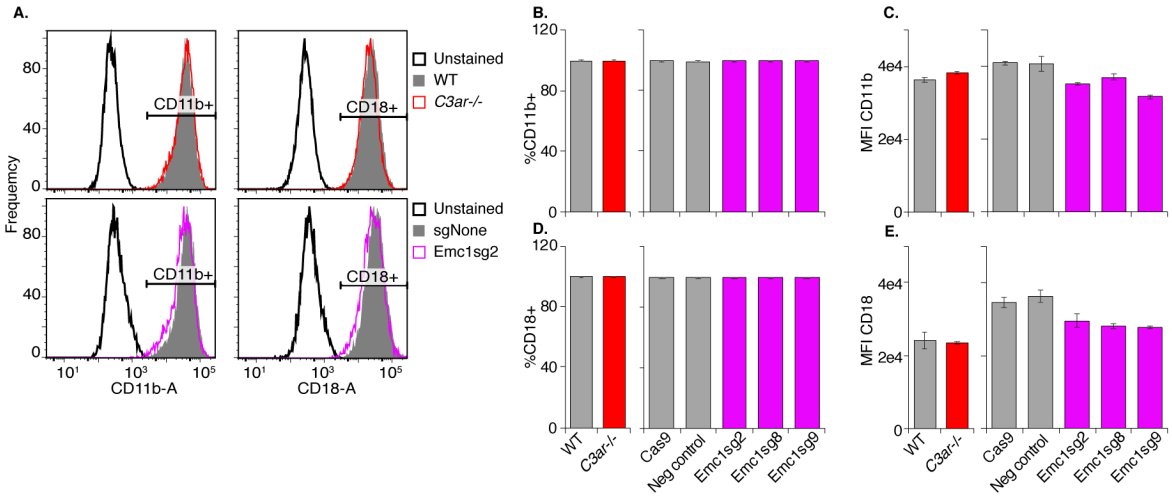

Figure 3.2: Emc1 and C3aR are not required for surface expression of CD18 or CD11b. BMDMs from *C3ar-/-* and WT mice, in addition to BMDMs expressing Cas9 and control or *Emc1*-targeting sgRNAs, were stained with CD18 and CD11b-specific antibodies and analyzed by flow cytometry (n=2 biological replicates). A. Representative histograms showing CD11b and CD18 levels in control, *C3ar-/-*, and *Emc1* CRISPRKO BMDMs. The percentage of CD11b (B) and CD18 (D) positive macrophages was analyzed. The mean fluorescence intensity of CD11b (C) and CD18 (D) were also measured.

To investigate whether the requirement of C3aR for phagocytosis extends to other types of particles that can be taken up by macrophages, we measured the capture of uncoated latex beads and FITC-labelled *E. coli* K12 in WT and *C3ar-/-* BMDMs (Fig. 3.1). We found that C3aR was not required for uptake of *E. coli* or latex beads (Fig. 3.1), suggesting that C3aR does not play a general role in phagocytosis.

To further validate the contribution of C3aR to phagocytosis, we treated macrophages with a specific non-peptide antagonist of C3aR, SB290157 (130) five minutes before challenge with *Hc* (Fig. 3.1). We found that the C3aR antagonist was able to inhibit macrophage phagocytosis of *Hc*, suggesting an acute role for C3aR in macrophage phagocytosis of fungi. Treatment with the antagonist seemed to have a stronger effect on phagocytosis at 60 min post-infection, which may reflect the difference in the dynamic ranges of the assay due to the use of a higher MOI in the antagonist experiment. The antagonist may also have off-target effects that can inhibit phagocytosis, or macrophages from *C3ar-/-* mice may up-regulate other surface receptors to compensate for chronic C3aR deficiency. C3aR signaling is dependent on pertussis toxin-sensitive Gαi (61), inhibition of which interferes with macrophage phagocytosis of Zymosan particles (131). We assessed whether Gαi inhibition by pre-treatment of macrophages with pertussis toxin (Ptx) would impact macrophage phagocytosis of *Hc* yeast, and whether Ptx treatment would synergize with C3aR deficiency. We found that Ptx pre-treatment inhibited macrophage phagocytosis of *Hc* (Fig. 3.1). Ptx treatment strongly phenocopies the phagocytosis defect in *C3ar-/-* BMDMs, and Ptx treatment modestly inhibits phagocytosis in *C3ar-/-* BMDMs (Fig. 3.1).

These findings show that C3aR-dependent Gαi activation promotes phagocytosis, although Gαi activation by other receptors, and C3aR coupling to a different Gα subunit, may play a minor role in *Hc* phagocytosis (Fig. 3.1). We also investigated whether C3aR genetically interacts with CR3 to promote phagocytosis by treating BMDMs with a CD18 blocking antibody (GAME-46) previously used to block CR3 in murine macrophages (43) (Fig. 3.1). As is consistent with previous results from thioglycollate-ellicited peritoneal macrophages (Thio-Pmacs) (43), WT BMDMs treated with the CD18 inhibitor had a modest defect in phagocytosis of *Hc*. Treatment of *C3ar-/-* BMDMs with the inhibitor did not further block phagocytosis of *Hc*, suggesting that CR3 participates in phagocytosis downstream of C3aR (Fig. 3.1).

We further reasoned that Emc1 may indirectly promote phagocytosis due to its role in stabilization of proteins with multiple transmembrane helices (119), such as C3aR. To test this hypothesis, we measured C3aR surface-expression in *Emc1* CRISPRKO BMDMs (Fig. 3.1). We saw a dramatic decrease in C3aR surface-expression in *Emc1*-targeted BMDMs compared to untransduced or control-targeted BMDMs (Fig. 3.1), suggesting that the EMC facilitates the proper folding and biosynthesis of GPCRs, such as C3aR, in macrophages. In contrast, *Emc1* CRISPRKO BMDMs did not show reduced surface expression of CD18 or CD11b (Fig. 3.2), verifying that the EMC is not as critical for proper folding of single-pass transmembrane proteins like integrins.

Since phagocytosis of *Hc* is delayed in *C3ar-/-* BMDMs, we expected lysis of infected BMDMs to show a corresponding delay. As expected, we found that *C3ar-/-*

BMDMs were slightly less susceptible to *Hc*-mediated lysis, as measured by an established assay (100, 132) (Fig. 3.3). Analysis of *Hc* colony forming units (CFUs) indicated that *C3ar-/-* macrophages were infected with fewer *Hc* yeast at the start of the experiment, and *Hc* yeasts did not have a major intracellular growth defect in the mutant macrophages (Fig. 3.3).

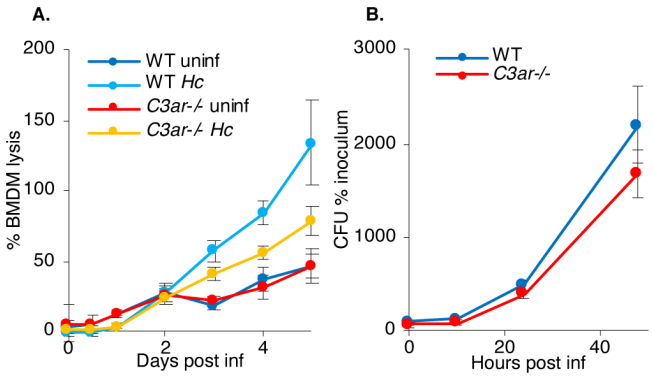

Figure 3.3: *C3ar-/-* BMDMs are partially resistant to *Hc*-induced lysis. BMDMs were infected with *Hc* (MOI=0.5), and macrophage lysis was quantified by measuring the release of lactate dehydrogenase (LDH) into the culture supernatants over-time (n=3 biological replicates, 3 technical replicates/biorep) (A). LDH release is presented as the percentage of total LDH present in the well (supernatant and macrophage lysate) at 2 hours post-infection. At the indicated time points, macrophages were lysed using water, and lysates were spread on agar plates. Colony forming units (CFUs) were enumerated (n=3 biological replicates, 2 technical reps/biorep) (B).

Serum complement promotes macrophage phagocytosis of Hc yeast

Since the canonical ligand for C3aR is C3a derived from C3 processing, we investigated whether serum represented a source of C3 that would react with *Hc* to generate C3a and promote phagocytosis. Macrophage infections discussed up to this point were conducted in the presence of 10% (for J774A.1 cells) or 20% (for BMDMs) heat-treated fetal bovine serum (FBS), which was not previously thought to harbor active complement components.

We infected WT and *C3ar-/-* BMDMs with mCherry+ *Hc* and FITC-labelled zymosan in the presence or absence of 20% heat-inactivated FBS, and monitored phagocytosis by flow cytometry. Surprisingly, we found that FBS promoted macrophage phagocytosis of *Hc*, and to a lesser extent zymosan, in a C3aR-dependent manner (Fig. 3.4). Even after 2h of co-culture, we did not observe efficient phagocytosis of *Hc* by BMDMs in serum-free media (Fig. 3.4). Phagocytosis of zymosan by BMDMs in serum-free media was more efficient than that of *Hc*, and was not dependent on C3aR (Fig. 3.4), as expected due to the role of other receptors, such as Dectin 1, in non-opsonic macrophage recognition of zymosan (83). The low level of *Hc* phagocytosis in serum-free media was also C3aR-independent. The ability of FBS to stimulate phagocytosis is not lot-dependent, as FBS from different lots and manufacturers promoted macrophage phagocytosis of *Hc* in a C3aR-dependent manner (Fig. 3.5). We also tested adult bovine serum, which was, surprisingly, able to stimulate phagocytosis of *Hc* in a partially C3aR-independent manner (Fig. 3.5). To assess whether FBS was promoting phagocytosis by opsonization of the yeast, we tested whether pre-incubation with FBS would be sufficient to stimulate phagocytosis of *Hc* in serum-free media (Fig. 3.4). We found that pre-incubation in FBS did not promote phagocytosis of *Hc* or zymosan (Fig. 3.4), suggesting either that FBS does not facilitate phagocytosis by opsonization, or that opsonization is labile. We also determined that incubating *Hc* with BMDM conditioned media containing FBS did not promote macrophage phagocytosis of *Hc* (Fig. 3.6), suggesting that BMDMs do not secrete a missing factor that would restore FBS-mediated opsonization of *Hc*.

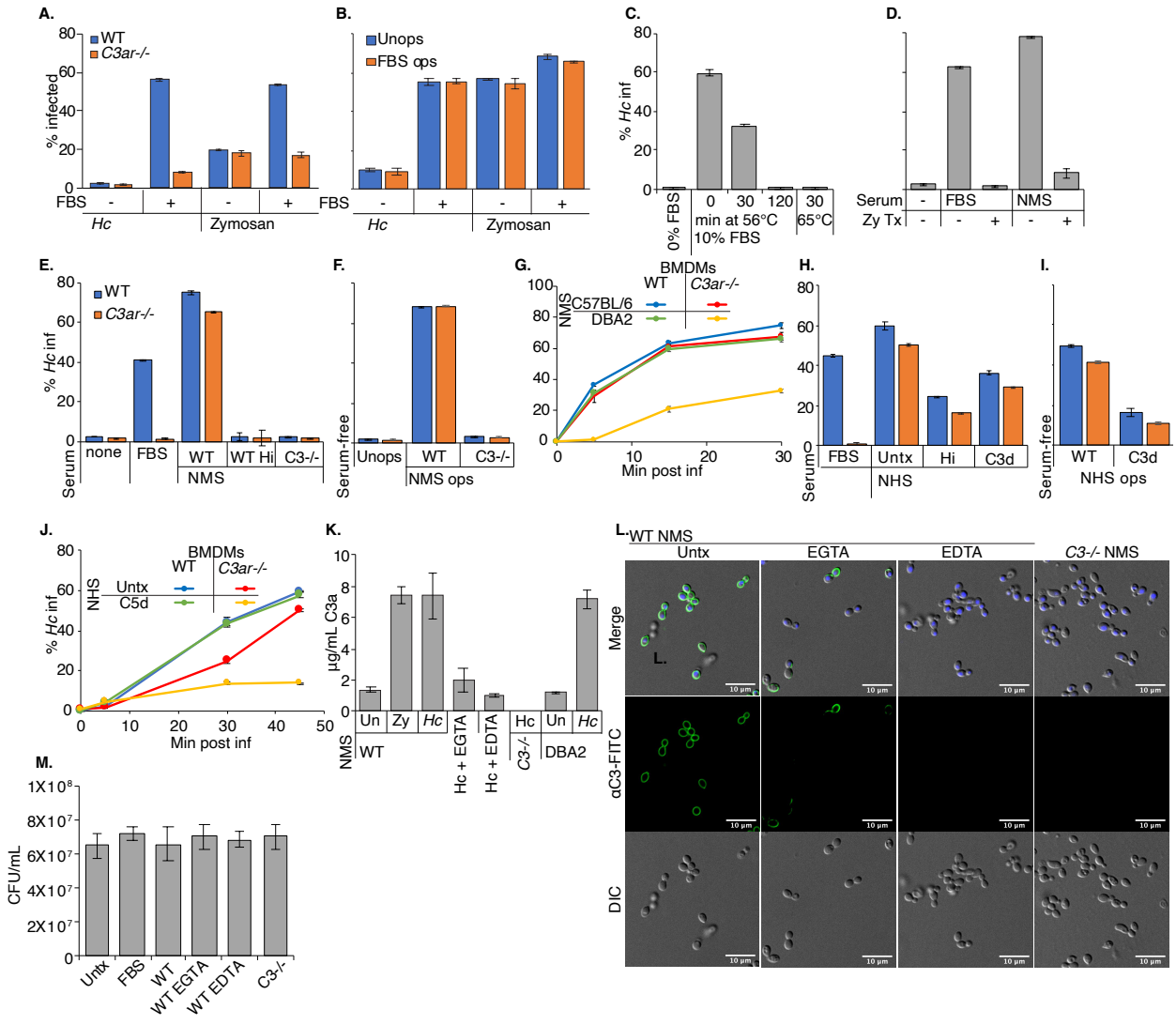

Figure 3.4: Serum complement promotes macrophage phagocytosis of *Hc* yeast. A. FBS stimulates macrophage phagocytosis of fungi in a C3aR-dependent manner. BMDMs were infected with mCherry-expressing *Hc* or FITC-labelled zymosan (30 min, MOI5) in the presence or absence of 20% heat-treated FBS (FBS). Phagocytosis was assessed via flow cytometry (n=3 biological replicates). B. FBS does not promote macrophage phagocytosis of *Hc* via opsonization. *Hc* and zymosan particles were pre-incubated with 10% heat-treated FBS for 30 min at 37°C, washed, and used to infect BMDMs (2h, MOI2). Phagocytosis was measured using flow cytometry (n=2 biological replicates). C-D. Prolonged or intense heat-treatment and zymosan treatment eliminates the phagocytosis-stimulating properties of FBS. C. Macrophage phagocytosis of *Hc* (MOI5, 45 min, n=3 biological replicates) was assessed in media supplemented

with 10% FBS that had been subjected to heat treatment (C) at 56°C for up to 2h, at 65°C for 30 min, or that had been pre-treated with zymosan (D) ($1X10^8$ particles/mL, 60 min at 37°C). Phagocytosis was measured by flow cytometry. E. Normal mouse serum (NMS) stimulates BMDM phagocytosis of *Hc* in a C3-dependenent manner. BMDMs were infected with *Hc* yeast (MOI=5, 60min) in serum-free media or media supplemented with 5% FBS, 5% NMS from WT mice, 5% NMS from C3-/- mice, or 5% heat-inactivated NMS (hiNMS) from WT mice, and phagocytosis was measured by flow cytometry (n=3 biological replicates). F. BMDMs in serum-free media were infected with *Hc* opsonized with 10% WT or C3-/- NMS. Phagocytosis was measured by flow cytometry (n=3 biological replicates). G. C5-deficient serum promotes macrophage phagocytosis of *Hc* in a C3aR-dependant manner. BMDMs were infected with *Hc* yeast (MOI5) in media supplemented with 5% NMS from C57BL/6 mice or DBA2 (C5-deficient) mice. Phagocytosis was measured by flow cytometry (n=2 biological replicates). H-J. Normal human serum (NHS) stimulates macrophage phagocytosis of *Hc* yeast. H. BMDMs were infected with *Hc* (MOI5, 60 min) in media supplemented with 5% untreated, heat-inactivated, or C3-depleted (C3d) NHS, and phagocytosis was monitored by flow cytometry (n=3 biological replicates). I. *Hc* was opsonized with 10% untreated or C3d NHS, used to infect BMDMs in serum-free media (MOI5, 60 min), and phagocytosis was monitored by flow cytometry (n=3 biological replicates) J. BMDMs were infected with *Hc* (MOI5) in media supplemented with 5% untreated or C5-depleted (C5d) NHS, and phagocytosis was monitored by flow cytometry (n=3 biological replicates). K-L. Mouse serum promotes complement opsonization of yeast and release of C3a via multiple pathways. *Hc* was incubated in 10% serum from WT, *C3-/-*, or DBA2 mice. 10 mM EGTA or EDTA were added to the reactions to chelate Ca^{2+} or Mg^{2+}, respectively. K. Supernatants were harvested following incubation, and mouse C3a levels were measured by ELISA (n=3 biological replicates). L. Yeast were stained with a FITC conjugated anti-mouse C3, and imaged using confocal microscopy (representative slices are shown from 2 biological replicates, scale bar = 10 μm). M. Yeast were incubated in 10% of the indicated serum for 30 min at 37°C, and fungal viability was measured by the CFU recovery.

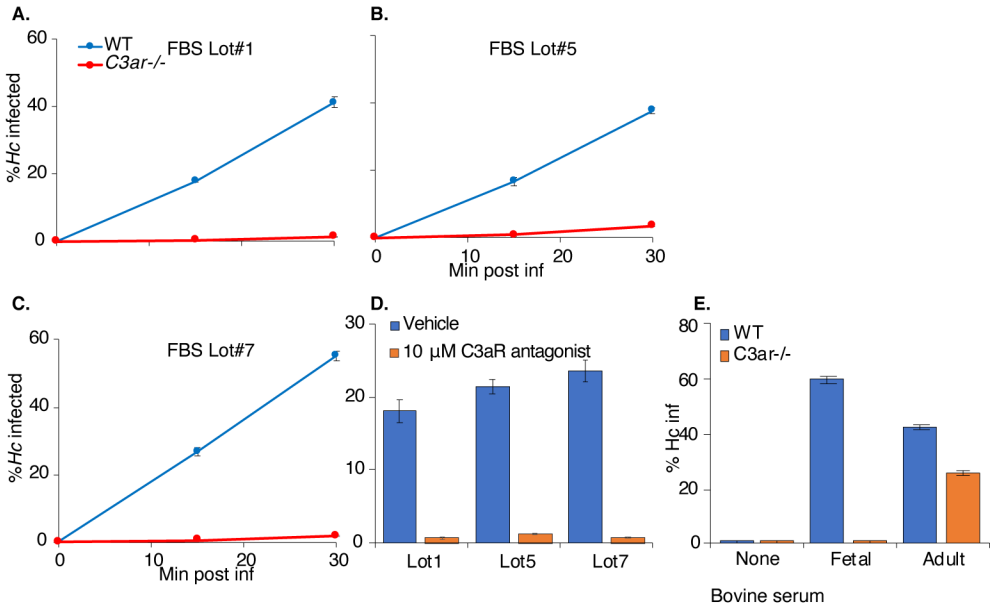

Figure 3.5: Different lots of FBS and adult bovine serum stimulate BMDM phagocytosis of *Hc* in a C3aR-dependent manner. (A-C) BMDMs from WT and *C3ar-/-* mice were infected with *Hc* in the presence of 20% FBS from three different lots from 2 separate suppliers. In addition, WT BMDMs differentiated in different lots of serum were treated with 10 μM of the C3aR antagonist and infected with *Hc* (D). Phagocytosis of *Hc* was measured by flow cytometry as described previously (n=2 biological replicates). E. Macrophages were infected with *Hc* in media supplemented with FBS or adult bovine serum, and phagocytosis was measured by flow cytonmetry (n=3 biological replicates).

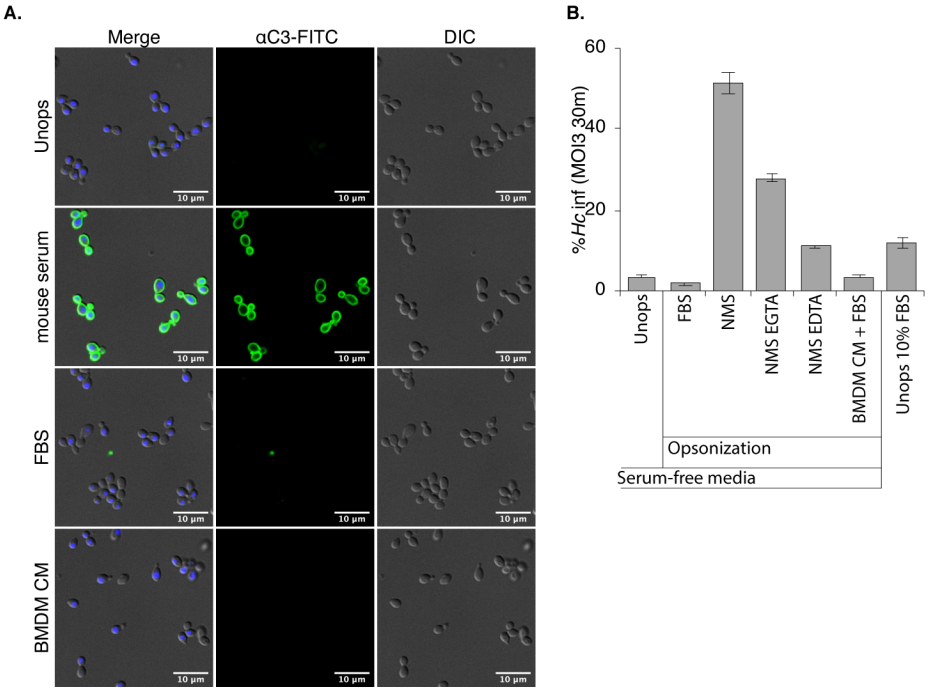

Figure 3.6: Macrophage conditioned media containing FBS does not promote opsonization that facilitates macrophage phagocytosis of *Hc* yeast in the absence of serum. BMDMs were cultured in media containing 10% FBS, and the BMDM conditioned media was harvested. *Hc* was incubated with macrophage conditioned media (BMDM CM), 10% FBS, or 10% normal mouse serum (NMS) with 10 mM EGTA or EDTA as indicated for 30 min at 37°C. A. Incubation with conditioned media or FBS does not lead to C3 deposition on the *Hc* surface. C3 deposition on *Hc* yeast was analyzed by immunofluorescence microscopy using a C3-specific antibody. Scale bar = 10 μm B. Pre-incubation of yeast with conditioned media does not improve macrophage phagocytosis of *Hc.* Yeast were washed 2X and used to infect BMDMs at an MOI of 3 for 30 min in serum-free media. Phagocytosis was assessed using flow cytometry as previously described (n=3 biological replicates).

Due to the surprising finding that serum incubated at 56°C for 30 min was able to stimulate phagocytosis, we tested whether increasing the duration or temperature of heat-treatment would affect this activity. We found that, while FBS heat-treatment at 56°C for 30 min reduced phagocytosis stimulation by 50%, treatment at 56°C for 2 h or at 65°C for 30 min nearly completely destroyed the ability of FBS to stimulate phagocytosis of *Hc* (Fig. 3.4). We further tested whether pre-incubating FBS with zymosan would deplete the phagocytosis stimulating properties of FBS. We found that pre-treating FBS and normal mouse serum (NMS) with zymosan also eliminated their ability to stimulate phagocytosis (Fig. 3.4). This suggests that a pathogen recognition component of serum that can be absorbed or inactivated by Zymosan, as opposed to a non-specific macrophage activation signal, is critical for the ability of FBS to stimulate phagocytosis. The ability of BMDMs in serum-free media to ingest zymosan and serum-opsonized *Hc* (Fig. 3.4) also suggests that BMDMs are not generally incompetent at phagocytosis in the absence of serum.

To establish a role for serum-derived C3 in macrophage recognition of *Hc*, we compared phagocytosis of *Hc* in media supplemented with no serum, FBS, or serum

collected from WT or *C3-/-* C57BL/6 mice (WT NMS or *C3-/-* NMS) (Fig. 3.4). We found that mouse serum promoted macrophage phagocytosis of *Hc* in a C3-dependent manner that was sensitive to heat inactivation (Fig. 3.4). Surprisingly, the ability of mouse serum to stimulate phagocytosis of *Hc* was not strongly dependent on C3aR (Fig. 3.4), suggesting an additional C3aR-independent, C3-dependent mechanism of phagocytosis. Since C5 can be activated downstream of C3, leading to the release of the potent chemoattractant C5a (63), we reasoned that serum from C57BL/6 mice might stimulate phagocytosis via C5. C5a release and recognition by C5aR would then stimulate phagocytosis and compensate for a C3aR-deficiency. To test this, we performed phagocytosis assays in media supplemented with serum from DBA2 mice, which has low levels of serum C5, but normal levels of C3 (133). We found that *C3ar-/-* BMDMs were defective at phagocytosis of *Hc* in media supplemented with DBA2 (C5-deficient), but not C57BL/6 (C5-sufficient) serum (Fig. 3.4), suggesting that C5a in C57BL/6 serum acts redundantly with C3a to promote macrophage phagocytosis of *Hc*.

We then determined whether human serum (NHS) had a similar C3-dependent effect on BMDM recognition of *Hc* by supplementing media in phagocytosis assays with 5% untreated NHS, or serum immuno-depleted for C3 or C5 (C3d/C5d) (Fig. 3.4). Similar to what we observed with mouse-serum-supplemented media, we found that NHS-supplemented media stimulated BMDM phagocytosis of *Hc* in a heat-labile and C3-dependent manner (Fig. 3.4). Phagocytosis of *Hc* in with untreated NHS was also less dependent on C3aR (Fig. 3.4). Of note, we observed more phagocytosis of *Hc* in heat-treated and C3d NHS than in heat-treated NMS or NMS from *C3-/-* mice, which

may suggest that other components of human serum, such as IgG antibodies that opsonize *Hc*, help to drive phagocytosis in the absence of complement. We also found that, similar to our observations in mouse serum, C5 in human serum contributes to C3aR-independent recognition of *Hc*, as *C3ar-/-* BMDMs had a stronger phagocytosis defect in C5d NHS than in untreated NHS (Fig. 3.4).

To confirm that incubating mouse serum with *Hc* yeast would promote opsonization with C3, as previously described (134), and to demonstrate C3a release, we incubated *Hc* yeast with mouse serum, and measured C3a release into the supernatant by ELISA, and C3 deposition on the *Hc* surface using immunofluorescence confocal microscopy (Fig. 3.4). We found that incubating WT C57BL/6 and DBA2 serum with *Hc* increased C3a levels in the supernatant (Fig. 3.4), suggesting C3a release. We observed robust C3 staining of *Hc* upon incubation with WT serum, and no C3 deposition after incubation with C3-/- sera (Fig. 3.4). To inhibit the classical/lectin pathways, or all activation pathways, we added EGTA or EDTA, respectively, to the indicated reactions. We did not observe C3 deposition or C3a release when Mg++ was chelated with EDTA (Fig. 3.4). We also saw C3 deposition, although with lower efficiency and with a less uniform distribution around the yeast cell-wall, and lower levels of C3a release, in the presence of EGTA (Fig. 3.4). These results confirm that *Hc* can activate the alternative complement pathway, as previously suggested (79). Due to the increased efficiency and uniformity of C3 deposition on yeast and the increased C3a release found in the absence of EGTA, we propose that the classical or lectin pathways also contribute to C3 opsonization of *Hc* yeast. We did not find evidence of C3

deposition on the cell-surface following incubation of *Hc* with heat-treated FBS or BMDM conditioned media containing heat-treated FBS (Fig. 3.6). We also did not find that incubation of *Hc* with mouse serum affected *Hc* viability, as we observed no difference in CFU recovery following serum incubation (Fig. 3.4).

To demonstrate that complement opsonization by mouse or human serum promotes macrophage phagocytosis of *Hc* yeast, we infected BMDMs in serum-free media with *Hc* opsonized by WT or *C3-/-* mouse serum (Fig. 3.4), or with untreated or C3-depleted NHS (Fig. 3.4). We found that opsonization with WT mouse serum, but not *C3-/-* serum, is sufficient to promote phagocytosis of *Hc* in serum-free media in a C3aR-independent manner, suggesting direct recognition of opsonized yeasts by CR3 (Fig. 3.4). This activity was blocked by EDTA and moderately inhibited by EGTA, suggesting contribution of both the classical/lectin and alternative pathways to phagocytosis stimulation through opsonization (Fig. 3.6). We similarly found that NHS-opsonized *Hc* was robustly recognized by BMDMs in serum-free media, and that C3d NHS-opsonized *Hc* were taken up less efficiently (Fig. 3.4). Previous work has shown C3 opsonization of *Hc* by human serum (134). The increased phagocytosis of C3d NHS-opsonized *Hc* may be due to opsonization by *Hc*-reactive IgGs in human serum.

Active complement C3 can also be secreted by macrophages (64-66). We measured the release of C3 into culture supernatants by ELISA, and found that *Hc* infection stimulated modest macrophage secretion of C3 (Fig. 3.7). However, we did not observe a phagocytosis defect when we infected *C3-/-* BMDMs with *Hc* or zymosan in

the presence of FBS (Fig. 3.7), suggesting that macrophage-derived C3 is not playing a major role in macrophage phagocytosis of *Hc* in our assay.

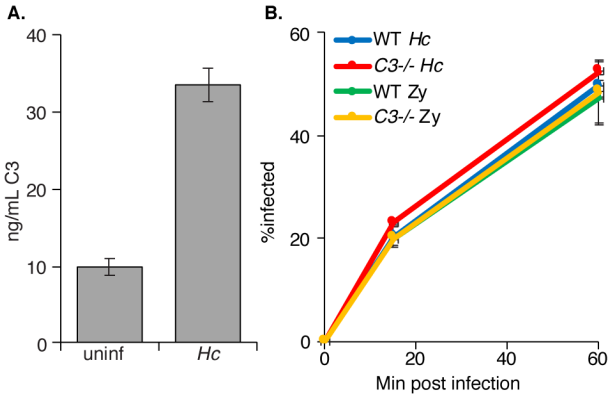

Figure 3.7: BMDM-derived C3 is not required for phagocytosis of *Hc* yeast or zymosan particles. A. BMDMs secrete C3 following infection with *Hc.* BMDMs were infected with *Hc* at an MOI2 for 24h, supernatants were harvested and C3 levels were quantified using a BD mouse C3 ELISA kit. B. *C3-/-* BMDMs are not defective in phagocytosis of *Hc* yeast or zymosan. WT and *C3-/-* BMDMs were infected with mCherry-expressing *Hc* or FITC-labelled zymosan (MOI2), and uptake over time was measured using flow-cytometry. Extracellular yeasts were excluded with calcofluor white staining.

C3aR localizes to the early Hc-containing phagosome

We next analyzed C3aR localization during macrophage phagocytosis of *Hc* and of latex beads, whose uptake does not depend on C3aR. These experiments were conducted in media supplemented with 20% FBS. Localization to the *Hc*-containing phagosome would implicate C3aR directly in fungal capture/ phagocytic cup formation, or as a passenger on the plasma membrane structures involved in *Hc* phagocytosis. Immunofluorescence confocal microscopy confirmed that C3aR is localized at the plasma membrane (Fig. 3.8). We observed C3aR localization to the *Hc*-containing phagosomes at 5- and 10-minutes post-infection, and with a lower frequency at 30 minutes post-infection (Fig. 3.9). Examples of C3aR-positive phagosomes are indicated by white arrows in the images. In contrast, we did not observe C3aR-positive bead-

containing phagosomes at the same frequency (Fig. 3.9), suggesting that C3aR localizes specifically to the *Hc*-containing phagosome, and not to latex bead-containing phagosomes. Selected insets (indicated by a white box in Figs Fig. 3.9) are enlarged to show phagosomal C3aR localization at 10 min post-infection (Fig. 3.9).

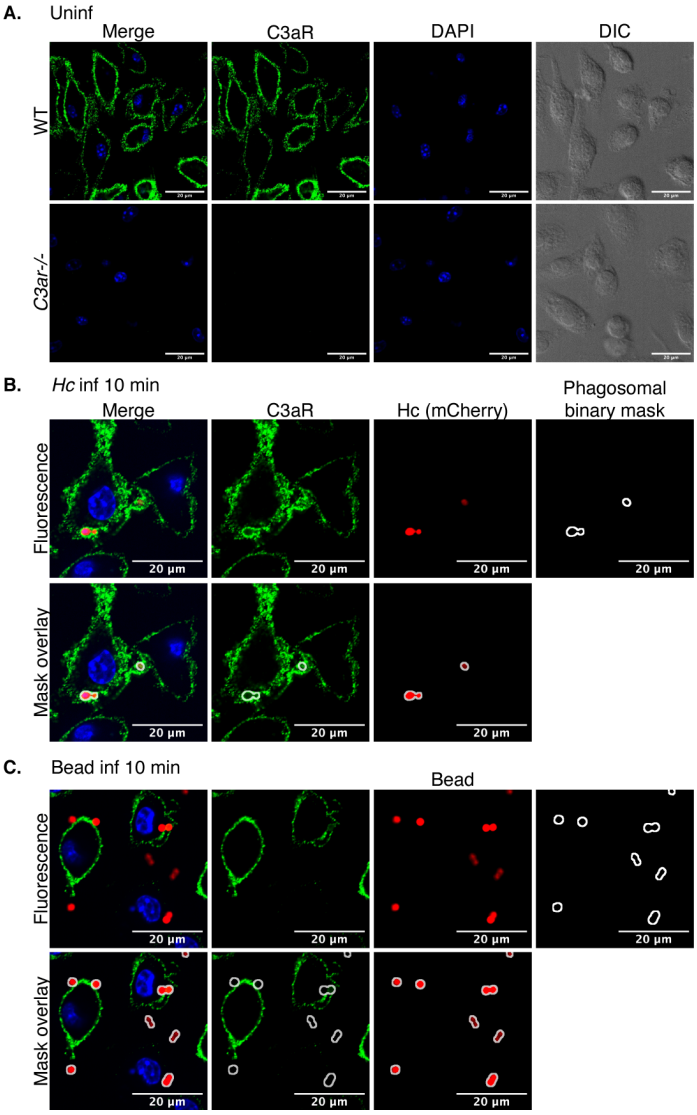

Figure 3.8: Analysis of C3aR localization in uninfected, *Hc*, and bead-infected BMDMs. A. Uninfected WT and *C3ar-/-* BMDMs were stained with a C3aR-specific antibody and imaged using confocal microscopy and optical sectioning. Representative slices of 2 biological replicates are shown. Scale bar = 20 µm. The antibody specifically detects C3aR, as staining was not observed in *C3ar-/-* BMDMs. C3aR exhibits punctate localization near the plasma membrane in WT BMDMs. B-C. Confocal images of *Hc* or bead-infected BMDMs stained with a C3aR-specific antibody are shown. Representative slices showing the region of interest mask derived from binary

operations on the B. *Hc* or C. bead fluorescent channel thresholding used to measure the phagosomal C3aR intensity of *Hc* and bead-containing phagosomes. The original and overlaid fluorescence images are shown.

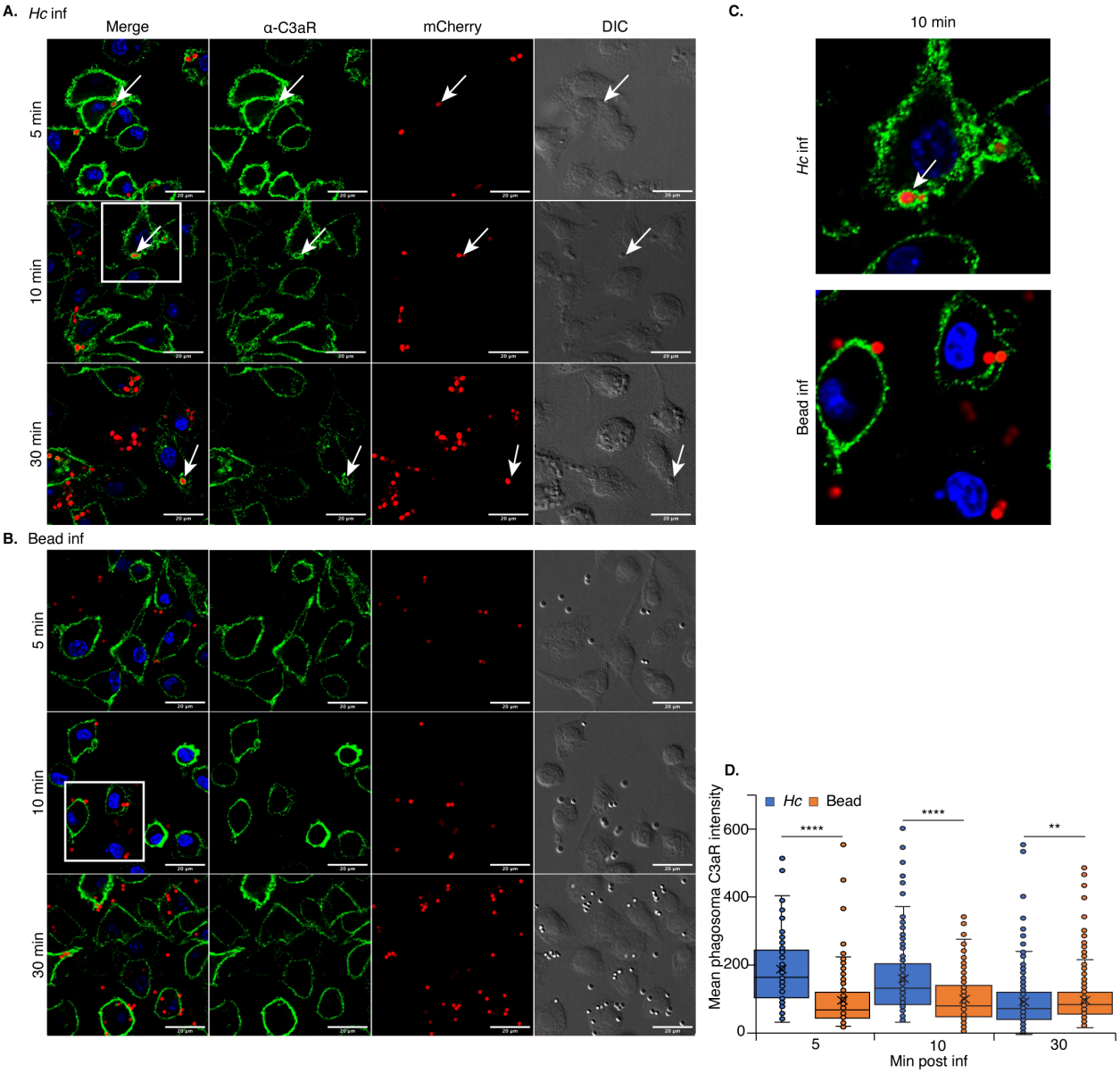

Figure 3.9: C3aR localizes to the early *Hc*-containing phagosome. C3aR localizes to *Hc*-containing phagosomes (A) to a greater extent than latex bead-containing phagosomes (B). BMDMs were infected with the indicated particles (MOI=5, n=2 biological replicates per time point). Cells were then stained with a C3aR-specific antibody and imaged by confocal microscopy. Representative images from a single slice are shown. Scale bar = 20 μm. C. Enlarged views of insets outlined in panels A and B by a white box. D. The mean fluorescence intensity of C3aR in the particle-containing phagosomes was quantified using ImageJ (N>91 phagosomes, **** $p<0.0001$, ** $p<0.01$ by two-tailed Wilcoxon rank-sum test).

To quantify C3aR localization to the *Hc* or bead-containing phagosome, we used imageJ to measure the mean intensity over background of the C3aR signal surrounding the *Hc* or bead particle. Our analysis revealed that *Hc*-containing phagosomes display significantly higher C3aR enrichment than bead-containing phagosomes at 5- and 10-minutes post-infection, but not at 30 minutes post-infection as the phagosomes mature (Fig. 3.9).

C3aR promotes the formation of actin-rich protrusions that facilitate capture of Hc yeast by local chemotaxis

Since C3a is a chemoattractant for macrophages (135), we investigated the role of macrophage migration in the C3aR-dependent capture of *Hc* yeast. Although macrophages did undergo chemotaxis towards *Hc* in trans-well migration assays, migration was not dependent on FBS or C3aR (Fig. 3.10). We also were not able to rescue the phagocytosis of *Hc* by *C3ar-/-* macrophages when the likelihood of *Hc*-macrophage interaction was increased by centrifugation of *Hc* onto the monolayer, or an extended pre-incubation on ice (Fig. 3.11). These experiments suggest that C3aR involvement in macrophage phagocytosis of *Hc* is not due to its role in facilitating long-range migration of macrophages towards yeast. However, these studies do not rule out a role for C3aR-dependent control of short-range chemotaxis in macrophage capture of *Hc* yeast.

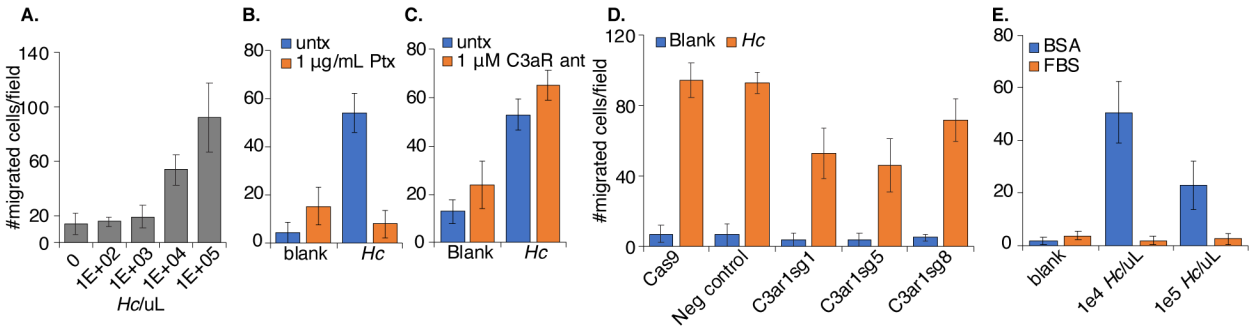

Figure 3.10: Macrophage-like cells undergo chemotaxis towards *Hc* yeast in a serum-independent manner, which is dependent on Gai, and partially dependent on C3aR. A. *Hc* stimulates chemotaxis of J774A.1 macrophage-like cells. *Hc* yeast were seeded into multiple-well plates at varying concentrations, and WT J774A.1 cells were seeded onto transwell permeable supports with 5 µm pores. Serum-free media supplemented with 0.25% BSA was used as the diluent in both the chamber and well unless otherwise indicated. After 3 h of migration, transwells were stained with crystal violet, and non-migratory cells were wiped off of the upper side of the transwell using a Q-tip. The number of migratory cells in each condition was quantified by microscopy (n=2 biogical replicates, 3 fields/biological replicate). B. Migration towards *Hc* is Gai-dependent. J774A.1 cells with or without pre-treatment with 1 μg/mL pertussis toxin (PTX) for 2 h were seeded into transwell permeable supports and migration towards 1e5 Hc/uL was quantified as described above. The number of migrating cells was quantified as described. C. The C3aR antagonist does not inhibit macrophage migration towards *Hc.* J774A.1 macrophages were treated with 1 μM SB290157, a C3aR antagonist, and migration towards *Hc* was assessed as described. D. C3aR-deficiency moderately impacts migration of J774A.1 cells towards *Hc.* Cas9-expressing J774A.1 macrophages transduced with non-targeting or C3aR-targeting sgRNAs were assessed for their ability to migrate towards *Hc* as described previously. E. *Hc*-dependent migration is abolished in the presence of FBS. The transwell migration assay was performed with media supplemented with BSA or 10% FBS to determine whether FBS affected the migration of macrophage-like cells towards *Hc* yeast.

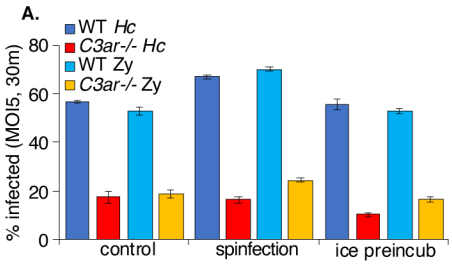

Figure 3.11: pre-incubation on ice or spinfection does not rescue phagocytosis of fungi in *C3ar-/-* BMDMs. A. BMDMs were infected with *Hc* or zymosan at an MOI=5 for 30 min. For the control condition, particles were added to the wells and allowed to settle onto the monolayer without intervention. For the 5 min spinfection, particles were added to the cells, and the plate was spun for 5 min at 550XG at RT before transferring to a 37°C, 5% CO_2 incubator. For the ice preincubation condition, BMDMs were pre-chilled

for 20 min on ice, and particles were allowed to settle onto the monolayer for 1 h on ice, then were transferred to a tissue culture incubator. Phagocytosis was measured as described previously (n=3 biological replicates).

To investigate this possibility, we performed live-cell confocal imaging of WT and *C3ar-/-* BMDMs during co-culture with mCherry-expressing *Hc* yeast in the presence of FBS (Fig 3.12). We observed evidence that BMDMs extend membrane ruffles in the direction of *Hc* yeast, and that the directional movement of these structures is dependent on C3aR (Fig 3.12). To better quantify and understand the role of F-actin in this process, We generated J774A.1 cells that express Lifeact-mEGFP, a probe that specifically labels F-actin (136), and performed live imaging of J774A.1 macrophages during co-culture with mCherry-labelled yeast in the presence of a C3aR antagonist (SB290157) or a vehicle control (Fig 3.12). These movies show macrophages extending actin-rich membrane protrusions in the direction of nearby *Hc* that promote rapid *Hc* capture and engulfment (example time series shown in Fig 3.12). In contrast, C3aR antagonist-treated macrophages showed much slower capture of *Hc* yeast, and failed to rapidly form such actin-rich, directed membrane protrusions (Fig 3.12). Membrane protrusions of macrophages that eventually captured *Hc* yeast were tracked and analyzed (137) (Fig. Fig 3.12). Treatment with the C3aR antagonist dramatically slowed capture of *Hc* yeast, as demonstrated by the lower phagocytosis rate and the lower mean velocity of the tracked protrusions (Fig Fig 3.12). Finally, the movement of the antagonist-treated membrane protrusions was less directional, as demonstrated by their lower outreach ratio (Fig 3.12).

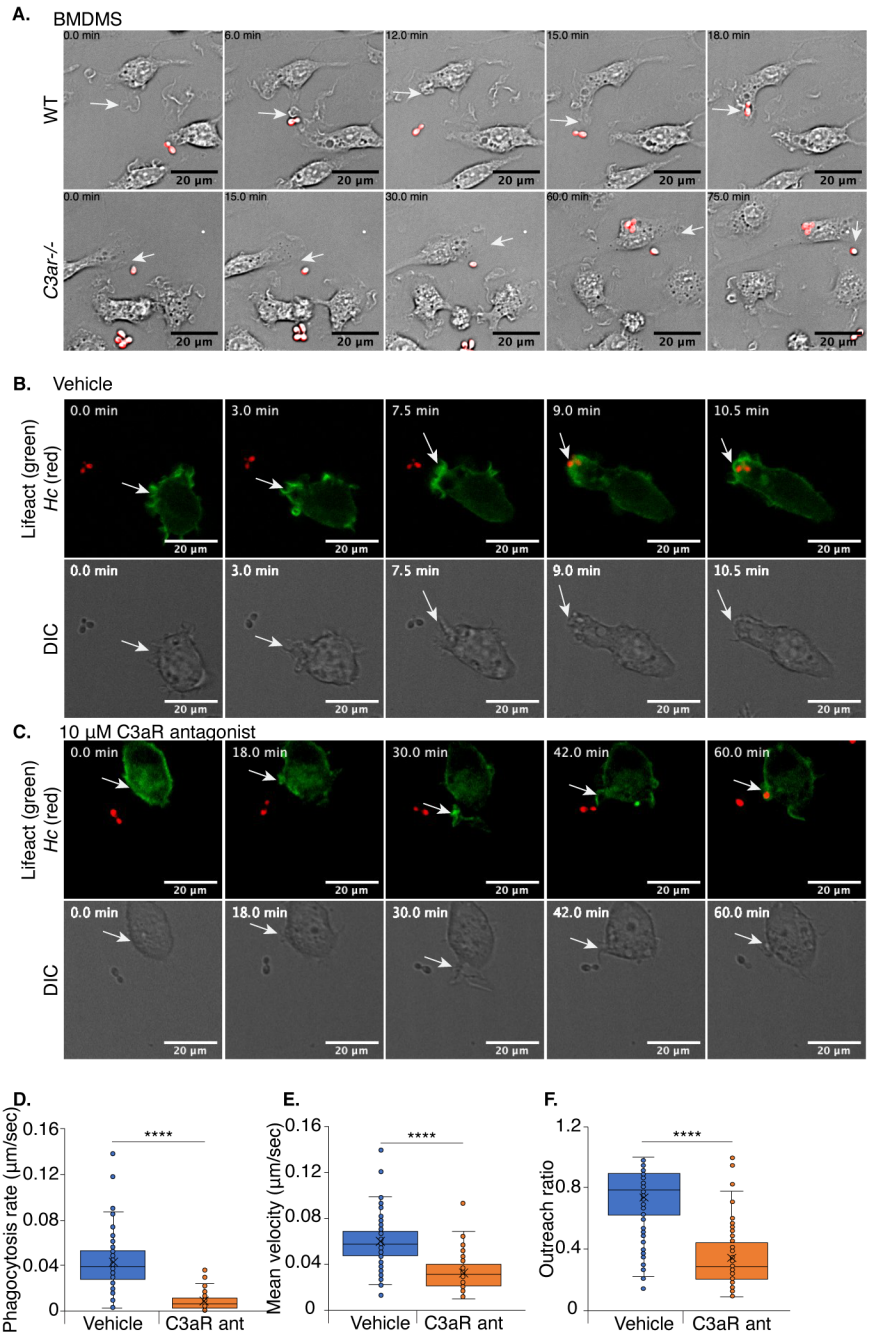

Figure 3.12: C3aR promotes the formation of actin-rich protrusions that facilitate capture of *Hc* yeast. A. WT and *C3ar-/-* BMDMs were co-cultured with m-Cherry-expressing *Hc* yeast, and the interactions were visualized using live-cell confocal microscopy in a temperature-and-CO_2 controlled chamber in media supplemented with FBS. Representative images from a time series showing WT BMDMs extending membrane ruffles (denoted by arrows) in the direction of *Hc* yeast, and the failure of *C3ar-/-* BMDMs to robustly exhibit this behavior. B-F. J774A.1 cells were engineered to express Lifeact-mEGFP to label F-actin, co-cultured with mCherry-expressing *Hc* yeast, and imaged using live-cell confocal microscopy. Cells were treated with a C3aR antagonist (10 µM SB290157) or a vehicle control. B. Representative images from a

confocal time series showing a macrophage extending an F-actin-rich protrusion towards an mCherry expressing *Hc* yeast, followed by phagocytosis and formation of an actin-rich phagosome. The corresponding DIC images are shown below. C. A similar time series of macrophages treated with SB290157 showing a failure to initiate formation of a membrane protrusion and much slower capture of *Hc* yeast. Scale bar = 20 μm. The movement of membrane structures that successfully caputured yeast were analyzed using MtrackJ to quantify the behaviors of these structures (D-F) (n=2 biological replicates, >50 tracks per replicate), including the phagocytosis rate, quantified as the time required for the macrophage to successfully engulf the yeast divided by the distance of the yeast to the macrophage at the start of the series (D), the mean velocity of the membrane structure closest to the yeast (E), and the outreach ratio quantified as the max displacement of the track divided by the length of the track (F) (**** $p<0.0001$ by two-tailed Wilcoxon rank sum test). These metrics demonstrate that macrophages treated with the C3aR antagonist are defective at the extension of membrane protrusions in the direction of *Hc* yeast that facilitate phagocytosis.

Live imaging experiments showed that C3aR facilitates the directional movement of actin-rich membrane protrusions towards *Hc* yeast that facilitate rapid phagocytosis (Fig. 3.12). This behavior likely requires a C3a gradient that diffuses away from the *Hc* yeast following complement cleavage at the fungal surface, as has been proposed for anaphylatoxin-mediated microbial capture (138). Consistent with this idea, the addition of recombinant C3a to BMDMs in the absence of a gradient was not sufficient to stimulate macrophage phagocytosis of *Hc* in serum-free media (Fig. 3.13). However, in addition to promoting local chemotaxis, C3a may also contribute to the local activation of phagocytosis receptors such as phagocytic integrins. We pre-treated BMDMS with phorbol 12-myristate 13-acetate (PMA), a PKC activator, and assessed phagocytosis of *Hc* by WT and *C3ar-/-* BMDMs in media with and without FBS supplementation (Fig. 3.13). Given that C3a is rapidly converted into its inactive form, C3adesarg, by host proteases (61), rC3a at the concentrations used might also not provide a strong enough sustained signal to promote macrophage activation and phagocytosis when added to

the cultures. In contrast, PMA treatment partially rescued BMDM phagocytosis of *Hc* in serum-free media and in *C3ar-/-* BMDMs in FBS (Fig. 3.13). We also found that thioglycollate-ellicited peritoneal macrophages (thio-Pmacs), which have been exposed to more activation signals than BMDMs, were better able to take up un-opsonized *Hc* in serum-free media, as previously reported (43), compared to BMDMs (Fig. 3.13). FBS did, however, increase the rate of *Hc* uptake by thio-Pmacs in a C3aR-dependent manner. These results suggest that using stimulated BMDMs or partially activated resident macrophages can rescue phagocytosis of *Hc* in serum-free media, suggesting that serum and C3aR-signaling influence the activity of other phagocytic receptors.

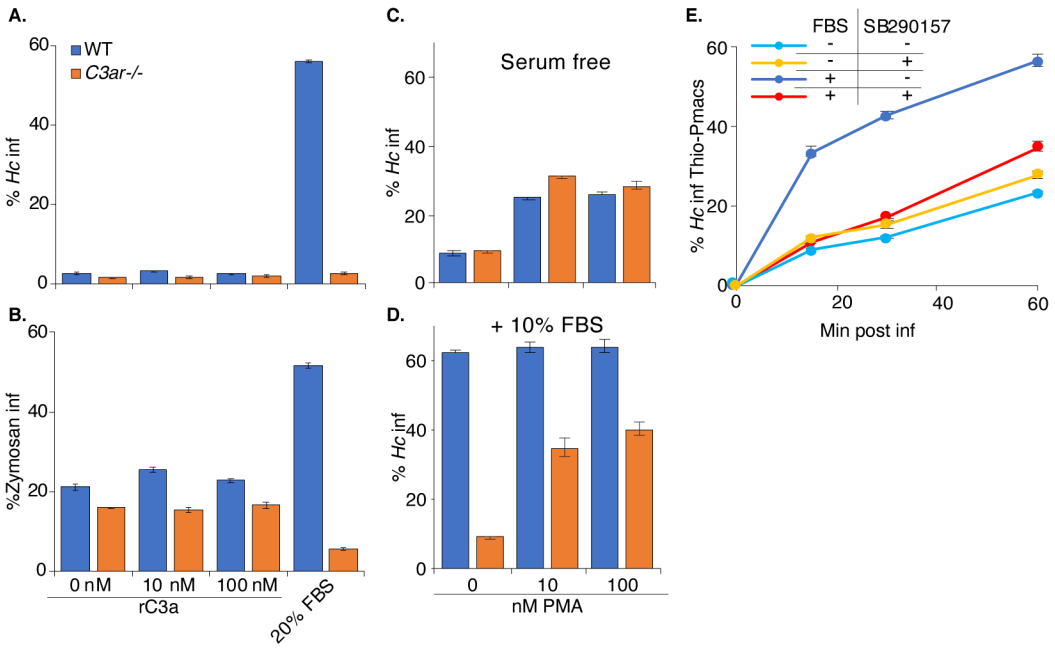

Figure 3.13: The macrophage activation state, but not recombinant C3a addition, determines the role of serum and C3aR in *Hc* uptake. BMDMs were pre-treated in serum-free or FBS-supplemented media with varying concentrations of recombinant mouse C3a (R&D systems) for 1 h, then infected with A. *Hc* or B. Zymosan at an MOI of 5 for 30 min. Phagocytosis was assessed by flow cytometry (n=2 biological replicates). C-D. BMDMs In serum-free (C) or FBS-supplemented (D) media were pre-treated with PMA for 2h and infected with *Hc* (MOI5, 60 min). Phagocytosis was measured by flow cytometry (n=3 biological replicates). E. Thioglycollate-ellicited peritoneal macrophages in serum-free or FBS-supplemented media were treated for 5 min with a C3aR

antagonist (SB290157, 10 μM) and infected with *Hc*. Phagocytosis was assessed by flow cytometry (n=3 biological replicates).

Chapter 4: The contribution of C3aR to the macrophage cytokine response to *Hc*, and the outcome of *Hc* infection in a mouse model

Introduction

Complement components can play pro or anti-inflammatory roles in innate immune regulation. Moreover, the combination of receptors engaged during phagocytosis of microbes are known to undergo crosstalk that modulates the cytokine response (139). *In vitro,* C3aR signaling has been demonstrated to either promote or dampen the production of inflammatory cytokines by macrophages depending on the cell-type or signal used (74). Whether C3aR plays a role in the macrophage cytokine response to fungi is unclear, though C5a has been shown to promote the cytokine response to *Candida albicans* (88).

In vivo, complement is protective against opportunistic pathogens, and facilitates clearance by phagocytes (84). Whether complement is important for control of endemic fungi is unknown. Excessive complement activation can also be damaging (77). C3aR plays a complicated role in bacterial and viral infection, where in some cases it can protect against infection (125), and in others exacerbate infection-induced damage (140) or interfere with microbial control (124). The role of C3aR in host defense against fungal infection is unknown, and may vary depending on the fungal replicative niche. Here, we investigate whether C3aR contributes to the cytokine response to *Hc* infection by macrophages, and whether C3 and C3aR play a role in mouse susceptibility to *Hc* infection.

C3aR plays opposing roles in the macrophage cytokine response to Hc and zymosan

Because C3aR has been implicated in modulating the cytokine response to microbial infection, we measured *Hc* and zymosan-induced cytokine release in *C3ar-/-* BMDMs or in C3aR-antagonist-treated thioglycollate-ellicited peritoneal macrophages (Thio-Pmacs) in the presence of FBS (Fig. 4.1). We observed a moderate decrease in TNFα secretion in *C3ar-/-* BMDMs infected with *Hc* at 2h post-infection, but this effect was diminished at 6h post-infection (Fig. 4.1). We were not able to detect IL-1β or IL-6 secretion in *Hc*-infected BMDMs. In Thio-Pmacs, we found that inhibition of C3aR did not affect TNFα or IL-1β secretion in response to *Hc*, but slightly inhibited IL-6 secretion at 2h, but not 6h post-infection (Fig. 4.1). Surprisingly, we observed C3aR ablation or treatment with the C3aR antagonist led to increased cytokine secretion in response to zymosan infection (Fig. 4.1). This may be due to weak agonist activity of the C3aR antagonist that manifests after extended incubation (141), or due to a role for C3aR in inhibiting zymosan-induced pro-inflammatory signaling following prolonged exposure, as has been documented for bacteria (125). We found that C3aR may play a minor role in increasing some pro-inflammatory cytokine production at early time-points following *Hc* infection, and that this depends on the macrophage cell-type used. It is unclear whether the effect on cytokine release is a consequence of altered phagocytosis kinetics, or due to a signaling role for C3aR.

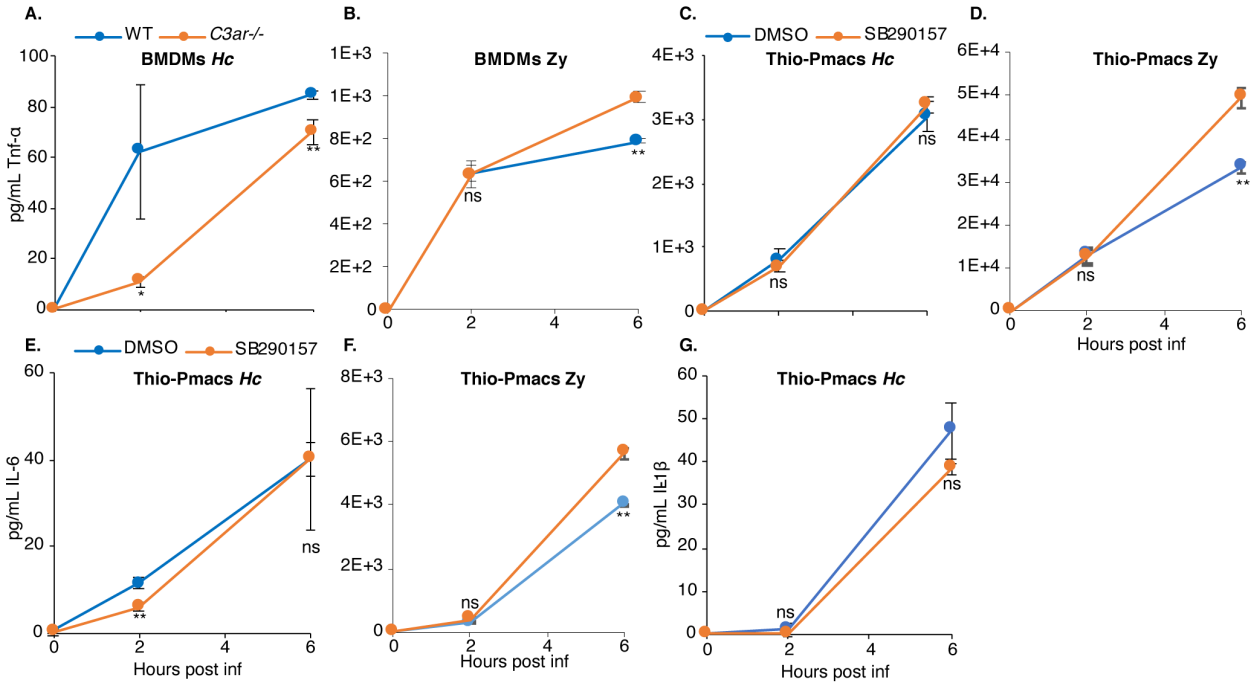

Figure 4.1: **C3aR-deficient macrophages show a minor delay in *Hc*-induced cytokine release, and increased zymosan-induced cytokine release.** A-B. WT and *C3ar-/-* BMDMs were infected with A. *Hc* or B. Zymosan (MOI10), and TNFα levels in macrophage supernatants were measured using the BD Cytometric Bead Array (CBA) kit (n=3 biological replicates). C-G. Thioglycollate-ellicited peritoneal macrophages were treated with the C3aR antagonist (SB290157, 10 μM) and infected with *Hc* (C, E, G) or zymosan (D, F) (MOI10). TNFα (C-D), IL-6 (E-F), and IL-1β (G) levels in culture supernatants were measured by CBA.

C3 and C3aR-deficient mice are not differentially susceptible to Hc infection

To determine whether C3aR influences disease progression in a mouse model of histoplasmosis, we compared the susceptibility of WT and *C3ar-/-* mice to a lethal and sub-lethal dose of *Hc* yeast administered intranasally (Fig. 4.2). C3aR is not required for mouse susceptibility to infection with *Hc* yeast. C3aR may moderately contribute to anti-histoplasma defense, as the *C3ar-/-* mice succumbed to infection faster than the WT mice at the lower lethal dose tested. The presence of other signals *in vivo*, such as C5aR, that promote macrophage phagocytosis of *Hc* may still allow *Hc* to access its replicative niche. In addition, C3aR is expressed on many other cell-types (71), and

regulates a wide variety of cellular functions (76), including T-cell homeostasis and differentiation (75). Thus, its role in non-myeloid cells may be important for host defense against fungi. Mice with C3aR specifically depleted in myeloid cells would clarify its role *in vivo*.

We also tested whether *C3-/-* mice were more susceptible to a sub-lethal dose of *Hc*, due to the increased susceptibility of these mice to opportunistic fungal infections. We did not find evidence that C3 is required for host resistance to *Hc* infection (Fig. 4.2), which may reflect the intracellular lifestyle of *Hc* and non-complement-mediated recognition of *Hc* by innate immune cells.

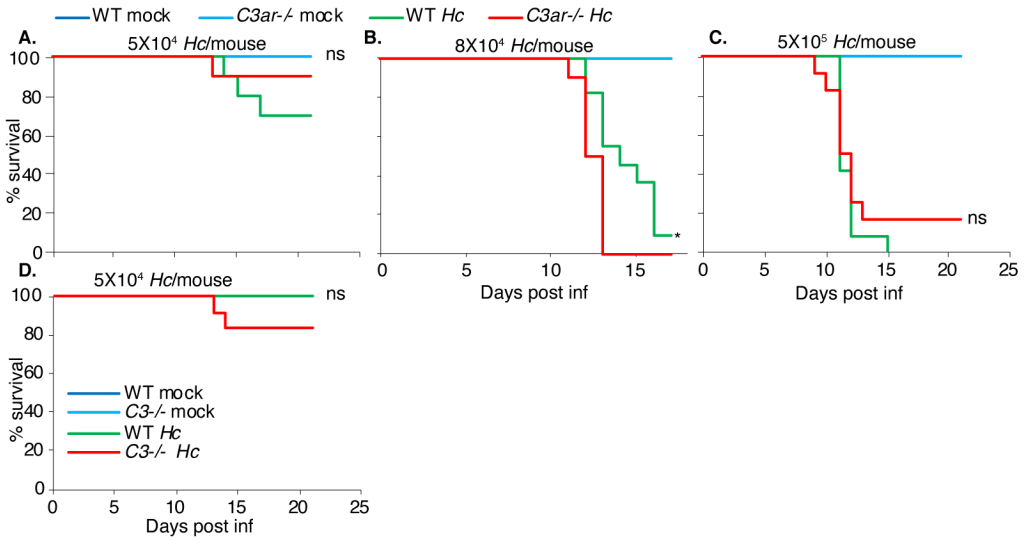

Figure 4.2: C3 and C3aR deficiency do not dramatically alter mouse susceptibility to *Hc* infection. A-C *C3ar-/-* mice (n≥10) and age-matched WT C57BL/6 mice (n≥10) were infected intranasally with varying doses of *Hc* yeast to initiate either a sub-lethal (A) or lethal (B-C) infection. D. *C3-/-* mice and age-matched WT mice were infected intranasally with a sub-lethal dose of *Hc* yeast. Susceptibility is illustrated by a Kaplan-Meier survival curve. ns = not significant, *$p < 0.05$ by logrank test.

Chapter 5: Discussion

We report a large-scale CRISPR-Cas9 screen conducted in macrophage-like cells challenged with *Hc* yeast. 361 genes emerged as high-confidence modifiers of macrophage susceptibility to *Hc*-mediated killing, vastly expanding our knowledge of the gene networks that underpin macrophage interaction with this important pathogen. Validation of top hits revealed an under-appreciated role for GPCR signaling through C3aR in serum-dependent macrophage phagocytosis of fungi. These results are particularly intriguing for *Histoplasma*, which is an intracellular fungal pathogen that thrives within the macrophage phagosome. Therefore, elucidating the molecular events that govern *Histoplasma* phagocytosis is particularly important for understanding *Hc* pathogenesis. Given that C3aR strongly enhances the efficiency of *Hc* phagocytosis, it may be a key host factor that promotes the intracellular lifestyle of this organism.

It was previously established that macrophage phagocytosis of *Hc* is not dependent on β-glucan recognition by Dectin-1 (43), and that *Hc* utilizes a number of mechanisms to minimize exposure of β-glucan on the cell surface (103, 104). In contrast, CR3 has been previously implicated in non-opsonic uptake of *Hc* (42, 43). Our work uncovers the important role of C3aR as a pattern recognition receptor for *Hc* and other fungi, potentially collaborating with CR3 to facilitate uptake of pathogenic yeasts (described in Fig. 5.1). We also discovered that C3aR-dependent phagocytosis requires serum, and that only mouse serum that was replete with C3 could stimulate phagocytosis, suggesting that fungal-reactive C3 releases a gradient of C3a emanating from the fungal surface that might be critical for the C3aR-dependent local chemotaxis

and stimulation of phagocytosis, as discussed below. Since *Hc* cannot engage PRRs such as Dectin-1, there is little uptake of *Hc* in the absence of serum. In contrast, the serum-independent, C3aR-independent phagocytosis of zymosan may be driven by Dectin-1. Given that *Hc* is introduced to the host via inhalation, and since complement activity is present in the bronchoalveolar fluid (67, 68), innate immune recognition of *Hc* likely occurs in the context of complement activation *in vivo*. Although we did not find major differences in the susceptibility of *C3ar-/-* or *C3-/-* mice to *Hc* infection, this does not rule out a role for complement and C3aR *in vivo*. Other receptors or signals in the host not recapitulated in our *ex vivo* models may drive macrophage phagocytosis of *Hc* and immune defense in the absence of complement or C3aR, allowing *Hc* access to its intracellular niche. Clarification of the role of complement in macrophage phagocytosis and pathogenesis of *Hc in vivo* will require additional study.

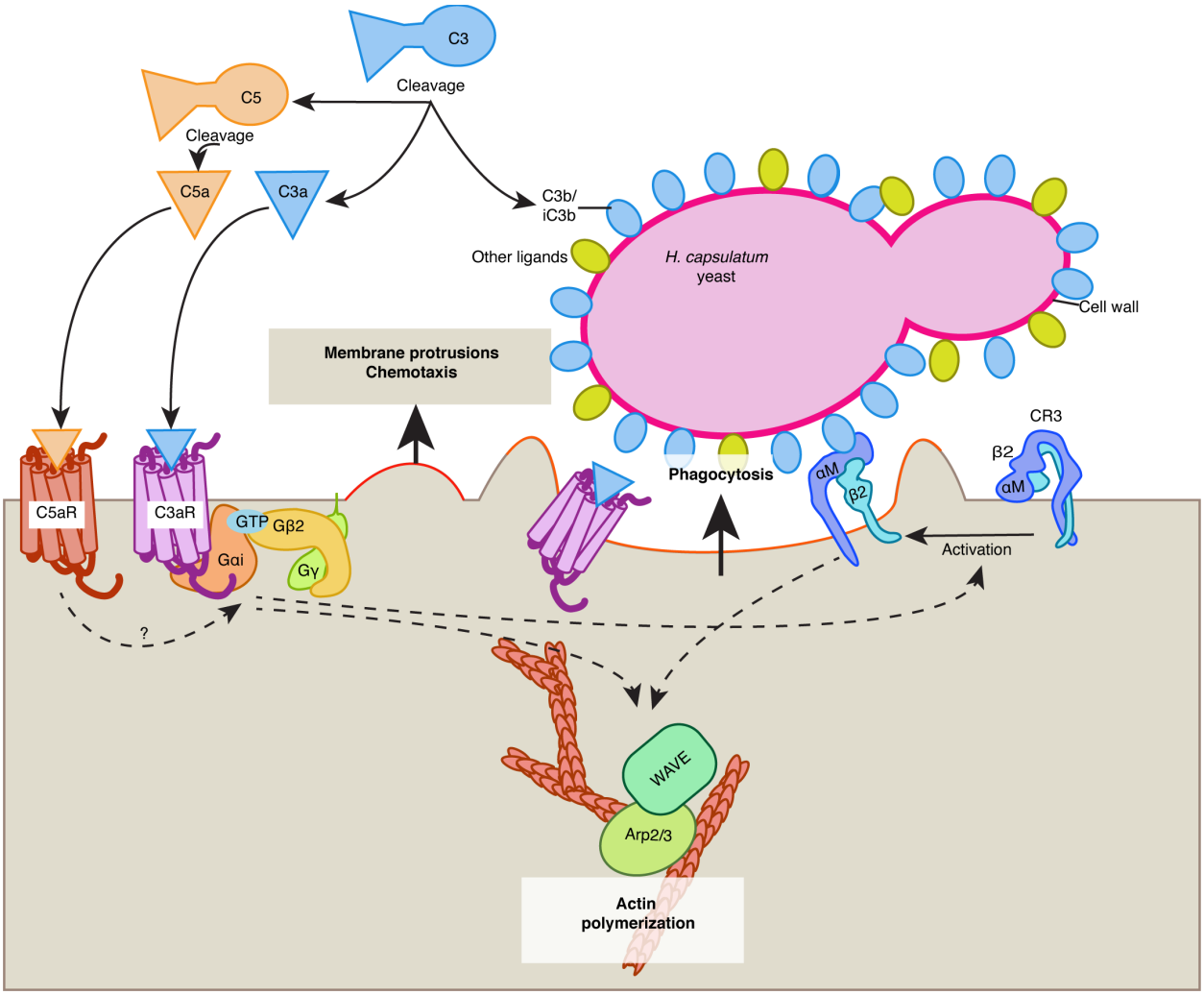

Figure 5.1: Model for the role of complement and C3aR in macrophage recognition of *Hc* yeast. We propose the following model for the role of complement and C3aR in macrophage recognition of *Hc*. C3, derived from serum, reacts with the *Hc* cell-wall, leading to C3b/iC3b deposition, and release of C3a, which diffuses away from the yeast surface leading to a concentration gradient of C3a emanating from the yeast cell-wall. C3a activates C3aR, which signals through Gαi and Gβ2 to promote the formation and directional movement of actin-rich membrane protrusions, and possibly to promote activation or increased motility of the integrin receptor CR3. Active CR3 can then directly recognize C3b/iC3b or other features of the *Hc* cell-wall. C3aR and/or CR3 activation then coordinates actin polymerization and phagocytic cup formation by regulating the activity of actin polymerization regulators Arp2/3 and SCAR/WAVE. In the presence of serum containing C5, the C5 convertases can similarly catalyze the cleavage of C5 at the fungal surface, leading to release of C5a and activation of C5aR, which can also drive local chemotaxis and activation of phagocytic integrins to promote phagocytosis.

The vast majority of genes identified in the screen were resistance-promoting hits, which may reflect limitations in the pooled screening approach, or the efficiency at which *Hc* evades macrophage defenses (in other words, it is challenging to increase macrophage sensitivity to *Hc*). Within these hits, we identified genes with previously described involvement in phagocytosis and *Hc* recognition, which validates our approach and is consistent with the requirement for *Hc* internalization to trigger the process of macrophage lysis. Our screen also revealed a role for GPCR signaling in *Hc*-host interactions. In addition to *C3ar*, the highest scoring protective hits included a set of genes that regulate signaling and receptor trafficking following GPCR engagement (120, 121). We validated that several of these genes, including *C3ar1, Gnb2,* and *Arrb2,* facilitate macrophage phagocytosis of *Hc.* While G-protein coupled receptor (GPCR) signaling is traditionally thought to play a role in chemotaxis rather than phagocytosis (50, 55), several studies have implicated G-protein activity directly in cytoskeleton coordination during phagocytosis (131, 142, 143). Both chemotaxis and phagocytosis depend on precise regulation of the actin cytoskeleton, and signaling often converges on the same signaling cytoskeleton remodeling machinery (55, 57). Additionally, previous studies have shown that the mobility and activity of phagocytosis receptors is increased at the leading edge of a cell (28, 144), and that active probing of the local environment by macrophages is critical for efficient binding of targets (58), suggesting strong coordination between chemotaxis and phagocytosis. We also identified the ER membrane complex, which facilitates the folding of transmembrane proteins with multiple membrane-spanning regions (118, 119). We showed that *Emc1* promotes

macrophage phagocytosis of *Hc*, and is required for surface expression of C3aR, but not CR3 subunits. Thus, we propose that the EMC indirectly participates in phagocytosis due to its role in folding receptors such as C3aR.

Many other genes and complexes identified may play important roles in *Hc* interaction with macrophages, and require further study to uncover the nature of their involvement. Systematic identification of genes relevant to different stages of *Hc* infection using cell-sorting based batch-retest screening, which has been used successfully to refine the contribution of screen hits to a particular process (31, 109), would help to clarify the role of these genes in macrophage phagocytosis of *Hc*, as well as intracellular replication and lysis. Such complexes include the ragulator complex and the chaperonin containing t-complex (CCT), and the retromer complex. The ragulator complex activates mTORC1 upon nutrient deprivation, which regulates autophagic flux that aids in defense against intracellular pathogens (117). This complex also has been found in screens for phagocytosis regulators (31), and has been shown to modulate phagocytic flux in microglia (145). The CCT is a molecular chaperone that promotes the folding and assembly of cytosolic proteins including G-protein complexes (146, 147), suggesting that this complex may indirectly affect phagocytosis of *Hc* due to involvement in G-protein activity. The retromer complex facilitates retrograde transport of endosomal cargo (148). Bacterial pathogens often hijack retrograde trafficking to establish an intracellular niche (149), and *Hc* may have evolved a similar strategy. On the other hand, this complex is important for recycling cell-surface receptors (53), and

its disruption may also interfere with the expression or activity of cell-surface receptors that promote recognition of *Hc*.

We identified several genes (*Alg3, Alg12, Dpm2, Dolpp1, Stt3b, Mogs, Mgat1*) that facilitate N-glycan biosynthesis (150), which likely play an indirect role in *Hc* interaction with macrophages through stabilization of cell-surface receptors or other transmembrane proteins. Cytosol-to-golgi sugar transporters identified in the screen (*Slc35a1, Slc35a2, Slc35b2*) are required for substrate glycosylation in the ER/golgi (151). It is also possible that *Hc* hijacks these pathways to promote nutrient acquisition and intracellular replication within the phagosome. Mitochondrial transporters (*Slc25a3, Slc25a32, Slc25a51, Slc25a19*) promote the import of metabolites that are critical for mitochondrial respiration and redox balance (152), and may affect nutrient acquisition by *Hc*, or regulate *Hc*-induced cellular stress and apoptosis. We also identified ubiquitin ligases such as *Ubr5* and *Trip12*, which regulate histone ubiquitylation upon DNA damage (153). *Ubr5* has also been shown to down-regulate TLR signaling (154). Validation in macrophage-like cells demonstrates that *Ubr5* is required for *Hc*-induced lysis, but not macrophage phagocytosis of *Hc*, suggesting that Ubr5 promotes intracellular replication of *Hc* or macrophage cell-death. Further study is needed to uncover the role of Ubr5 in the pathogenesis of *Hc*.

Of note, we did not uncover regulators of the integrated stress response (ISR), such as transcription factor *Chop*, and pseudokinase *Trib3*, as resistance-promoting hits in the screen. We were expecting to find these genes due to previously documented role of Trib3 and Chop in *Hc*-induced lysis of MCSF-differentiated BMDMs (98, 100),

though BMDMs from *Trib3-/-* and *Chop-/-* mice are only partially resistant to *Hc*-mediated lysis, suggesting a contribution of other cell-death promoting pathways in BMDMs. In addition, the contribution of these pathways to cell-death may be cell-type specific, as lysis of GM-CSF-differentiated BMDMs by *Hc* is dependent on TNF receptor (155). Our screen was conducted using J774A.1 cells, which are macrophage-like but differ from BMDMs in their responses to other intracellular pathogens (122). Thus, the ISR may not be as critical for *Hc*-mediated lysis of J774A.1 cells. In support of this hypothesis, we have observed that these cells show less robust transcriptional induction of both *Trib3* and *Chop* compared to BMDMs during infection with *Hc* (98). While lysis of both BMDMs and J774A.1 cells by *Hc* is dependent on the secreted virulence factor Cbp1 (100), the exact mechanisms by which Cbp1 triggers macrophage cell-death is unknown, and may depend on the cell-type. Finally differences in the MOI, *Hc* strain, or other experimental details may alter this pathway. Several important caveats of our screen are suggested by the failure to uncover Trib3 and Chop. These include the use of a cell-line that does not fully reproduce aspects of macrophage biology, and the less physiologically relevant use of a high MOI infection with an uracil auxotroph strain of *Hc* in the presence of exogenous uracil. In addition, despite our attempts to maintain high coverage (>1000X) of the libraries during the screening process, we likely introduced bottlenecks due to batch-to-batch variation in doubling time, or stochasticity in *Hc* lysis kinetics during screening, as exhibited by the moderate degree of correlation between screen replicates. Batch re-testing of top hits in a single pool at higher coverage, which has been successfully employed to refine genome-wide pooled screens (31, 109), will

improve our confidence in the identification of true modifiers of macrophage susceptibility to *Hc* infection

Since the identification of C3aR as a phagocytosis-promoting receptor was intriguing, we further characterized its role in macrophage phagocytosis of *Hc* and other targets. While we found that C3aR was required for phagocytosis of several fungal species, C3aR did not play a general role in phagocytosis, as *C3ar-/-* macrophages were not defective in uptake of *E. coli* or latex beads. Previous studies have demonstrated that C3aR promotes phagocytosis of damaged neurons (140, 156), myelin particles (128) and protein aggregates (126). C3aR has also been implicated in macrophage phagocytosis of uropathogenic *E. coli* (125), but not *Pseudomonas aeruginosa* (124). Further study is needed to determine the shared characteristics of particles that require C3aR for optimal phagocytosis, such as particle size, reactivity with complement, or other biochemical properties. Nonetheless, the identification of C3aR as an important phagocytosis-promoting receptor for fungi implies that it may contribute to host defense against fungal pathogens. Such study will be essential to determining the therapeutic benefit of targeting complement or C3aR in the treatment of invasive fungal infections.

We found that heat-treated fetal bovine serum (FBS) added to the macrophage media promoted fungal phagocytosis in C3ar-dependent but opsonization-independent manner. This suggests that FBS promotes phagocytosis predominantly by generating C3a that activates C3aR, although the mechanism by which FBS-derived C3a might play a role independent of C3b opsonization is unclear. One explanation for this

discrepancy is that opsonization of *Hc* in FBS does occur, but bovine C3b/iC3b is more rapidly degraded or is not recognized efficiently by mouse complement receptors. Other possibilities, in the absence of opsonization, include non-canonical activation of FBS-derived C3 that leads to C3a release but fails to deposit C3b at the *Hc* surface. It is also possible that C3a, or another ligand present in FBS, is passively absorbed by the fungal surface, and leads to C3aR-dependent phagocytosis. C3a has been previously shown to bind the cell-wall of *Candida albicans* (73).

We also showed that mouse and human serum was able to stimulate macrophage phagocytosis of *Hc* in a C3-dependent manner, and that C3-dependent opsonization of *Hc* promoted macrophage phagocytosis, consistent with studies showing a role for C3b/C3bi in recognition of fungal pathogens (80). Surprisingly, the ability of serum from C57BL/6 mice and normal human serum to promote macrophage phagocytosis of *Hc* was not strongly dependent on C3aR. We demonstrated that C5a-C5aR signaling compensated for C3aR deficiency, since macrophage phagocytosis of *Hc* in the presence of C5 immuno-depleted human serum, or serum from C5-deficient DBA2 mice was more strongly dependent on C3aR. This is consistent with previous work implicating C5a and C5aR in innate immune recognition and phagocytosis of fungi by neutrophils (62, 88, 157). However, we have yet to experimentally confirm the role of C5aR in *Hc* recognition. The strong dependency of FBS-mediated phagocytosis on C3aR also suggests that C5 levels or activity in FBS are lower than in mouse or human serum. This may be due to species-specific differences in either serum composition, cross-reactivity with receptors expressed on mouse macrophages, or due to changes in

serum composition that occur after birth. Preliminary evidence suggests that macrophage phagocytosis of *Hc* in adult bovine serum is less dependent on C3aR compared to phagocytosis in FBS, suggesting the latter possibility. Additionally, complement activity can have direct microbicidal effects. However, the thick fungal cell-wall is thought to prevent MAC formation, and pathogens including *Candida albicans* have evolved strategies to interfere with complement activity (69, 82). We did not observe attenuation of *Hc* viability following incubation with mouse serum, though whether *Hc* can directly interfere with the microbicidal functions of complement will require more study.

To investigate the role of C3aR in macrophage phagocytosis of *Hc,* we demonstrated that C3aR localizes to the *Hc* containing phagosome at early time-points during infection. Localization of C3aR to the phagosome suggests direct involvement of C3aR in *Hc* recognition or cytoskeleton remodeling. Alternatively, C3aR might not directly participate in phagosome formation, but reside at the plasma membrane sites that participate in *Hc* phagocytosis.

Live imaging of actin dynamics in macrophages during *Hc* infection revealed that C3aR promotes the directional movement of actin-rich membrane protrusions that aid in the capture of *Hc* yeast. This is consistent with the ability of C3a to promote chemotaxis of innate immune cells, including macrophages (72), and the role of G-protein signaling in activating cytoskeleton remodeling at the leading edge and the phagocytic cup (131, 142, 143). We did not find strong evidence that C3aR promotes chemotaxis towards *Hc* yeast in trans-well assays, and we were not able to restore phagocytosis in *C3ar-/-*

macrophages by forcing contact between macrophages and *Hc,* suggesting that C3aR participates in short-distance hunting rather than long-distance migration during fungal phagocytosis, as has been proposed for anaphylatoxin-mediated phagocytosis (138). Of note, we did find that, in the absence of serum, J774A.1 cells migrated towards *Hc* yeast in trans-well assays in a pertussis-toxin-sensitive manner, suggesting the intriguing possibility that a molecule generated by *Hc* can promote macrophage chemotaxis, as has been described for *Candida albicans* (60).

C3aR may also promote optimal phagocytosis by spatially coordinating receptor mobility (144) or activation (121) at the leading edge. A role for receptor activation is supported by the partial rescue of *Hc* phagocytosis in the absence of C3aR or in serum-free media by activating macrophages with PMA or using thioglycollate-ellicited peritoneal macrophages. We believe that, as previously suggested (138), a gradient of C3a diffusing away from the *Hc* surface is important for this activity, as the uniform distribution of recombinant C3a alone was not sufficient to stimulate macrophage phagocytosis in the absence of serum. C3aR likely cooperates with receptors, such as CR3, that can directly recognize ligands on the *Hc* surface, such as C3b/iC3b, or other ligands such as Hsp60 that may require robust inside-out activation of phagocytic integrins for efficient recognition. More investigation is needed to untangle the precise mechanism by which the C3-C3a-C3aR pathway contributes to *Hc* recognition, especially to determine whether it promotes efficient binding and internalization independent of its role in local chemotaxis.

C3a-C3aR activity has been shown to both amplify and inhibit pro-inflammatory responses to other agents (74), and C5aR enhances the cytokine response to *Candida albicans* (158). We found that C3aR plays a minor role only at early time points macrophage cytokine response to *Hc* in the presence of FBS. This may be due a signaling role for C3aR, or simply due to delayed phagocytosis/capture, which would slow the interaction between fungal PAMPS, and other macrophage receptors, especially receptors that are active in phagosomes. FBS-derived C3a might also be less potent at modulating pro-inflammatory signaling via mouse C3aR, and repeating these experiments in the presence of C5-deficient autologous serum or C3a peptide would clarify the role of C3aR the macrophage inflammatory response to *Hc*. It is also worth noting that *Hc* does not initiate a strong pro-inflammatory cytokine response in resting macrophages, possibly limiting our ability to uncover a contribution of C3aR to this response. On the other hand, C3aR-deficient macrophages secreted higher levels of pro-inflammatory cytokines when stimulated with zymosan for 6 h than control macrophages, suggesting that C3aR dampens the inflammatory response to zymosan. The difference in PAMP exposure between *Hc* and zymosan may account for the differences in the role of C3aR, as *Hc* is much less immune stimulatory than zymosan.

Complement and C3aR involvement has been reported in the pathogenesis of various inflammatory diseases, such as asthma (129, 159), neurodegeneration (127, 156, 160), and sepsis (111), where uncontrolled complement activity exacerbates host damage. On the other hand, complement and C3aR can be important for defense against certain bacterial pathogens (69, 125), and C3 is vital for host defense against

opportunistic fungal pathogens (84, 85, 157, 161). Surprisingly, we did not find that *C3-/-* mice were more susceptible to *Hc* infection, which was unexpected given importance of complement in resistance to other fungi. We also do not know whether *C3-/-* mice would be more resistant to a lethal challenge with Hc, nor whether *C3-/-* mice have a defect in fungal burden control or in mounting an effective immune response against *Hc*. While we also do not find that *C3ar-/-* mice show dramatically altered susceptibility to *Hc* infection, more investigation is needed to clarify whether C3aR affects fungal recognition, intracellular replication of *Hc,* host susceptibility to other fungal pathogens, or modulates the immune response to fungi *in vivo*. Additional study is also needed to understand the role of complement in innate immune recognition of *Hc in vivo.* One key difference between *Hc* and the fungi that have been previously studied, such as *C. albicans* and *C. neoformans*, is that *Hc* predominantly replicates intracellularly within macrophages (97). The intracellular life-cycle of *Hc* may help to shield the fungus from complement attack, rendering complement less potent once *Hc* has established its intracellular niche. Better understanding the role of complement and C3aR in disease progression *in vivo* will be essential to determine the therapeutic benefit of targeting complement or C3aR in the treatment of invasive fungal infections.

Chapter 6: Materials and Methods

Strains and culture conditions

J774A.1 cells (ATCC) were cultured in Dulbecco's modified Eagle medium high glucose (DMEM, UCSF media production) with 10% heat-inactivated fetal bovine serum (FBS; Corning or Atlanta), penicillin and streptomycin (pen/strep, UCSF media production). Cells were passaged by detaching with a disposable cell scraper. HEK293T cells (ATCC) were cultured in DMEM with 10% FBS and pen/strep. Platinum-E (Plat-E) retroviral packaging cells (CellBioLabs) were a gift from Jason Cyster (UCSF) and were maintained in DMEM supplemented with 10% FBS, pen/strep, glutamine, and 10mM HEPES (UCSF media production). Plat-E and HEK293T cells were passaged by detaching cells using 0.05% Trypsin-EDTA (UCSF media production). WT C57BL/6J (stock 000664), Rosa26-Cas9 (stock 26179), *C3ar-/-* (stock 33904), *C3-/-* (stock 29661), and DBA2/J (stock 000671) mice were obtained from Jackson Laboratories and/or bred in the UCSF mouse barrier facility. Bone marrow from 6-to 8-week-old female mice was isolated from femurs and tibias, and differentiated into bone marrow-derived macrophages (BMDMs) by culturing in BMM (bone marrow macrophage media) + 10mM HEPES as described previously (162). BMM contains 10% CMG-conditioned media and 20% FBS. Mammalian cells were frozen in complete media supplemented with 10% DMSO and 50% FBS, and stored in liquid nitrogen. Thioglycollate-ellicited peritoneal macrophages (Thio-Pmacs) were isolated and cultured as previously described (43, 46). Briefly, 8-12-week-old mice were injected I.P. with 3% thioglycollate broth. Four days later, mice were euthanized, peritoneal lavage was collected, and cells

were cultured in RPMI supplemented with 10% FBS, pen-strep, glutamine, sodium-pyruvate, non-essential amino acids, and β-mercaptoethanol for 24h in tissue-culture conditions prior to phagocytosis or cytokine release assays. *Histoplasma capsulatum* (*Hc*) strain G217B (ATCC 26032) and G217B *ura5Δ* were kind gifts from William Goldman (University of North Carolina, Chapel Hill). mCherry-expressing *Hc* was generated as described previously (49). The *Hc cpb1* mutant strain, G217Bura5Δcbp1::T-DNA with a Ura5-containing episomal vector, was generated previously (98, 100). *Hc* cultures were grown on *Histoplasma* macrophage medium (HMM) agarose plates or in liquid HMM on an orbital shaker as previously described, and stocks generated from single colonies were frozen in HMM with 15% glycerol in single-use aliquots (163). Mammalian cells and *Hc* cultures were maintained in humidified tissue-culture incubators at 37°C with 5% CO_2. *Hc* was grown on HMM-agar plates (supplemented with 0.175 mg/mL uracil to grow *Hc ura5Δ*) for 1-2 weeks, and passaged in 1:25 HMM liquid culture every-other day for five days to obtain logarithmic-phase *Hc* yeast-cultures (OD_{600}=5-7). Yeast cells were collected, resuspended in Ca^{++} and Mg^{++}-free D-PBS (D-PBS), sonicated for 3 seconds on setting 2 using a Fisher Scientific Sonic Dismembrator Model 100, and counted using a hemocytometer. Where indicated, *Hc* was killed by incubating with 4% paraformaldehyde (PFA, electron microscopy sciences) in PBS for 20 min at RT and washed twice. *Hc* yeast were adjusted to the appropriate concentration in D-PBS. For macrophage infections, *Hc* was added to the macrophage cultures, and allowed to settle onto the cells unless otherwise specified. *Candida albicans* (*Ca*) strain Sc5314 (ATCC MYA-2876) was a kind gift from

Alexander Johnson (UCSF). *Ca* was grown on YEPD (2% peptone, 1% yeast extract, 2% glucose) agar or liquid media at 30°C. *Coccidioides posadasii* Silveira strain was a generous gift from Dr. Bridget Barker (Northern Arizona University). Coccidioides arthroconidia were obtained as previously described (164), by growing Coccidioides on 2xGYE (2% glucose 1% yeast extract) solid agar in flasks at 30°C for 4-6 weeks. At the time of collection, arthroconidia were dislodged with a cell scraper in PBS, filtered through miracloth to remove hyphal fragments, resuspended in PBS and stored at 4C for up to 6 months. Arthroconidia concentration was measured by counting arthroconidia on hemocytometer.

Generation of stable J774A.1 cell-lines for CRISPRKO and live-cell imaging experiments

Gene-targeting sequences were cloned into the pMCB306 lentiguide-puro vector as previously described (165). Table 2.2 lists the CRISPR targeting sequences used. Table 6.1 lists the oligonucleotides used in this study. The lentiviral Lifeact-monomeric eGFP-Blast vector was a kind gift from Diane Barber (UCSF). The Ef1a-Cas9-Blast lentiviral vector (pMCB393) was generated previously (112). To generate lentivirus particles, HEK293T cells were transfected using polyethylenimine (PEI) with second-generation (sgRNA, Lifeact) or third-generation (Ef1a-Cas9-Blast) packaging plasmids and the desired transfer plasmid. Lentivirus was harvested 48-and 72-h later, and filtered through a 0.45 µm polyvinylidene fluoride (PVDF) or polyethersulfone (PES) filter (Millipore). Viruses were concentrated using the Lenti-X concentrator (Takara) according to the manufacturer's instructions. Concentrated lentivirus (Cas9: 20X, lentiguide-puro: 1-2X, Lifeact: 5X) was added to J774A.1 cells for 12-24 h (with 8 µg/mL

polybrene for Cas9), after which virus-containing media was removed and cells were grown in complete DMEM. Starting at 3 days post-transduction, cells were grown under selection with Blasticidin (2 µg/mL) or puromycin (2.5 µg/mL) for 3 days, and expanded without selection for at least 3 days or until the desired number of cells was obtained. To obtain clonal Cas9-expressing J774A.1 cells, live cells were harvested and single-cell sorted using a FACSAriaII cell-sorter into 96-well plates containing complete media supplemented with 50% sterile-filtered J774A.1 conditioned media, and expanded for 3 weeks. The Cas9 activity of the J7-Cas9 clones was determined following transduction with the lentiguide-puro-eGFP vector containing a GFP-targeting sgRNA, and measuring eGFP silencing after puromycin selection by flow cytometry. The J7-Cas9 clone with the highest eGFP-silencing activity was used to generate the pooled CRISPR libraries and individual CRISPRKO cell-lines. The efficiency of Cas9-mediated gene-targeting was assessed by PCR-amplifying the targeted locus in control and CRISPRKO cells, performing Sanger sequencing, and analyzing sequencing chromatograms using the TIDE webtool (166). CRISPR targeting efficiency as measured by TIDE analysis for the sgRNAs used is shown in Table 2.2.

Pooled CRISPR-Cas9 screens

We used pooled mouse sgRNA sub-libraries that were generated previously (112), some of which are available on Addgene (#1000000121-1000000130). Each library covers 500-1500 genes with 10 sgRNAs/gene and includes 750 negative control sgRNAs (375 non-targeting and 375 safe-targeting sgRNAs). We performed screens on all of the sub-libraries, except for the Mouse Unique sub-libraries, which contain mouse

genes that do not have known orthologues in humans. Taken together, our screens covered 16,781 mouse genes. Lentivirus was generated by transfecting HEK293T cells seeded in 15 cm dishes with sgRNA plasmids and second-generation packaging plasmid as described previously(167). Lentivirus was harvested at 48-and 72 h post-transfection, filtered through 0.45 µm PES filters, pooled, then concentrated using the Lenti-X concentrator (Takara) according to the manufacturer's instructions. J774A.1 cells stably expressing LentiCas9-Blast (generation described above) were incubated with 2X concentrated lentivirus for 24h at 1000X coverage in T-225 or T-175 flasks at an MOI of 0.2-0.5 as determined by flow cytometry of mCherry expression at 3 days post-transduction. We then performed selection for transductants using puromycin (2.5 µg/mL) for 3 days until >90% of the cells were mCherry-positive by flow cytometry. Cells were allowed to recover from puromycin selection for three days before screening. Cells were split into two conditions, and screening was performed in duplicate. One condition was infected with *Hc ura5Δ* and subjected to 2-3 pulses of uracil to initiate fungal growth and macrophage lysis (see Table 2.1 for details specific to each sub-library). J774A.1 CRISPRKO libraries, seeded at 1000X library coverage in T-225 or T-150 flasks, were infected with *Hc ura5Δ* at a multiplicity of infection (MOI) of 5 yeast/macrophage. Yeast were allowed to settle onto the monolayer and incubated for 2 h. The cells were washed once with D-PBS to remove extracellular yeast, and incubated in the presence of 0.35 mg/mL uracil for 2 d until ~50% of the monolayer was cleared. Then, the monolayer was washed 3X with D-PBS to remove dead macrophages and extracellular yeast, and incubated for 2-5 days in complete media without uracil to allow the monolayer to

recover. Recovery was assessed by visual assessment of confluency. Uracil was then re-introduced to the culture media for 1-2 d to re-initiate fungal growth and lysis. The addition and removal of uracil was performed 1-2 times depending on the speed at which the monolayer recovered. Uninfected cells were passaged in parallel every 2 d by detaching adherent cells with a cell-scraper, counting using a hemocytometer, and re-seeding into new flasks at 1000X coverage. Uninfected cells were pulsed with uracil during passaging to match the *Hc* infection. At the end of the screening period, monolayers were washed and harvested by detaching with a cell-scraper. Genomic DNA was extracted from the cells using the DNA blood midi or maxi kit according to the manufacturer's instructions, with the inclusion of a brief centrifugation step after cell lysis to remove un-lysed *Hc* yeast before addition of ethanol and application to the column. Guide frequencies were quantified by PCR amplification and deep sequencing using an illumina NextSeq 500 as previously described(165).

Analysis of CRISPR-Cas9 Screens

Sub-library screens were analyzed separately using casTLE version 1.0 as previously described (114). Briefly, the distribution of guides was compared between the uninfected and *Hc*-infected samples, and guide enrichments were calculated as log ratios between the infected and uninfected samples. A maximum likelihood estimator was used to estimate the effect size for each gene and the log-likelihood ratio (confidence score, or casTLE score) by comparing the distribution of the 10 gene-targeting guides to the distribution of negative control guides. An effect size of 1 roughly corresponds to one $\log_2$ fold change of the gene-targeting guides compared to the

negative controls. P values were determined by permuting the gene-targeting guides in the screen and comparing to the distribution of negative controls using casTLE, and false discovery rate (FDR) thresholds for defining hits were calculated using the Benjamini-Hochberg procedure. We used an FDR threshold of 5% to define hits. Results from the separate sub-library screens were concatenated and visualized using JavaTreeview (168). GO-biological process analysis was performed using Gorilla (169) using an un-ranked list of genes that passed the 5% FDR cutoff as the target list and all of the genes detected in the screen as the background list.

Competitive fitness assays in J774A.1 cells

J774A.1-Cas9 (WT) cells were mixed with CRISPRKO J774A.1-Cas9 cells harboring the lentiguide-puro vector, which drives expression of a gene-targeting sgRNA and an eGFP marker (75% WT cells, 25% CRISPRKO cells). $3.5X10^5$ cells/well were seeded in tissue culture (TC)-treated 6-well plates. 12-24 h later, the cells were infected with *Hc ura5Δ* at an MOI of 5, which was incubated with the monolayer for 2 h followed by a D-PBS wash step. The cells were incubated in complete media containing 0.35 µg/mL uracil for 2 d, until lysis of >50% of the monolayer was observed. Then cells were recovered by washing 3X with D-PBS, and incubating in complete media in the absence of uracil for 2 d. Uninfected cells were detached by scraping and passaged to prevent overcrowding, and were subjected to the same washing and media conditions as the *Hc*-infected cells. Following the recovery period, surviving cells were harvested and stained, and GFP-expression was analyzed by flow cytometry.

Generation of CRISPR-knockout BMDMs

The pSIN MuLV sgRNA retroviral transfer plasmid (U6 guide tracer EF1a Thy1.1 P2A Neo) was a kind gift from Jason Cyster (UCSF). The sgRNA cloning site, U6 promoter, and selection marker of pSIN was replaced to match that of pMCB306 using the Gibson Assembly Cloning Kit (NEB) to generate the transfer plasmid (BAS2186) used for these studies. Oligos used for this cloning are listed in Table 6.1 Gene-targeting sgRNA sequences (Table 2.2) were cloned into the vector as previously described for pMCB306 (165). To generate viral particles for expression of sgRNAs, Plat-E retroviral packaging cells were transfected with the transfer plasmid in antibiotic-free complete DMEM. Virus was harvested at 48 h and 72 h post-transfection and filtered through a 0.45µm PES filter. Bone marrow from female 6-8-week-old Rosa26-Cas9 mice was isolated and cultured for 2 d in BMM as described above. Non-adherent bone marrow cells were harvested, and $2X10^6$ cells per well were infected with 2 mL fresh MuLV supernatant by centrifugation (2400 RPM, 2 h, RT) in 6-well non-TC-treated plates with 10 µg/mL polybrene. Viral supernatant was removed, and cells were incubated overnight in BMM. Both adherent and non-adherent bone marrow cells were infected with viral supernatant again as described above with the 72h viral harvest. 24h after the second viral infection, BMDMs were grown under puromycin selection (4 µg/mL) for 3 days, grown for an additional 3-5 days in BMM without puromycin, and harvested as previously described. Retroviral infection and selection were verified by Thy1.1 staining and flow cytometry. The efficiency of Cas9-mediated gene-targeting was assessed by PCR-amplifying the targeted locus in control and CRISPRKO cells,

performing sanger sequencing, and analyzing sequencing chromatograms using the TIDE webtool (166). Results are shown in Table 2.2.

Competitive Hc phagocytosis assays

WT and CRISPRKO J774A.1 cells were mixed as described above (75% WT and 25% CRISPRKO), seeded at $3X10^5$ cells/well in tissue-culture-treated 12-well plates, and incubated for 12-24 h prior to infection. *Hc* yeast expressing mCherry were added to the monolayers (MOI2), and incubated for 1h at 37°C. Cells were washed with ice-cold HBSS and harvested by pipetting in HBSS. Similarly, Cas9-expressing BMDMs (WT) were mixed with Cas9-BMDMs transduced with a retroviral vector driving expression of a gene-targeting sgRNA (CRISPRKO) (75% WT and 25% CRISPRKO). BMDMs were added at $5X10^5$ cells/well to non-TC-treated 12-well plates in BMM for 12-24 h and infected with mCherry-expressing *Hc* for 1 h in BMM. Phagocytosis and GFP or Thy1.1 expression was measured using flow cytometry.

FITC labelling of Zymosan and Coccidioides posadasii arthroconidia

FITC-labelling was performed as described previously for *Hc* yeast (43). Briefly, zymosan A (Sigma) was sonicated for 3 seconds on setting 2 using a Fisher Scientific Sonic Dismembrator Model 100, washed with 0.05 M sodium carbonate-bicarbonate buffer, and adjusted to $2X10^8$ particles/mL. *C. posadasii* arthroconidia were adjusted to $5X10^8$ conidia/mL, and washed in a sodium carbonate-bicarbonate buffer. Fungi were incubated with in 0.05M sodium carbonate-bicarbonate buffer (pH 9.5) with 0.16mg/mL FITC (Fisher, dissolved in DMSO at 5mg/mL) for 15 min at room temperature, protected from light, then washed twice with HBSA (HBSS + 0.25% BSA). Labelled zymosan was

resuspended in D-PBS, counted using a hemocytometer, and frozen in single-use aliquots at -20°C. FITC-labelled arthroconidia were resuspended in PBS and counted on a hemocytometer. FITC-labelled arthroconidia were kept at 4°C and protected from light until used in phagocytosis experiments.

Serum

Fetal bovine serum (FBS) was purchased from Atlanta Biologicals or Corning unless otherwise indicated, and stored in 500 mL bottles at -80°C. Serum was thawed to 37°C and heat-treated by incubating in a 56°C water bath for 30 min with one inversion. Following heat-treatment, serum was aliquoted and stored at -20°C. Where indicated, serum was pre-treated with zymosan at $1X10^8$ particles/mL for 60 min at 37°C. Zymosan was removed by centrifugation and sterile filtration (0.22 µm PVDF filter) before addition to macrophage media. Adult bovine serum (USA origin) was purchased from Sigma. To collect mouse serum, 8-12 week-old male mice were euthanized using CO_2, and blood was collected by cardiac puncture. Blood was placed in a 1.5 mL Eppendorf tube and allowed to coagulate by incubation at room temperature for 1 h, and for an additional 30 min on ice. Coagulated blood was centrifuged, and the supernatant was harvested. Serum was used fresh or stored at -80°C in single-use aliquots. Untreated, C3-depleted, and C5-depleted pooled human serum was purchased from Complement Technology, Inc.

Macrophage phagocytosis assays

BMDMs were thawed and seeded in BMM in 12-well non-TC-treated plates at $5X10^5$ cells/well (flow cytometry) or onto ethanol-sterilized glass coverslips in TC-treated

24-well plates at 2X10^5 cells/well (microscopy), and allowed to adhere for 12-24 h. Thioglycollate-ellicited macrophages were seeded in complete media in 24-well TC-treated plates at 6X10^5 F4/80+ cells/well and allowed to adhere for 12-24h. Prior to infection, the cells were washed with D-PBS and fresh media was added. For some experiments, macrophages were pre-treated with the following compounds and vehicle controls: pertussis toxin (Sigma, 1 µg/mL, 2 h), SB290157 (Sigma, 1 µM, 5 min), anti-CD18 clone GAME-46 or isotype control (BD, 10 µg/mL, 90 min), recombinant C3a (R&D systems, 1 h), and phorbal 12-myristate 13-acetate (Sigma, 2 h). To ensure a consistent MOI, prior to infection, a well of cells was harvested using dissociation buffer, and counted using a hemocytometer. The count was used to calculate the number of cells that had adhered to the dish to determine the number of fungal cells or particles to add to the well for the appropriate MOI. For *Hc* phagocytosis assays, mCherry-expressing *Hc* yeast was added to the macrophage monolayer. For Zymosan phagocytosis assays, FITC-labelled zymosan was sonicated and added to the monolayer. Fluorescein-conjugated *E. coli* bioparticles (Invitrogen) were prepared according to the manufacturer's instructions and added to macrophage monolayers (MOI4). Carboxylate-modified microspheres (2.0 µm and 0.5 µm) were sonicated and added to the macrophage monolayers (MOI2). Phagocytosis of the above substrates was analyzed by flow cytometry. Logarithmic cultures of *Candida albicans* yeast grown in YEPD liquid media were harvested, washed 3X with D-PBS, counted, and added to macrophage monolayers on coverslips at an MOI of 3. Coverslips were washed 2X with DPBS and stained with 35 µg/mL calcofluor white M2R (CFW, Sigma) for 1 min. Then,

the coverslips were washed, fixed with 4% PFA at 37°C for 20 min. PFA was quenched by washing 3X with 100 mM glycine. Cells were permeabilized with 0.1% Triton-X-100 (5 min), and blocked with 1% BSA. Both intracellular and extracellular *C. albicans* yeast were detected by staining with a FITC-conjugated anti-*C. albicans* antibody (abcam, 1:1000) overnight 4°C. FITC-labelled *C. posadasii* arthroconidia were added to the coverslip an MOI of 1, then spun for 15 min at 550g to ensure contact between macrophages and arthroconidia. At the indicated times, the coverslips were washed and stained with 35 µg/mL CFW (2 min), washed once, fixed with 4% PFA, then washed with PBS. For *C. albicans* and *C. posadasii* experiments, Coverslips were mounted and imaged at 40X magnification. 16 fields along a grid were automatically selected. To determine the phagocytosis rate, the cell-counter plugin in ImageJ was used to manually count the total number of macrophages and the number of macrophages with at least one intracellular fungus, determined by exclusion of CFW staining. The phagocytosis rate was calculated as the number of macrophages with at least one intracellular fungal particle divided by the total number of macrophages.

Serum opsonization and analysis of C3 deposition by immunofluorescence microscopy

Hc was incubated at $1X10^8$ yeast/mL with 10% serum and the indicated chelators (10 mM EGTA or EDTA) in PBS for 30 min at 37°C. The yeast were washed twice with PBS, and co-cultured with BMDMs, or stained with a FITC-conjugated anti-mouse C3 antibody (MP Biomedicals, 1:200) for 1h at RT. Following staining, yeast were washed twice with PBS, and fixed with 4% PFA after spinning onto poly-L-Lysine-coated

coverslips. Coverslips were washed 2X and imaged at 60X magnification to visualize mouse C3 deposition on the cell-wall.

Analysis of C3aR localization by immunofluorescence microscopy

$2X10^5$ BMDMs were seeded onto ETOH-sterilized glass coverslips in 24-well plates. Phagocytosis was synchronized by pre-incubating macrophage monolayers on ice, and centrifuging mCherry *Hc* yeast or fluorescent latex beads (MOI=5) at 4°C onto the monolayers, followed by incubation at 37°C for up to 30 min. Coverslips were washed with D-PBS and fixed with 4% PFA for 20min at RT. Coverslips were blocked with PBS + 5% FBS for 1 h at RT, and stained with an anti-mouse C3aR antibody (Clone 14D4, Hycult, 1:1000) overnight at 4°C in 5% FBS. Coverslips were washed with 5% FBS and stained with AlexaFluor-488-conjugated goat anti-rat IgG (Invitrogen, 1:500) for 1 h at RT. Coverslips were imaged at 60X magnification. Optical sectioning was performed to obtain Z-stacks (0.4 µm step-size, 5 µm thickness), and 6 fields were manually selected (using DIC to find macrophages in association with *Hc* or beads) and imaged per coverslip. To quantify C3aR localization to the *Hc* or bead-containing phagosome, we used imageJ to define a 0.5 µm-thick phagosome perimeter outside of the *Hc* or bead particle. We set a threshold on the *Hc* (>600) or bead (>800) channel pixel values and generated a binary mask. The mask was then dilated, outlined, and dilated an additional two times. Example binary masks are shown in Fig. 3.8.Then, we use the 3D ROI manager (170) plugin in ImageJ to generate 3D ROI objects from the binary mask, and to quantify the mean intensity of the C3aR signal within the

phagosomal volume. We subtracted the background signal, measured on phagosomes in *C3ar-/-* BMDMs subjected to the same staining and analysis pipeline.

Live cell-imaging and cell tracking

$2X10^4$ BMDMs or $5X10^3$ Lifeact-meGFP-expressing J774A.1 macrophages (generated as described in "generation of stable cell-lines") were seeded into 96-well glass-bottom plates (Cellvis) and allowed to adhere for 12-24 h. For experiments with J774A.1 cells, culture media was replaced with fresh phenol-red-free DMEM containing 10% FBS with either a vehicle control (DMSO) or 10 μM C3aR antagonist (SB290157) and incubated for 5 min. mCherry-expressing yeast were added to the cells (MOI5), and centrifuged briefly (15 sec) to facilitate contact with the macrophages. BMDMs were imaged every minute for 2 hours at 40X magnification, and J774A.1 cells were imaged every 90 sec for 45 min at 20X magnification. An Okolab stagetop incubator with temperature and humidity control was used to maintain optimal conditions (37°C and 5% CO_2). Four fields were imaged per duplicate well. Actin-rich (eGFP+) membrane protrusions of macrophages that capture *Hc* yeast were tracked manually using the imageJ plugin MtrackJ (171). Tracking was started at the membrane point closest to the *Hc* yeast when the yeast first appeared close to the location at which it was eventually captured. The position of the yeast was used as a reference. The track was terminated when the *Hc* was successfully engulfed (as visualized by formation of an actin collar around the *Hc* yeast), or when the imaging period ended. The phagocytosis rate is reported as the distance from the J774A.1 cell-membrane to the *Hc* target at the start of tracking divided by the time elapsed until the yeast was successfully engulfed. The

mean velocity (mean displacement/time across tracked points) and outreach ratio of the tracks (the max displacement/net displacement) were calculated as described (137).

Confocal microscopy

For fixed imaging, coverslips were mounted onto slides using vectashield antifade mounting media, with or without DAPI (Vector labs) and sealed using nail polish. Fluorescence confocal microscopy was performed using a using a Nikon Ti-Eclipse inverted microscope with a Yokogawa spinning disk CSU-X1 and an Andor Clara CCD camera. Image processing and analysis was performed using ImageJ (FIJI).

Flow cytometry

Primary macrophages (BMDMs and Thio-Pmacs) were washed and harvested using HBSS-based cell dissociation buffer (Thermo scientific) by incubating at 37°C for 10 min and pipetting with ice-cold HBSS. J774A.1 cells were washed with ice-cold HBSS, and harvested by spraying cells off of the well with ice-cold HBSS using a P-1000 pipette. Cells were kept on ice and protected from light for subsequent steps. Cells were stained with fixable viability dye efluor450 (ebioscience; 1:1000) for competitive fitness assays and CD11b/CD18 staining, or fixable viability dye efluor780 (ebioscience; 1:500) for phagocytosis assays for 20 min. Cells were washed with FACS buffer (2% FBS and 5 mM EDTA in PBS) prior to staining with antibodies and/or CFW (1 μg/mL) in FACS buffer for 15-20min. The following antibodies and dilutions were used: PerCP-conjugated anti-Thy1.1 (clone OX-7, biolegend, 1:100), PE, FITC, or AlexaFluor647-conjugated anti-CD11b antibody (clone M1/70, UCSF mAB core, 1:500 for BMDMs, 1:1000 for J774A.1), AlexaFluor-647-conjugated anti-F4/80 (BM8, UCSF mAB core,

1:500), and AlexaFluor-647-conjuaged anti-CD18 antibody (M18/2, Biolegend, 1:100). Cells were washed with FACS buffer. For phagocytosis and competitive fitness assays, cells were washed with D-PBS, and fixed using BD stabilizing fixative for 15min, washed with D-PBS, and kept on ice prior to data acquisition. For indirect flow cytometry measurement of C3aR expression, staining was conducted as described previously (71). $5X10^5$ BMDMs were fixed using BD stabilizing fixative (20min on ice). Cells were blocked for 20min with PBS5 (PBS+5% FBS) and stained with a C3aR antibody (Clone 14D4, Hycult, 1:500) in PBS5 for 20min on ice. Cells were washed with PBS5 and stained with APC-conjugated goat anti-rat IgG (Biolegend, 1:200) for 20 min. Cells were washed with PBS5, and resuspended in PBS. Flow cytometry acquisition was performed using a BD LSRII or Fortessa analyzer in the UCSF Parnassus Flow Core (RRID:SCR_018206). Analysis was performed using FlowJo v. 7 or 10. Where necessary, compensation was performed with single-color controls using FlowJo.

Trans-well migration assay

Cells and *Hc* were resuspended in migration media (DMEM with 0.5% fatty acid-free BSA, pen/strep, and 10 mM HEPES) or complete DMEM with 10% FBS. Inhibitors were added to both the well and the insert when used. 6.5 mm transwell permeable supports with polycarbonate membranes and 5 µm pores (Costar) were used. Migration assays were performed in duplicate. 600 µL *Hc* G217B yeast was added at the indicated concentration to the well of a 24-well transwell plate. $2X10^5$ J774A.1 cells in 100 µL media were seeded into the transwell insert, and plates were incubated at 37°C with 5% CO_2 for 3 h with minimal disturbance. Media was removed from the insert,

which was dipped once in D-PBS, then placed in crystal violet stain (0.5% crystal violet, 20% methanol) for 10 min at RT. Supports were rinsed with dH_2O, and a Q-tip was used to gently wipe cells off of the top of the membrane, and dried at RT. Membranes were mounted on slides, and 3 fields per membrane were imaged using a Leica DM 1000 microscope at 10X magnification. Cells in each microscopic field were counted manually using the cell counter plugin in ImageJ.

Cytotoxicity assays

$7.5X10^4$ BMDMs were seeded per well of a 48-well plate and infected with *Hc* G217B at an MOI of 0.5 in the presence of pheno-red-free BMM. $1.875X10^4$ J774A.1 cells were seeded per well of a 48-well plate and infected with *Hc* at an MOI of 5 in phenol-red-free complete DMEM. Where indicated, media was supplemented with 0.35 mg/mL uracil. To recover J774A.1 cells from infection with *Hc ura5Δ*, cells were washed with D-PBS, and grown in complete media that did not contain uracil for 3 days. Recovered cells were re-seeded and incubated with complete media with or without uracil supplementation. At the indicated time points, the amount of lactate dehydrogenase (LDH) in the culture supernatant was measured as described previously (172). Macrophage lysis is calculated as the percentage of total LDH from uninfected macrophages lysed in 1% Triton-X at day 0 of infection. Due to continued replication of macrophages during the experiment, the total LDH at later time points is greater than the total LDH from the first time point, resulting in an apparent lysis that is greater than 100%. To quantify cell depletion and recovery during infections of J774A.1 cells, we measured macrophage DNA remaining in the wells as previously described (101).

Briefly, we washed the cells with D-PBS, added ddH_2O to the well to lyse the macrophages, and measured the amount of macrophage DNA in the wells using the picoGreen DsDNA reagent (Invitrogen). Fluorescence intensities were measured using the quantitative plate read option on an Mx3000P QPCR machine (Agilent).

Intracellular fungal growth assay

$7.5X10^4$ BMDMs were seeded per well of a 48-well plate and infected in triplicate with *Hc* at an MOI of 0.5. At the indicated time points, culture supernatants were removed and 500 µL ddH_2O was added. Macrophages were osmotically and mechanically lysed by pipetting up-and-down and sonicating (3 seconds at setting 2), and lysates were plated on HMM agarose at the appropriate dilutions as described previously (98). After incubation at 37°C with 5% CO_2 for 12-14 days, colony forming units (CFUs) were enumerated. To prevent analysis of extracellular replication, CFUs were not monitored after the onset of macrophage lysis.

CBA and ELISA assays

BMDMs were seeded at $3X10^5$ cells/well in 48-well plates (TC-treated), and infected with *Hc* in triplicate (MOI=10 for CBA and MOI=2 for C3 ELISA). Thio-Pmacs were seeded at $8X10^5$ F4/80+ cells/well and infected with *Hc* in triplicate (MOI=10). Experiments were performed in media supplemented with FBS. Supernatants were collected at the indicated times, snap-frozen in LN_2 and stored at -80°C. Supernatants were filtered using 0.2 µm Acroprep 96-well filter plates by centrifugation. TNF-α, IL-1β, and IL-6 levels were measured using the appropriate mouse CBA flex set (BD) according to the manufacturer's instructions. Data were acquired using a BD LSRII or

Fortessa flow cytometer and analyzed using FCAP array software (BD). The Mouse Complement C3 ELISA kit (Abcam) was used according to the manufacturer's instructions to quantify C3 levels in macrophage culture supernatant. Mouse serum was incubated with *Hc* and zymosan at $10X10^8$ particles/mL for 30 min at 37°C. The reaction was stopped by addition of 10 mM EDTA and incubation on ice. *Hc* and zymosan were pelleted by centrifugation, and the supernatant was filtered using Spin-X cellulose acetate spin filters. Supernatants were diluted 1:200. A mouse C3a ELISA pair (BD) was used as previously described (159) according to manufacturer's instructions to measure C3a levels in the supernatants using filter plates. Briefly, corning High-Bind plates were coated with 4 µg/mL capture antibody in pH 6.5 binding buffer. PBS+10% FBS was used for blocking, and PBS+Δ10% FBS +0.05% Tween-20 was used to dilute samples, standards, and detection antibody solutions. Biotinylated C3a detection antibody was used at 6.25 ng/mL, and avidin-HRP was used at a 1:5000 dilution.

Mouse infections

C3ar-/- mice (B6.129S4(C)-*C3ar1*^{tm1Cge}*/BaoluJ*, JAX:033904) were purchased from Jackson laboratories and bred in the UCSF mouse barrier facility, and *C3-/-* mice (B6.129S4-C3^{tm1crr}/J, JAX:029661) were purchased from Jackson laboratories. Some of these mice were bred in the UCSF moues barrier facility. 8-12-week-old mice were used for infections, and age-matched WT mice (C57BL/6J, JAX:000664) were purchased from the Jackson laboratories. *Hc* strain G217B yeast were grown to mid-logarithmic phase (OD_{600} = 5-7), and washed with PBS. Yeast suspensions were sonicated for 3 seconds on setting 2 using a Fisher Scientific Sonic Dismembrator model 100, and

counted using a hemocytometer. The culture was diluted in PBS to deliver the inoculum in 25 µl. Mice were isoflurane anesthetized and the inoculum was delivered intranasally. Mice were monitored daily for signs of disease, including weight loss, hunching, panting, and lack of grooming. Animals were euthanized if they exhibited 3 days of sustained weight loss greater than 25% of their maximum weight, in addition to one other symptom, or if they were deemed moribund (lack of movement or responsiveness).

RNA isolation and qRT-PCR

J774A.1 cells were infected with *Hc* at an MOI of 5 for 24 h. RNA isolation using QIAzol reagent (Qiagen), reverse transcription, and qRT-PCR was performed as described previously to measure the abundance of *TRIB3* and *CHOP* normalized to *HPRT* levels in infected macrophages (98). Primer sequences are listed in Table 6.1.

Statistical analysis

Two-tailed t-tests were performed using Excel (Microsoft). Logrank and Wilcoxon rank-sum tests were performed using R. Details of the statistical analysis are listed in the figure legends. Error bars indicate Standard Deviation.

Ethics statement

All mouse experiments were performed in compliance with the *National Institutes of Health Guide for the Care and Use of Laboratory Animals* and were approved by the Institutional Animal Care and Use Committee at the University of California San Francisco (protocol AN18753-03A). Mice were euthanized by CO_2 narcosis and cervical dislocation consistent with American Veterinary Medical Association guidelines.

Table 6.1: Oligonucleotides used in this study

Name	Sequence (5'-3')
Gnb2sg1_fw_7251	TGGGACAGCTACACCACTAAC
Gnb2sg1_rv_7252	GGTGATGATTTGGTTGTCGTCC
Gnb2sg3_fw_7253	CTCTCTTGCACTGCCCATCA
Gnb2sg3_rv_7254	TCCTGGATCCCTGGTCTTCC
Gnb2sg7_fw_7255	GGCTCCCCCACTATTTCGG
Gnb2sg7_rv_7256	GTCATCTGATCCCGTGGTGAA
Nckap1Lsg8_fw_7257	CGTGGAAGTGATGGAGCGAT
Nckap1Lsg8_rv_7258	CTCGAAAACCCAGTGAGGCA
Nckap1Lsg9_10_fw_7259	AAGGGGTAGGTAATGCCAGC
Nckap1Lsg9_10_rv_7260	AAAACAACCTGGGGGCTGAT
Galesg3_fw_7261	GGTGCTAGCTGGGGCATTTA
Galesg3_rv_7262	TGGAGGGGAGGGTCAGTG
Galesg7_fw_7263	GAGAAGCGGCAGTGTTCTCT
Galesg7_rv_7264	ACCTGTCCCGTCCTCTGTAG
Galesg10_fw_7265	TCTGTAACTGATGCCCGTCG
Galesg10_rv_7266	CTGCATACCAGCTGCCAAGA
Tnfrsf1asg2_8_fw_7267	TTCGAATCTGCTCGTGAGTGT
Tnfrsf1asg2_8_rv_7268	CGGTTAAGACTAAGAGCGCGT
Tnfrsf1asg6_fw_7269	GAACCAGTTCCAACGCTACC
Tnfrsf1asg6_rv_7270	GCTTATCCCCTAACGTCCTGG
Fermt3_fw_7271	GAGCACGAGTCAGCTAGCAA
Fermt3_rv_7272	ACAACCTTTGTCAGGTCATGC
Alg3sg5_fw_7273	ACTTCTGGTTACTCGGCTCA
Alg3sg5_rv_7274	AAATGGGCTTGGGTCAGGTA
Alg3sg7_fw_7275	CCCAGGTGGAGGGTTTCATC
Alg3sg7_rv_7276	GGACACGGTAAGAGGCACAA
Alg3sg9_fw_7277	GTTGGGGTTGGCCCTTAAGTA
Alg3sg9_rv_7278	AGGAGATCCGTCTCTTCGGT
Ubr5sg1_5_fw_7279	ACACACGCTCGGCGG
Ubr5sg1_5_rv_7280	CTCCGCCGAGTTCAACGAG
Ubr5sg8_fw_7281	CGTAAAGTGCTGTTAGCTGCG
Ubr5sg8_rv_7282	AAGTGCATGTGGTACCTAGCTT
Rab21sg1_2_fw_7283	AGGAGACGCCATTAGAGGGA
Rab21sg1_2_rv_7284	GACTTTTCCGGGTCCTCTCC
Rab21sg8_fw_7285	GTAGCATTCAGTGTGTGCCC
Rab21sg8_rv_7286	GCACTTAAGGTCTCTGCAGTGTTA
Atl2sg3_fw_7287	GATCGTAACCACGGAGAGCA

Name	Sequence (5'-3')
Atl2sg3_rv_7288	GCGCTGGTGACATCAGGTAG
Atl2sg6_fw_7289	TGCTTGACTGAAATAGAGGACC
Atl2sg6_rv_7290	TGGGGTCAATTTGAAAGACACT
Atl2sg7_fw_7291	CAGTTGATGTAAGGAGCCATGTTA
Atl2sg7_rv_7292	CCGATTTCTCTGAACTCCCCAG
Arrb2sg2_fw_7293	CTTATGTGTACCGACCCTCCG
Arrb2sg2_rv_7294	GCACCACGCCATCTAGGAAA
Arrb2sg4_fw_7295	TGGTGCTTGTGGATCCTGAC
Arrb2sg4_rv_7296	AAGGAGGCGTTTCAACTGGT
Arrb2sg9_fw_7297	TTCCTCCTCTTCCCAAGGCT
Arrb2sg9_rv_7298	TGGCCTGCTTTGTGACATCT
EMC6seqFw_5977	ACTCGGTTTTCTCCACAGCTC
EMC6seqRv_5978	ACCCGGTGTTAATTCTGGCA
Lamtor4sg2Rv2_6024	GAGCAGTGAGGCCGCTAAAA
Lamtor4sg2Fw2_6025	GACCCCTCACATGGCTATCAA
Lamtor4sg5.6Fw2_6026	GAGAAGGAAGGCTCCGCTAC
Lamtor4sg5.6.target_Rv_5987	ATGGCAAGCAAGGAACCACA
EMC7sg4Fw2_6027	GATCCGGCTCGGGATGATG
EMC7sg4Rv2_6028	CTGGATACCCTTCCAGCGTC
EMC7sg6Fw2_6029	TGGTTAGCTGCTTCCACTTGT
EMC7sg6Rv2_6030	AAACTGGGTATCCTCACCGC
EMC7sg7targetFw_5999	TGGCTTGCTTTGTTTGTGTGT
EMC7sg7targetRv_6000	TGTTCCTAAAGACACTAGTTTCCCA
Emc1sg2seq_fw_6095	TTAGTGTGGGTCTGACGGGG
Emc1sg8seq_fw_6096	TCCTCTCTATGGCTCTGCGG
Emc1sg9seq_fw_6097	GCCTTAGCCGACTACCCTTG
Emc1sg2seq_rv_6098	TGGGCATCTATGTCTCTTCAGT
Emc1sg8seq_rv_6099	TGGGTTGACATCTTACGACTCTT
Emc1sg9seq_rv_6100	GCCCTCCGTTGGATACAGTG
PacI_306ClonSite_fwd_6372	ctcactccttctctaggcgccggaattgaagatctttaatTTTGGTTAGTACCGGGCC
AgeI_306ClonSite_rv2_6373	CATCACTTTCCCAGTTTACCC
BmgBIpurogibson_fw_6417	tgctgaagcaggccggcgacgtggaggagaaccccggccccATGACCGAGTACAAGCCCACGG
EcoRVPuro-RV_stop_6419	gagcctggaccactgatgatatctaaTCAGGCACCGGGCTTGCGGGT
mouseC3ar1seq_fw_6486	TTCTGAGGAAGGAGTGCTAACG
mouseC3ar1seq_Rv_6487	GGCGGTTCTCACGTTTCGAT
OAS5595_mouseITGB2.1targetseq_fw	gctctcggggagacctagac
OAS5596_mouseITGB2.2targetseq_fw	tgggtgtctaggcttccaac
OAS5597_mouseITGB2.3targetseq_fw	tctatcccttcccccaactc

Name	Sequence (5'-3')
OAS5598_mouseITGB2.1targetseq_rv	gtcaatggccatggttcttc
OAS5599_mouseITGB2.2targetseq_rv	tcccaaggttgaaaggagtg
OAS5600_mouseITGB2.3targetseq_rv	caccccaatggaattcaaag
mHPRT1-F	AGGTTGCAAGCTTGCTGGT
mHPRT1-R	TGAAGTACTCATTATAGTCAAGGGCA
mTrb3_fwd2	TGCAGGAAGAAACCGTTGGAG
mTrb3_rev2	CTCAGGCTCATCTCTCACTCG
CHOP F	CTGGAAGCCTGGTATGAGGAT
CHOP R	CAGGGTCAAGAGTAGTGAAGGT

References

1. Brown GD, Denning DW, Gow NA, Levitz SM, Netea MG, White TC. Hidden killers: human fungal infections. Science translational medicine. 2012;4(165):165rv13.
2. Bongomin F, Gago S, Oladele RO, Denning DW. Global and Multi-National Prevalence of Fungal Diseases-Estimate Precision. J Fungi (Basel). 2017;3(4).
3. Brown GD, Denning DW, Levitz SM. Tackling Human Fungal Infections. Science (New York, NY). 2012;336(6082):647-.
4. Sil A, Andrianopoulos A. Thermally Dimorphic Human Fungal Pathogens-Polyphyletic Pathogens with a Convergent Pathogenicity Trait. Cold Spring Harbor perspectives in medicine. 2015;5(8).
5. Kauffman CA. Histoplasmosis: a clinical and laboratory update. Clinical microbiology reviews. 2007;20(1):115-32.
6. Van Dyke MCC, Thompson GR, Galgiani JN, Barker BM. The Rise of Coccidioides: Forces Against the Dust Devil Unleashed. Front Immunol. 2019;10:2188.
7. Erwig LP, Gow NA. Interactions of fungal pathogens with phagocytes. Nature reviews Microbiology. 2016;14(3):163-76.
8. Casadevall A. Immunity to Invasive Fungal Diseases. Annual review of immunology. 2022;40:121-41.
9. Freeman SA, Grinstein S. Phagocytosis: receptors, signal integration, and the cytoskeleton. Immunological reviews. 2014;262(1):193-215.

10. Urban CF, Backman E. Eradicating, retaining, balancing, swarming, shuttling and dumping: a myriad of tasks for neutrophils during fungal infection. Current opinion in microbiology. 2020;58:106-15.
11. Desai JV, Lionakis MS. The role of neutrophils in host defense against invasive fungal infections. Curr Clin Microbiol Rep. 2018;5(3):181-9.
12. Clark C, Drummond RA. The Hidden Cost of Modern Medical Interventions: How Medical Advances Have Shaped the Prevalence of Human Fungal Disease. Pathogens. 2019;8(2).
13. Mednick AJ, Feldmesser M, Rivera J, Casadevall A. Neutropenia alters lung cytokine production in mice and reduces their susceptibility to pulmonary cryptococcosis. European journal of immunology. 2003;33(6):1744-53.
14. Wuthrich M, Deepe GS, Jr., Klein B. Adaptive immunity to fungi. Annual review of immunology. 2012;30:115-48.
15. Epelman S, Lavine KJ, Randolph GJ. Origin and functions of tissue macrophages. Immunity. 2014;41(1):21-35.
16. Mosser DM, Edwards JP. Exploring the full spectrum of macrophage activation. Nature reviews Immunology. 2008;8(12):958-69.
17. Gautier EL, Shay T, Miller J, Greter M, Jakubzick C, Ivanov S, et al. Gene-expression profiles and transcriptional regulatory pathways that underlie the identity and diversity of mouse tissue macrophages. Nature immunology. 2012;13(11):1118-28.
18. Martin CJ, Peters KN, Behar SM. Macrophages clean up: efferocytosis and microbial control. Current opinion in microbiology. 2014;17:17-23.

19. Kim SY, Nair MG. Macrophages in wound healing: activation and plasticity. Immunol Cell Biol. 2019;97(3):258-67.

20. Wager CML, Wormley FL, Jr. Classical versus alternative macrophage activation: the Ying and the Yang in host defense against pulmonary fungal infections. Mucosal Immunology. 2014;7(5):1023-35.

21. Deepe GS, Jr., Seder RA. Molecular and cellular determinants of immunity to Histoplasma capsulatum. Research in immunology. 1998;149(4-5):397-406; discussion 509-10.

22. Brummer E, Kurita N, Yoshida S, Nishimura K, Miyaji M. KILLING OF HISTOPLASMA-CAPSULATUM BY GAMMA-INTERFERON-ACTIVATED HUMAN MONOCYTE-DERIVED MACROPHAGES - EVIDENCE FOR A SUPEROXIDE ANION-DEPENDENT MECHANISM. Journal of Medical Microbiology. 1991;35(1):29-34.

23. Gilbert AS, Wheeler RT, May RC. Fungal Pathogens: Survival and Replication within Macrophages. Cold Spring Harbor perspectives in medicine. 2015;5(7):a019661.

24. Leopold Wager CM, Hole CR, Wozniak KL, Wormley FL, Jr. Cryptococcus and Phagocytes: Complex Interactions that Influence Disease Outcome. Front Microbiol. 2016;7:105.

25. Flannagan RS, Jaumouillé V, Grinstein S. The cell biology of phagocytosis. Annu Rev Pathol. 2012;7:61-98.

26. Underhill DM, Ozinsky A. Phagocytosis of microbes: complexity in action. Annual review of immunology. 2002;20:825-52.

27. Ostrowski PP, Grinstein S, Freeman SA. Diffusion Barriers, Mechanical Forces, and the Biophysics of Phagocytosis. Developmental cell. 2016;38(2):135-46.

28. Torres-Gomez A, Cabañas C, Lafuente EM. Phagocytic Integrins: Activation and Signaling. Front Immunol. 2020;11:738.

29. Mylvaganam S, Freeman SA, Grinstein S. The cytoskeleton in phagocytosis and macropinocytosis. Current biology : CB. 2021;31(10):R619-r32.

30. Li K, Underhill DM. C-Type Lectin Receptors in Phagocytosis. Current topics in microbiology and immunology. 2020;429:1-18.

31. Haney MS, Bohlen CJ, Morgens DW, Ousey JA, Barkal AA, Tsui CK, et al. Identification of phagocytosis regulators using magnetic genome-wide CRISPR screens. Nat Genet. 2018;50(12):1716-27.

32. Fairn GD, Grinstein S. How nascent phagosomes mature to become phagolysosomes. Trends in immunology. 2012;33(8):397-405.

33. Di Paolo G, De Camilli P. Phosphoinositides in cell regulation and membrane dynamics. Nature. 2006;443(7112):651-7.

34. Stenmark H. Rab GTPases as coordinators of vesicle traffic. Nature reviews Molecular cell biology. 2009;10(8):513-25.

35. Canton J. Phagosome maturation in polarized macrophages. J Leukoc Biol. 2014;96(5):729-38.

36. Yates RM, Hermetter A, Russell DG. The kinetics of phagosome maturation as a function of phagosome/lysosome fusion and acquisition of hydrolytic activity. Traffic. 2005;6(5):413-20.

37. Hatinguais R, Willment JA, Brown GD. PAMPs of the Fungal Cell Wall and Mammalian PRRs. Current topics in microbiology and immunology. 2020;425:187-223.

38. Höft MA, Hoving JC, Brown GD. Signaling C-Type Lectin Receptors in Antifungal Immunity. Current topics in microbiology and immunology. 2020;429:63-101.

39. Brown GD, Taylor PR, Reid DM, Willment JA, Williams DL, Martinez-Pomares L, et al. Dectin-1 is a major beta-glucan receptor on macrophages. The Journal of experimental medicine. 2002;196(3):407-12.

40. Goodridge HS, Reyes CN, Becker CA, Katsumoto TR, Ma J, Wolf AJ, et al. Activation of the innate immune receptor Dectin-1 upon formation of a 'phagocytic synapse'. Nature. 2011;472(7344):471-5.

41. Stappers MHT, Clark AE, Aimanianda V, Bidula S, Reid DM, Asamaphan P, et al. Recognition of DHN-melanin by a C-type lectin receptor is required for immunity to Aspergillus. Nature. 2018;555(7696):382-6.

42. Bullock WE, Wright SD. ROLE OF THE ADHERENCE-PROMOTING RECEPTORS, CR3, LFA-1, AND P150,95, IN BINDING OF HISTOPLASMA-CAPSULATUM BY HUMAN MACROPHAGES. Journal of Experimental Medicine. 1987;165(1):195-210.

43. Lin JS, Huang JH, Hung LY, Wu SY, Wu-Hsieh BA. Distinct roles of complement receptor 3, Dectin-1, and sialic acids in murine macrophage interaction with Histoplasma yeast. J Leukoc Biol. 2010;88(1):95-106.

44. Tan SM. The leucocyte β2 (CD18) integrins: the structure, functional regulation and signalling properties. Biosci Rep. 2012;32(3):241-69.

45. Li X, Utomo A, Cullere X, Choi MM, Milner DA, Jr., Venkatesh D, et al. The β-glucan receptor Dectin-1 activates the integrin Mac-1 in neutrophils via Vav protein signaling to promote Candida albicans clearance. Cell Host Microbe. 2011;10(6):603-15.

46. Huang JH, Lin CY, Wu SY, Chen WY, Chu CL, Brown GD, et al. CR3 and Dectin-1 Collaborate in Macrophage Cytokine Response through Association on Lipid Rafts and Activation of Syk-JNK-AP-1 Pathway. PLoS pathogens. 2015;11(7):e1004985.

47. Netea MG, Van der Graaf C, Van der Meer JW, Kullberg BJ. Recognition of fungal pathogens by Toll-like receptors. Eur J Clin Microbiol Infect Dis. 2004;23(9):672-6.

48. Coady A, Sil A. MyD88-Dependent Signaling Drives Host Survival and Early Cytokine Production during Histoplasma capsulatum Infection. Infection and Immunity. 2015;83(4):1265-75.

49. Van Prooyen N, Henderson CA, Hocking Murray D, Sil A. CD103+ Conventional Dendritic Cells Are Critical for TLR7/9-Dependent Host Defense against Histoplasma capsulatum, an Endemic Fungal Pathogen of Humans. PLoS pathogens. 2016;12(7):e1005749.

50. Van Haastert PJ, Devreotes PN. Chemotaxis: signalling the way forward. Nature reviews Molecular cell biology. 2004;5(8):626-34.

51. Shi C, Pamer EG. Monocyte recruitment during infection and inflammation. Nature reviews Immunology. 2011;11(11):762-74.

52. Neupane AS, Willson M, Chojnacki AK, Vargas ESCF, Morehouse C, Carestia A, et al. Patrolling Alveolar Macrophages Conceal Bacteria from the Immune System to Maintain Homeostasis. Cell. 2020;183(1):110-25.e11.

53. Pavlos NJ, Friedman PA. GPCR Signaling and Trafficking: The Long and Short of It. Trends Endocrinol Metab. 2017;28(3):213-26.

54. Wang X, Iyer A, Lyons AB, Korner H, Wei W. Emerging Roles for G-protein Coupled Receptors in Development and Activation of Macrophages. Front Immunol. 2019;10:2031.

55. Rougerie P, Miskolci V, Cox D. Generation of membrane structures during phagocytosis and chemotaxis of macrophages: role and regulation of the actin cytoskeleton. Immunological reviews. 2013;256(1):222-39.

56. Szymczak WA, Deepe GS, Jr. The CCL7-CCL2-CCR2 axis regulates IL-4 production in lungs and fungal immunity. Journal of immunology (Baltimore, Md : 1950). 2009;183(3):1964-74.

57. Heinrich V, Lee CY. Blurred line between chemotactic chase and phagocytic consumption: an immunophysical single-cell perspective. Journal of cell science. 2011;124(Pt 18):3041-51.

58. Flannagan RS, Harrison RE, Yip CM, Jaqaman K, Grinstein S. Dynamic macrophage "probing" is required for the efficient capture of phagocytic targets. The Journal of cell biology. 2010;191(6):1205-18.

59. Wen X, Xu X, Sun W, Chen K, Pan M, Wang JM, et al. G-protein-coupled formyl peptide receptors play a dual role in neutrophil chemotaxis and bacterial phagocytosis. Molecular biology of the cell. 2019;30(3):346-56.

60. Edens HA, Parkos CA, Liang TW, Jesaitis AJ, Cutler JE, Miettinen HM. Non-serum-dependent chemotactic factors produced by Candida albicans stimulate chemotaxis by binding to the formyl peptide receptor on neutrophils and to an unknown receptor on macrophages. Infect Immun. 1999;67(3):1063-71.

61. Klos A, Tenner AJ, Johswich KO, Ager RR, Reis ES, Köhl J. The role of the anaphylatoxins in health and disease. Mol Immunol. 2009;46(14):2753-66.

62. Sun D, Zhang M, Liu G, Wu H, Zhu X, Zhou H, et al. Real-Time Imaging of Interactions of Neutrophils with Cryptococcus neoformans Demonstrates a Crucial Role of Complement C5a-C5aR Signaling. Infect Immun. 2016;84(1):216-29.

63. Noris M, Remuzzi G. Overview of complement activation and regulation. Semin Nephrol. 2013;33(6):479-92.

64. Ezekowitz RA, Sim RB, Hill M, Gordon S. Local opsonization by secreted macrophage complement components. Role of receptors for complement in uptake of zymosan. The Journal of experimental medicine. 1984;159(1):244-60.

65. Goodrum KJ. Complement component C3 secretion by mouse macrophage-like cell lines. J Leukoc Biol. 1987;41(4):295-301.

66. Luo C, Chen M, Madden A, Xu H. Expression of complement components and regulators by different subtypes of bone marrow-derived macrophages. Inflammation. 2012;35(4):1448-61.

67. Wong SSW, Daniel I, Gangneux JP, Jayapal JM, Guegan H, Dellière S, et al. Differential Interactions of Serum and Bronchoalveolar Lavage Fluid Complement Proteins with Conidia of Airborne Fungal Pathogen Aspergillus fumigatus. Infect Immun. 2020;88(9).

68. Bolger MS, Ross DS, Jiang H, Frank MM, Ghio AJ, Schwartz DA, et al. Complement levels and activity in the normal and LPS-injured lung. Am J Physiol Lung Cell Mol Physiol. 2007;292(3):L748-59.

69. Lambris JD, Ricklin D, Geisbrecht BV. Complement evasion by human pathogens. Nature reviews Microbiology. 2008;6(2):132-42.

70. Lee CY, Herant M, Heinrich V. Target-specific mechanics of phagocytosis: protrusive neutrophil response to zymosan differs from the uptake of antibody-tagged pathogens. Journal of cell science. 2011;124(Pt 7):1106-14.

71. Quell KM, Karsten CM, Kordowski A, Almeida LN, Briukhovetska D, Wiese AV, et al. Monitoring C3aR Expression Using a Floxed tdTomato-C3aR Reporter Knock-in Mouse. Journal of immunology (Baltimore, Md : 1950). 2017;199(2):688-706.

72. Zwirner J, Werfel T, Wilken HC, Theile E, Gotze O. Anaphylatoxin C3a but not C3a(desArg) is a chemotaxin for the mouse macrophage cell line J774. European journal of immunology. 1998;28(5):1570-7.

73. Sonesson A, Ringstad L, Nordahl EA, Malmsten M, Mörgelin M, Schmidtchen A. Antifungal activity of C3a and C3a-derived peptides against Candida. Biochimica et biophysica acta. 2007;1768(2):346-53.

74. Coulthard LG, Woodruff TM. Is the complement activation product C3a a proinflammatory molecule? Re-evaluating the evidence and the myth. Journal of immunology (Baltimore, Md : 1950). 2015;194(8):3542-8.

75. Liszewski MK, Kolev M, Le Friec G, Leung M, Bertram PG, Fara AF, et al. Intracellular complement activation sustains T cell homeostasis and mediates effector differentiation. Immunity. 2013;39(6):1143-57.

76. Hajishengallis G, Reis ES, Mastellos DC, Ricklin D, Lambris JD. Novel mechanisms and functions of complement. Nature immunology. 2017;18(12):1288-98.

77. Ricklin D, Reis ES, Lambris JD. Complement in disease: a defence system turning offensive. Nat Rev Nephrol. 2016;12(7):383-401.

78. Galgiani JN, Yam P, Petz LD, Williams PL, Stevens DA. Complement activation by Coccidioides immitis: in vitro and clinical studies. Infect Immun. 1980;28(3):944-9.

79. Ratnoff WD, Pepple JM, Winkelstein JA. Activation of the alternative complement pathway by Histoplasma capsulatum. Infect Immun. 1980;30(1):147-9.

80. Kozel TR. Activation of the complement system by pathogenic fungi. Clinical microbiology reviews. 1996;9(1):34-46.

81. Zaragoza O, Taborda CP, Casadevall A. The efficacy of complement-mediated phagocytosis of Cryptococcus neoformans is dependent on the location of C3 in the polysaccharide capsule and involves both direct and indirect C3-mediated interactions. European journal of immunology. 2003;33(7):1957-67.

82. Harpf V, Rambach G, Würzner R, Lass-Flörl C, Speth C. Candida and Complement: New Aspects in an Old Battle. Front Immunol. 2020;11:1471.

83. Taylor PR, Tsoni SV, Willment JA, Dennehy KM, Rosas M, Findon H, et al. Dectin-1 is required for beta-glucan recognition and control of fungal infection. Nature immunology. 2007;8(1):31-8.

84. Tsoni SV, Kerrigan AM, Marakalala MJ, Srinivasan N, Duffield M, Taylor PR, et al. Complement C3 plays an essential role in the control of opportunistic fungal infections. Infect Immun. 2009;77(9):3679-85.

85. Shapiro S, Beenhouwer DO, Feldmesser M, Taborda C, Carroll MC, Casadevall A, et al. Immunoglobulin G monoclonal antibodies to Cryptococcus neoformans protect mice deficient in complement component C3. Infect Immun. 2002;70(5):2598-604.

86. Pillemer L, Blum L, Lepow IH, Ross OA, Todd EW, Wardlaw AC. The properdin system and immunity. I. Demonstration and isolation of a new serum protein, properdin, and its role in immune phenomena. Science (New York, NY). 1954;120(3112):279-85.

87. McDonald JU, Rosas M, Brown GD, Jones SA, Taylor PR. Differential dependencies of monocytes and neutrophils on dectin-1, dectin-2 and complement for the recognition of fungal particles in inflammation. PLoS One. 2012;7(9):e45781.

88. Cheng SC, Sprong T, Joosten LA, van der Meer JW, Kullberg BJ, Hube B, et al. Complement plays a central role in Candida albicans-induced cytokine production by human PBMCs. European journal of immunology. 2012;42(4):993-1004.

89. Speth C, Rambach G. Complement Attack against Aspergillus and Corresponding Evasion Mechanisms. Interdiscip Perspect Infect Dis. 2012;2012:463794.

90. Pfaller MA, Diekema DJ. Epidemiology of invasive mycoses in North America. Critical reviews in microbiology. 2010;36(1):1-53.

91. Deepe GS, Jr., Gibbons RS, Smulian AG. Histoplasma capsulatum manifests preferential invasion of phagocytic subpopulations in murine lungs. J Leukoc Biol. 2008;84(3):669-78.

92. Jones GS, Sepúlveda VE, Goldman WE. Biodiverse Histoplasma Species Elicit Distinct Patterns of Pulmonary Inflammation following Sublethal Infection. mSphere. 2020;5(4).

93. Horwath MC, Fecher RA, Deepe GS, Jr. Histoplasma capsulatum, lung infection and immunity. Future microbiology. 2015;10(6):967-75.

94. Garfoot AL, Rappleye CA. Histoplasma capsulatum surmounts obstacles to intracellular pathogenesis. The FEBS journal. 2016;283(4):619-33.

95. Eissenberg LG, Goldman WE, Schlesinger PH. HISTOPLASMA-CAPSULATUM MODULATES THE ACIDIFICATION OF PHAGOLYSOSOMES. Journal of Experimental Medicine. 1993;177(6):1605-11.

96. Strasser JE, Newman SL, Ciraolo GM, Morris RE, Howell ML, Dean GE. Regulation of the macrophage vacuolar ATPase and phagosome-lysosome fusion by Histoplasma capsulatum. Journal of Immunology. 1999;162(10):6148-54.

97. Ray SC, Rappleye CA. Flying under the radar: Histoplasma capsulatum avoidance of innate immune recognition. Semin Cell Dev Biol. 2019;89:91-8.

98. English BC, Van Prooyen N, Ord T, Ord T, Sil A. The transcription factor CHOP, an effector of the integrated stress response, is required for host sensitivity to the fungal intracellular pathogen Histoplasma capsulatum. PLoS pathogens. 2017;13(9):e1006589.

99. Woods JP. Revisiting old friends: Developments in understanding Histoplasma capsulatum pathogenesis. Journal of Microbiology. 2016;54(3):265-76.

100. Isaac DT, Berkes CA, English BC, Hocking Murray D, Lee YN, Coady A, et al. Macrophage cell death and transcriptional response are actively triggered by the fungal virulence factor Cbp1 during H. capsulatum infection. Mol Microbiol. 2015;98(5):910-29.

101. Sebghati TS, Engle JT, Goldman WE. Intracellular parasitism by Histoplasma capsulatum: fungal virulence and calcium dependence. Science (New York, NY). 2000;290(5495):1368-72.

102. Ray SC, Rappleye CA. Mac1-Dependent Copper Sensing Promotes Histoplasma Adaptation to the Phagosome during Adaptive Immunity. mBio. 2022;13(2):e0377321.

103. Rappleye CA, Eissenberg LG, Goldman WE. Histoplasma capsulatum alpha-(1,3)-glucan blocks innate immune recognition by the beta-glucan receptor. Proceedings of the National Academy of Sciences of the United States of America. 2007;104(4):1366-70.
104. Garfoot AL, Shen Q, Wuthrich M, Klein BS, Rappleye CA. The Eng1 beta-Glucanase Enhances Histoplasma Virulence by Reducing beta-Glucan Exposure. mBio. 2016;7(2).
105. Guimaraes AJ, de Cerqueira MD, Zamith-Miranda D, Lopez PH, Rodrigues ML, Pontes B, et al. Host membrane glycosphingolipids and lipid microdomains facilitate Histoplasma capsulatum internalisation by macrophages. Cell Microbiol. 2019;21(3):e12976.
106. Long KH, Gomez FJ, Morris RE, Newman SL. Identification of heat shock protein 60 as the ligand on Histoplasma capsulatum that mediates binding to CD18 receptors on human macrophages. Journal of immunology (Baltimore, Md : 1950). 2003;170(1):487-94.
107. Newman SL, Bucher C, Rhodes J, Bullock WE. PHAGOCYTOSIS OF HISTOPLASMA-CAPSULATUM YEASTS AND MICROCONIDIA BY HUMAN CULTURED MACROPHAGES AND ALVEOLAR MACROPHAGES - CELLULAR CYTOSKELETON REQUIREMENT FOR ATTACHMENT AND INGESTION. Journal of Clinical Investigation. 1990;85(1):223-30.
108. Kampmann M, Bassik MC, Weissman JS. Functional genomics platform for pooled screening and generation of mammalian genetic interaction maps. Nature Protocols. 2014;9(8):1825-47.
109. Jeng EE, Bhadkamkar V, Ibe NU, Gause H, Jiang L, Chan J, et al. Systematic Identification of Host Cell Regulators of Legionella pneumophila Pathogenesis Using a Genome-wide CRISPR Screen. Cell Host Microbe. 2019;26(4):551-63.e6.

110. Park RJ, Wang T, Koundakjian D, Hultquist JF, Lamothe-Molina P, Monel B, et al. A genome-wide CRISPR screen identifies a restricted set of HIV host dependency factors. Nat Genet. 2017;49(2):193-203.

111. Napier BA, Brubaker SW, Sweeney TE, Monette P, Rothmeier GH, Gertsvolf NA, et al. Complement pathway amplifies caspase-11-dependent cell death and endotoxin-induced sepsis severity. The Journal of experimental medicine. 2016;213(11):2365-82.

112. Morgens DW, Wainberg M, Boyle EA, Ursu O, Araya CL, Tsui CK, et al. Genome-scale measurement of off-target activity using Cas9 toxicity in high-throughput screens. Nature communications. 2017;8:15178.

113. Worsham PL, Goldman WE. Selection and characterization of ura5 mutants of Histoplasma capsulatum. Molecular & general genetics : MGG. 1988;214(2):348-52.

114. Morgens DW, Deans RM, Li A, Bassik MC. Systematic comparison of CRISPR/Cas9 and RNAi screens for essential genes. Nature biotechnology. 2016;34(6):634-6.

115. Devreotes P, Horwitz AR. Signaling networks that regulate cell migration. Cold Spring Harb Perspect Biol. 2015;7(8):a005959.

116. Moser M, Nieswandt B, Ussar S, Pozgajova M, Fässler R. Kindlin-3 is essential for integrin activation and platelet aggregation. Nat Med. 2008;14(3):325-30.

117. Jewell JL, Russell RC, Guan KL. Amino acid signalling upstream of mTOR. Nature reviews Molecular cell biology. 2013;14(3):133-9.

118. Chitwood PJ, Hegde RS. The Role of EMC during Membrane Protein Biogenesis. Trends Cell Biol. 2019.

119. Shurtleff MJ, Itzhak DN, Hussmann JA, Schirle Oakdale NT, Costa EA, Jonikas M, et al. The ER membrane protein complex interacts cotranslationally to enable biogenesis of multipass membrane proteins. Elife. 2018;7.

120. Irannejad R, von Zastrow M. GPCR signaling along the endocytic pathway. Current opinion in cell biology. 2014;27:109-16.

121. Block H, Stadtmann A, Riad D, Rossaint J, Sohlbach C, Germena G, et al. Gnb isoforms control a signaling pathway comprising Rac1, Plcβ2, and Plcβ3 leading to LFA-1 activation and neutrophil arrest in vivo. Blood. 2016;127(3):314-24.

122. Andreu N, Phelan J, de Sessions PF, Cliff JM, Clark TG, Hibberd ML. Primary macrophages and J774 cells respond differently to infection with Mycobacterium tuberculosis. Scientific reports. 2017;7:42225.

123. Haas PJ, van Strijp J. Anaphylatoxins: their role in bacterial infection and inflammation. Immunologic research. 2007;37(3):161-75.

124. Mueller-Ortiz SL, Hollmann TJ, Haviland DL, Wetsel RA. Ablation of the complement C3a anaphylatoxin receptor causes enhanced killing of Pseudomonas aeruginosa in a mouse model of pneumonia. Am J Physiol Lung Cell Mol Physiol. 2006;291(2):L157-65.

125. Wu KY, Zhang T, Zhao GX, Ma N, Zhao SJ, Wang N, et al. The C3a/C3aR axis mediates anti-inflammatory activity and protects against uropathogenic E coli-induced kidney injury in mice. Kidney Int. 2019;96(3):612-27.

126. Lian H, Litvinchuk A, Chiang AC, Aithmitti N, Jankowsky JL, Zheng H. Astrocyte-Microglia Cross Talk through Complement Activation Modulates Amyloid Pathology in Mouse

Models of Alzheimer's Disease. The Journal of neuroscience : the official journal of the Society for Neuroscience. 2016;36(2):577-89.

127. Litvinchuk A, Wan YW, Swartzlander DB, Chen F, Cole A, Propson NE, et al. Complement C3aR Inactivation Attenuates Tau Pathology and Reverses an Immune Network Deregulated in Tauopathy Models and Alzheimer's Disease. Neuron. 2018;100(6):1337-53.e5.

128. Zhang LY, Pan J, Mamtilahun M, Zhu Y, Wang L, Venkatesh A, et al. Microglia exacerbate white matter injury via complement C3/C3aR pathway after hypoperfusion. Theranostics. 2020;10(1):74-90.

129. Humbles AA, Lu B, Nilsson CA, Lilly C, Israel E, Fujiwara Y, et al. A role for the C3a anaphylatoxin receptor in the effector phase of asthma. Nature. 2000;406(6799):998-1001.

130. Ames RS, Lee D, Foley JJ, Jurewicz AJ, Tornetta MA, Bautsch W, et al. Identification of a selective nonpeptide antagonist of the anaphylatoxin C3a receptor that demonstrates antiinflammatory activity in animal models. Journal of immunology (Baltimore, Md : 1950). 2001;166(10):6341-8.

131. Huang NN, Becker S, Boularan C, Kamenyeva O, Vural A, Hwang IY, et al. Canonical and noncanonical g-protein signaling helps coordinate actin dynamics to promote macrophage phagocytosis of zymosan. Molecular and cellular biology. 2014;34(22):4186-99.

132. Decker T, Lohmann-Matthes ML. A quick and simple method for the quantitation of lactate dehydrogenase release in measurements of cellular cytotoxicity and tumor necrosis factor (TNF) activity. J Immunol Methods. 1988;115(1):61-9.

133. Nilsson UR, Müller-Eberhard HJ. Deficiency of the fifth component of complement in mice with an inherited complement defect. The Journal of experimental medicine. 1967;125(1):1-16.

134. Zhang MX, Klein B. Activation, binding, and processing of complement component 3 (C3) by Blastomyces dermatitidis. Infect Immun. 1997;65(5):1849-55.

135. Daffern PJ, Pfeifer PH, Ember JA, Hugli TE. C3a is a chemotaxin for human eosinophils but not for neutrophils. I. C3a stimulation of neutrophils is secondary to eosinophil activation. The Journal of experimental medicine. 1995;181(6):2119-27.

136. Riedl J, Crevenna AH, Kessenbrock K, Yu JH, Neukirchen D, Bista M, et al. Lifeact: a versatile marker to visualize F-actin. Nature methods. 2008;5(7):605-7.

137. Svensson CM, Medyukhina A, Belyaev I, Al-Zaben N, Figge MT. Untangling cell tracks: Quantifying cell migration by time lapse image data analysis. Cytometry Part A : the journal of the International Society for Analytical Cytology. 2018;93(3):357-70.

138. Heinrich V, Simpson WD, 3rd, Francis EA. Analytical Prediction of the Spatiotemporal Distribution of Chemoattractants around Their Source: Theory and Application to Complement-Mediated Chemotaxis. Front Immunol. 2017;8:578.

139. Underhill DM, Goodridge HS. Information processing during phagocytosis. Nature Reviews Immunology. 2012;12(7):492-502.

140. Vasek MJ, Garber C, Dorsey D, Durrant DM, Bollman B, Soung A, et al. A complement-microglial axis drives synapse loss during virus-induced memory impairment. Nature. 2016;534(7608):538-43.

141. Mathieu MC, Sawyer N, Greig GM, Hamel M, Kargman S, Ducharme Y, et al. The C3a receptor antagonist SB 290157 has agonist activity. Immunol Lett. 2005;100(2):139-45.
142. Peracino B, Borleis J, Jin T, Westphal M, Schwartz JM, Wu L, et al. G protein beta subunit-null mutants are impaired in phagocytosis and chemotaxis due to inappropriate regulation of the actin cytoskeleton. The Journal of cell biology. 1998;141(7):1529-37.
143. Pan M, Neilson MP, Grunfeld AM, Cruz P, Wen X, Insall RH, et al. A G-protein-coupled chemoattractant receptor recognizes lipopolysaccharide for bacterial phagocytosis. PLoS Biol. 2018;16(5):e2005754.
144. Freeman SA, Vega A, Riedl M, Collins RF, Ostrowski PP, Woods EC, et al. Transmembrane Pickets Connect Cyto- and Pericellular Skeletons Forming Barriers to Receptor Engagement. Cell. 2018;172(1-2):305-17.e10.
145. Shen K, Sidik H, Talbot WS. The Rag-Ragulator Complex Regulates Lysosome Function and Phagocytic Flux in Microglia. Cell Rep. 2016;14(3):547-59.
146. Willardson BM, Tracy CM. Chaperone-mediated assembly of G protein complexes. Subcell Biochem. 2012;63:131-53.
147. Kubota H, Hynes G, Willison K. The chaperonin containing t-complex polypeptide 1 (TCP-1). Multisubunit machinery assisting in protein folding and assembly in the eukaryotic cytosol. Eur J Biochem. 1995;230(1):3-16.
148. Bonifacino JS, Rojas R. Retrograde transport from endosomes to the trans-Golgi network. Nature reviews Molecular cell biology. 2006;7(8):568-79.
149. Personnic N, Barlocher K, Finsel I, Hilbi H. Subversion of Retrograde Trafficking by Translocated Pathogen Effectors. Trends Microbiol. 2016.

150. Stanley P, Taniguchi N, Aebi M. N-Glycans. In: Varki A, Cummings RD, Esko JD, Stanley P, Hart GW, Aebi M, et al., editors. Essentials of Glycobiology. Cold Spring Harbor (NY): Cold Spring Harbor Laboratory Press
Copyright 2015-2017 by The Consortium of Glycobiology Editors, La Jolla, California. All rights reserved.; 2015. p. 99-111.
151. Hadley B, Litfin T, Day CJ, Haselhorst T, Zhou Y, Tiralongo J. Nucleotide Sugar Transporter SLC35 Family Structure and Function. Comput Struct Biotechnol J. 2019;17:1123-34.
152. Ruprecht JJ, Kunji ERS. The SLC25 Mitochondrial Carrier Family: Structure and Mechanism. Trends Biochem Sci. 2020;45(3):244-58.
153. Gudjonsson T, Altmeyer M, Savic V, Toledo L, Dinant C, Grøfte M, et al. TRIP12 and UBR5 suppress spreading of chromatin ubiquitylation at damaged chromosomes. Cell. 2012;150(4):697-709.
154. Cho JH, Kim SA, Seo YS, Park SG, Park BC, Kim JH, et al. The p90 ribosomal S6 kinase-UBR5 pathway controls Toll-like receptor signaling via miRNA-induced translational inhibition of tumor necrosis factor receptor-associated factor 3. The Journal of biological chemistry. 2017;292(28):11804-14.
155. Deepe GS, Jr., Buesing WR. Deciphering the pathways of death of Histoplasma capsulatum-infected macrophages: implications for the immunopathogenesis of early infection. Journal of immunology (Baltimore, Md : 1950). 2012;188(1):334-44.
156. Surugiu R, Catalin B, Dumbrava D, Gresita A, Olaru DG, Hermann DM, et al. Intracortical Administration of the Complement C3 Receptor Antagonist Trifluoroacetate Modulates Microglia Reaction after Brain Injury. Neural Plast. 2019;2019:1071036.

157. Sun D, Sun P, Li H, Zhang M, Liu G, Strickland AB, et al. Fungal dissemination is limited by liver macrophage filtration of the blood. Nature communications. 2019;10(1):4566.

158. Zipfel PF, Skerka C. Complement, Candida, and cytokines: the role of C5a in host response to fungi. European journal of immunology. 2012;42(4):822-5.

159. Roy RM, Paes HC, Nanjappa SG, Sorkness R, Gasper D, Sterkel A, et al. Complement component 3C3 and C3a receptor are required in chitin-dependent allergic sensitization to Aspergillus fumigatus but dispensable in chitin-induced innate allergic inflammation. mBio. 2013;4(2).

160. Brennan FH, Jogia T, Gillespie ER, Blomster LV, Li XX, Nowlan B, et al. Complement receptor C3aR1 controls neutrophil mobilization following spinal cord injury through physiological antagonism of CXCR2. JCI Insight. 2019;4(9).

161. Mershon KL, Vasuthasawat A, Lawson GW, Morrison SL, Beenhouwer DO. Role of complement in protection against Cryptococcus gattii infection. Infect Immun. 2009;77(3):1061-70.

162. Hwang LH, Mayfield JA, Rine J, Sil A. Histoplasma requires SID1, a member of an iron-regulated siderophore gene cluster, for host colonization. PLoS pathogens. 2008;4(4):e1000044.

163. Worsham PL, Goldman WE. Quantitative plating of Histoplasma capsulatum without addition of conditioned medium or siderophores. Journal of medical and veterinary mycology : bi-monthly publication of the International Society for Human and Animal Mycology. 1988;26(3):137-43.

164. Mead HL, Van Dyke MCC, Barker BM. Proper Care and Feeding of Coccidioides: A Laboratorian's Guide to Cultivating the Dimorphic Stages of C. immitis and C. posadasii. Curr Protoc Microbiol. 2020;58(1):e113.

165. Deans RM, Morgens DW, Okesli A, Pillay S, Horlbeck MA, Kampmann M, et al. Parallel shRNA and CRISPR-Cas9 screens enable antiviral drug target identification. Nat Chem Biol. 2016;12(5):361-6.

166. Brinkman EK, Chen T, Amendola M, van Steensel B. Easy quantitative assessment of genome editing by sequence trace decomposition. Nucleic acids research. 2014;42(22):e168.

167. Bassik MC, Kampmann M, Lebbink RJ, Wang SY, Hein MY, Poser I, et al. A Systematic Mammalian Genetic Interaction Map Reveals Pathways Underlying Ricin Susceptibility. Cell. 2013;152(4):909-22.

168. Saldanha AJ. Java Treeview--extensible visualization of microarray data. Bioinformatics. 2004;20(17):3246-8.

169. Eden E, Navon R, Steinfeld I, Lipson D, Yakhini Z. GOrilla: a tool for discovery and visualization of enriched GO terms in ranked gene lists. BMC bioinformatics. 2009;10:48.

170. Ollion J, Cochennec J, Loll F, Escudé C, Boudier T. TANGO: a generic tool for high-throughput 3D image analysis for studying nuclear organization. Bioinformatics. 2013;29(14):1840-1.

171. Meijering E, Dzyubachyk O, Smal I. Methods for cell and particle tracking. Methods Enzymol. 2012;504:183-200.

172. Isaac DT, Coady A, Van Prooyen N, Sil A. The 3-Hydroxy-Methylglutaryl Coenzyme A Lyase HCL1 Is Required for Macrophage Colonization by Human Fungal Pathogen Histoplasma capsulatum. Infection and Immunity. 2013;81(2):411-20.

Publishing Agreement

It is the policy of the University to encourage open access and broad distribution of all theses, dissertations, and manuscripts. The Graduate Division will facilitate the distribution of UCSF theses, dissertations, and manuscripts to the UCSF Library for open access and distribution. UCSF will make such theses, dissertations, and manuscripts accessible to the public and will take reasonable steps to preserve these works in perpetuity.

I hereby grant the non-exclusive, perpetual right to The Regents of the University of California to reproduce, publicly display, distribute, preserve, and publish copies of my thesis, dissertation, or manuscript in any form or media, now existing or later derived, including access online for teaching, research, and public service purposes.

DocuSigned by:
Allison Cohen
EC54858DBEF44AC...
Author Signature

5/28/2022
Date